THESIS FOR THE DEGREE OF DOCTOR OF PHILOSOPHY

Lipid-based liquid crystals as drug delivery vehicles for antimicrobial peptides

LUKAS BOGE

Department of Chemistry and Chemical Engineering

CHALMERS UNIVERSITY OF TECHNOLOGY

Gothenburg, Sweden 2018

Lipid-based liquid crystals as drug delivery vehicles for antimicrobial peptides

LUKAS BOGE
ISBN 978-91-7597-809-3

Doktorsavhandlingar vid Chalmers tekniska högskola
Ny serie nr 4490
ISSN 0346-718X

Department of Chemistry and Chemical Engineering
Chalmers University of Technology
SE-412 96 Gothenburg
Sweden
Telephone + 46(0)317721000

Cover: Cryogenic transmission electron microscopy (cryo-TEM) reveals the repeating cubic liquid crystalline structure of a cubosome particle. More images and further details are presented in section 4.2 in this thesis. One side of the cubosome particle equals 100 nm.

Printed by Chalmers Reproservice
Gothenburg, Sweden 2018

Lipid-based liquid crystals as drug delivery vehicles for antimicrobial peptides

LUKAS BOGE
Department of Chemistry and Chemical Engineering
CHALMERS UNIVERSITY OF TECHNOLOGY

ABSTRACT

The development of antimicrobial resistance is a great challenge within health sectors worldwide. Thus, demand for new, efficient treatments is urgent in order to treat various bacterial infections. Antimicrobial peptides (AMPs) are a group of antibiotics that have gained more and more attraction in the past decade. AMPs suffer from relatively low stability due to proteolytic and chemical degradation. As a consequence, carrier systems to protect the AMPs are highly needed to achieve efficient treatments in the clinic.

In this thesis, lipid-based liquid crystalline (LC) structures have been examined as carriers for AMPs. LC structures of polar lipids have potential to be used as carriers and delivery systems in various pharmaceutical applications. This is due to their ability to solubilize and encapsulate hydrophilic, hydrophobic and amphiphilic substances. An important feature of these LC systems is that they can coexist with an excess of water, which enables fragmentation of the highly viscous gels into LC nanoparticles (LCNPs), i.e. cubosomes and hexosomes, in the presence of a suitable stabilizer. Peptides and proteins can be incorporated into the lipid self-assembled structures, thereby protecting them from chemical and proteolytic degradation. Cubosomes and hexosomes were investigated as drug delivery vehicles for the three AMPs: i) AP114, an improved plectasin derivative originating from the fungus *Pseudoplectania nigrella*, ii) DPK-060, derived from the endogenous human protein kininogen and iii) LL-37, a human AMP found in the cathelicidin family. Phase behavior, different preparation methodologies of the LCNPs, antimicrobial effect and proteolytic protection of the AMPs were studied. Moreover, the interaction between AMP-loaded particles with bacteria and bacterial mimicking membranes was investigated. Formulations aimed for pulmonary and topical administration were also evaluated. Results showed that cubic LC phases were most sensitive to the incorporation of AMPs. Depending on the nature of the AMP, different changes in the curvature of the systems were observed. Cubosomes loaded with AMPs exhibited good antimicrobial activity and were found to protect the proteolytic sensitive LL-37 from enzymatic degradation. Data strongly suggested that the release of AMP from the particles cannot solely be explained by the antimicrobial effect. Cubosomes loaded with LL-37 are thought to adsorb onto bacterial membranes, resulting in cell death.

Keywords: Liquid crystals, liquid crystalline nanoparticles, cubosome, hexosome, phase behavior, antimicrobial peptide, AMP, glycerol monooleate, proteolysis, antimicrobial effect, antimicrobial resistance, bacterial membrane, membrane interaction, infection, topical delivery, pulmonary delivery

LIST OF PUBLICATIONS

The thesis is based on the work described in the following papers:

Paper 1 ***Lipid-based liquid crystals as carriers for antimicrobial peptides: phase behavior and antimicrobial effect***
Lukas Boge, Helena Bysell, Lovisa Ringstad, David Wennman, Anita Umerska, Viviane Cassisa, Jonny Eriksson, Marie-Laure Joly-Guillou, Katarina Edwards and Martin Andersson
Langmuir, **2016**, *32*, p. 4217–4228

Paper 2 ***Cubosomes post-loaded with antimicrobial peptides: characterization, bactericidal effect and proteolytic stability***
Lukas Boge, Anita Umerska, Nada Matougui, Helena Bysell, Lovisa Ringstad, Jonny Eriksson, Mina Davoudi, Katarina Edwards and Martin Andersson
International Journal of Pharmaceutics, **2017**, 526, p. 400-412

Paper 3 ***Freeze-dried and rehydrated liquid crystalline nanoparticles stabilized with disaccharides for drug-delivery of the plectasin derivative AP114 antimicrobial peptide***
Lukas Boge, Amanda Västberg, Anita Umerska, Helena Bysell, Jonny Eriksson, Katarina Edwards, Anna Millqvist-Fureby and Martin Andersson
Journal of Colloid and Interface Science, **2018**, 522, p. 126-135

Paper 4 ***The interaction of antimicrobial peptide LL-37 loaded cubosomes with model and bacterial membranes***
Lukas Boge, Kathryn Browning, Randi Nordström, Mario Campana, Josefin Seth Caous, Maja Hellsing, Lovisa Ringstad and Martin Andersson
Manuscript in preparation

Paper 5 ***Cubosomes for topical delivery of the antimicrobial peptide LL-37***
Lukas Boge, Karin Hallstensson, Lovisa Ringstad, Jenny Johansson, Therese Andersson, Mina Davoudi, Per Tomas Larsson, Margit Mahlapuu, Joakim Håkansson and Martin Andersson
Submitted for publication

The papers listed above are appended at the end of this thesis

CONTRIBUTION REPORT

Paper 1 Responsible for all experimental work (except cryo-TEM imaging and *in vitro* bacterial studies), data evaluation and writing of the manuscript.

Paper 2 Responsible for all experimental work (except cryo-TEM imaging and *in vitro* bacterial studies), data evaluation and writing of the manuscript.

Paper 3 Involved in planning of the study and did part of the experimental work (SAXS measurements) and wrote the manuscript.

Paper 4 Did major part of the experimental work (except cryo-TEM/ET imaging), responsible for data analysis and writing of the manuscript. Co-analyzed neutron reflectivity data.

Paper 5 Involved in planning the study, did minor part of experimental work (SAXS measurements and peptide quantification in release studies), responsible for data evaluation and writing of the manuscript.

RELATED PUBLICATIONS, NOT INCLUDED IN THIS THESIS

I. ***Lipid-based nanoformulations for peptide delivery***
Nada Matougui, Lukas Boge, Anne-Claire Groo, Anita Umerska, Lovisa Ringstad, Helena Bysell and Patrick Saulnier
International Journal of Pharmaceutics, 2016, 502, p. 80-97

II. ***Evaluation of toxicity of glycerol monooleate nanoparticles on PC12 cell line***
Filippo Valente, Helena Bysell, Edi Simoni, Lukas Boge, Mimmi Eriksson, Alessandro Martini and Laura Astolfi
International Journal of Pharmaceutics, 2018, 539, p. 23-30

ACKNOWLEDGEMENT

My supervisor **Martin Andersson**. Thank you for your support and many clever ideas during these years. Especially those ideas making me think the other way around. You have encouraged me to initiate new collaborations, which have taken this research to a higher level. It has been a pleasure having you as supervisor; you possess excellent mentor and management skills. Sorry for always mixing up “was” and “were”, “were” and “where”, “has” and “have” and “is” and “are” in my texts… ;-)

My co-supervisor and manager at RISE Research Institutes of Sweden, **Lovisa Ringstad**. Thank you for giving me freedom and confidence to finish my investigations and taking care of administrative (often money related) issues. It has been plenty of fun working in close collaboration with you. I hope our careers will intersect in the future!

Former co-supervisor **Helena Bysell**, one of the persons responsible for that this happened at all. Thank you for seeing the opportunity to have me as an industrial PhD student in the FORMAMP-project and letting me jump on this train. It has been an exciting journey that has come to an end, making room for new adventurers. Thank you for your enthusiasm and guidance during highs and lows.

Again, thank you for your time and engagement in this project!

I would also like to thank:

Anders Palmqvist, my examiner, and **Hanna Härelind**, director of studies, for watching that I was on track with my PhD studies over these years.

Szymon Sollami-Delekta and **Amanda Västberg**, for performing excellent research within your master thesis projects. You have both contributed a lot to this thesis!

Kathryn Browning, **Liv Sofia Elinor Damgaard**, **Maja Hellsing** and **Mario Campana**, my neutron reflectivity dream-team ☺

Anita Umerska, **Viviane Cassisa**, and **Mina Davoudi** for performing *in vitro* bacterial studies included in three of the papers included in this thesis

Camilla Holmlund, **Jonny Eriksson** and **Katarina Edwards** for taking incredible cryo-TEM images shown in this thesis

All co-authors of my papers. By working together we can make science of higher impact!

All people involved in the **FORMAMP-project**, for valuable discussions and input during these intense and fun years. I would like to thank **Randi Nordström**, **Oliver Andrén**, **René Rozenbaum** and **Nada Matougui** for great collaboration and support during the FORMAMP roller coaster. I have learned a lot from all of you, and really enjoyed hanging out with you during project meetings and conferences.

My colleagues at **RISE** in Stockholm, Södertälje, Borås and Göteborg. Special thanks to **Johan Andersson**, **Mimmi Eriksson**, **Eva Sjöström** and **Martin Arvidsson** (ex-RISE) for always being around for a coffee break or for going out for a beer or two.

Members of **M.A. Research group** at Chalmers, Especially I would like to thank **Anand Kumar Rajasekharan**, **Simon Isaksson**, **Saba Atefyekta**, **Mats Hulander**, **Gustav Sundell** and **Astrid Pihl** for fun times at conferences, courses and for sharing knowledge and experiences.

National Microscopy Infrastructure, NMI, (VR-RFI 2016-00968) for providing assistance in microscopy

ISIS Neutron and Muon Source at **Rutherford Appleton Laboratory** (Didcot, UK) is acknowledged for beam-time allocation at CRISP from the **Science and Technology Facilities Council**

The MAX IV Laboratory (Lund, Sweden) for beam-time allocation at synchrotron beamline I911-SAXS

The research performed in this study were carried out at **RISE Research Institutes of Sweden** (Stockholm, Sweden) and funded by the European Union's Seventh Framework Program (FP7/2007-2013), under Grant Agreement No. 604182 within the **FORMAMP project** and by **RISE Research Institutes of Sweden** (Stockholm, Sweden)

Last, but not least

Kasper and **Jonathan**, my brothers in arms

LIST OF ABBREVIATIONS

AMP	Antimicrobial peptide
2D	Two dimensional
3D	Three dimensional
AB	*Acinetobacter baumannii*
BHI	Brain heart infusion broth
BHI_{100}	Brain heart infusion broth diluted 100 times in water
CFU	Colony forming units
CmSi	Contrast matched silicon
CmSi-buffer	Buffer prepared in H_2O/D_2O-mixture
Cryo-ET	Cryogenic transmission electron tomography
Cryo-TEM	Cryogenic transmission electron microscopy
d-buffer	Buffer prepared in D_2O
dDMPC	1,2-dimyristoyl-d54-sn-glycero-3-phosphocholine
dDMPG	1,2-dimyristoyl-d54-sn-glycero-3-[phospho-rac-(1-glycerol)] sodium salt
DLS	Dynamic light scattering
DOPC	1,2-dioleoyl-sn-glycero-3-phosphocholine
DPPS	1,2-Dipalmitoyl-sn-glycero-3-phosphoserine
EC	*Escherichia coli*
ESBL EC	Extended spectrum beta-lactamase producing *Escherichia coli*
GFP	Green fluorescent protein
GFP-EC	Green fluorescent protein producing *Escherichia coli*
GMO	Glycerol monooleate
h-buffer	Buffer prepared in H_2O
hDMPC	1,2-dimyristoyl-sn-glycero-3-phosphocholine
hDMPG	1,2-dimyristoyl-sn-glycero-3-phospho-(1'-rac-glycerol) sodium salt
HNE	Human neutrophil elastase
HPLC	High performance liquid chromatography
LC	Liquid crystal or liquid crystalline
LCNP	Liquid crystalline nanoparticle
MIC	Minimum inhibitory concentration
MMA	Mean molecular area
MRSA	Methicillin-resistant *Staphylococcus aureus*
MTT	Methylthiazolyldiphenyl-tetrazolium bromide
MWCO	Molecular weight cut-off
NR	Neutron reflectivity
OA	Oleic acid
P407	Poloxamer 407
PA	*Pseudomonas aeruginosa*
PC	Phosphatidyl choline
PE	*Pseudomonas aeruginosa* elastase
QCM-D	Quartz crystal microbalance with dissipation monitoring
RDA	Radial diffusion assay
SA	*Staphylococcus aureus*
SAXS	Small angle x-ray scattering

SE	*Staphylococcus epidermis*
SEM	Scanning electron microscopy
SLD	Scattering length density
UPLC	Ultra-performance liquid chromatography
wt %	Weight %

TABLE OF CONTENTS

1. INTRODUCTION

It is the middle of the summer, the sun is burning on your back. You are at your summer house far away from the civilized and stressful city life. In a desperate attempt to escape the heat of the sun, you crawl out of your comfortable lounger and head off to the kitchen to prepare a cool drink. On your way, crossing the old garden, you accidently step on a rusty nail in the grass. You reach down to investigate your foot and find the rusty nail has penetrated the skin between your toes. By jumping on the right leg, you manage to reach a chair on the veranda. You sit down, taking a couple of deep breaths. After another look at the foot, you decide to remove the nail. You grab the rusty nail between your thumb and index finger. While holding your breath, you remove it with a quick motion. The pain is intense and it starts bleeding. You find some old plasters in the kitchen, trying to stop the blood.

The next day, you wake up with a swollen foot and it hurts even more than before. You wait another few days to see if it gets any better. It is impossible to lean on the foot because of the pain. You finally decide to drive to the nearest town, to the small hospital. The doctor quickly concludes that the foot is infected by bacteria, most likely originating from the rusty nail. The doctor prescribes you a 7-day penicillin cure. However, the foot does not get better. On the 5^{th} day of penicillin the wound has become an ulcer, the foot is even more swollen and has turned blue. You wake up in the middle of the night sweating, realizing you have a fever. You are feeling dizzy, and it is hard to communicate with you. The world spins around, you fall into a deep sleep.

A quick ambulance ride back to the local hospital, facing the same doctor you met a few days ago. He looks very concerned about your situation and decides to let the ambulance drive you to the infection unit at another hospital in a bigger city. Upon arrival, nurses and doctors immediately surround you. They monitor your heartbeat and takes blood samples for analysis. The diagnosis: sepsis. Your blood is full of exponentially growing bacteria. Through a cannula in your right arm an antibiotic cocktail slowly enters your bloodstream. It does not help. Over the next couple of days different antibiotics are tried to heal you, without progress. The doctor enters your room telling you that the analysis of your blood samples in the lab is ready. The bacterium causing the infection is resistant to all available antibiotics and you are waiting for an inescapable death.

What can you do?

1.1. Antimicrobial resistance: a global threat

Development of antimicrobial resistance of pathogenic bacteria is a great challenge within the health sector, all around the world. Decades of over and misuse of penicillin and other antibiotic drugs, both in humans and in animals, have led to this current unpleasant situation. The discoverer of penicillin, Alexander Fleming, did ironically predict this future very precisely in his Nobel lecture held in 1945 [1]:

> "*The time may come when penicillin can be bought by anyone in the shops. Then there is the danger that the ignorant man may easily under-dose himself and by exposing his microbes to nonlethal quantities of the drug make them resistant."*

And he was so right. Resistant bacteria began to pop up everywhere where penicillin was used. Today, estimations point out that up to 70 % of the hospital acquired infections in the United States are caused by bacteria resistant to one or more antibiotics [2]. Since the discovery and deployment of penicillin in the 1940's, bacteria have developed resistance to all new types of antibiotics, often after a few years of use. In the past 40 years only two classes of antibiotics used clinically have been discovered and reached the market [2, 3]. It is estimated points out that research needs to be funded with approximately £1.5 billion over 10 years to explore and evaluate new antibiotics [4]. Novel candidates currently in clinical trials include various antibodies, lysins, probiotics, bacteriophages, immune stimulation, vaccines and antimicrobial peptides (AMPs) [4]. It comes as no surprise that antimicrobial resistance is listed as one of the biggest threats to global health and development by the World Health Organization (WHO) as high rates of resistance development is observed around the planet. In the latest WHO report "*Antimicrobial resistance: global report on surveillance"* (2014) it was found that more than 50% of the pathogenic bacteria causing common infections in hospitals and out in society (e.g. *Escherichia coli* and *Staphylococcus aureus*) had reduced susceptibility to antibiotic treatments [5]. The demand for new and efficient treatments is urgent. It is doubtless a must in order to treat various bacterial infections, large or small, in the near future.

1.2. Antimicrobial peptides and their function

AMPs, also referred to as host-defense peptides, are present in almost all organisms as part of their innate defense system. Thus, they make up the body's first response towards pathogens, e.g. bacteria. They have been around in animals and plants for millions of years, in co-evolution with bacteria, without losing their ability to kill them [6]. Pioneering work in the field was carried out in the 1960's by Zeya and Spitznagel, as they found bactericidal protein fractions extracted from guinea pig polymorphonuclear leukocytes [7, 8]. In the 1970's Boman and co-workers studied the immune system of insects and found and characterized several bactericidal proteins [9-11] and later Zasloff and co-workers discovered the AMP

magainin in frog skin [12]. Since then about 2500 AMPs have been discovered and characterized [13]. Until 2015, only a handful of AMPs could be found in clinical trials, but many more in discovery and preclinical phases [4, 14-16]. Only two AMPs have today regulatory approval for clinical use in the treatment of infections; polymyxin and gramicidin S [17, 18]. AMPs are promising therapeutics to treat various infectious diseases due to their fast and non-specific mechanism of action [6, 15]. Hence, they are said to be less prone to induce high levels of resistance compared to conventionally used antibiotics. However, it has been shown that bacteria may also develop resistance to AMPs and this issue needs to be carefully studied before translation into clinics [19]. Beside the antibacterial properties of AMPs, they can also display antifungal, antitumor, antiviral and wound healing properties [6]. Hence, they play an important role in the innate host immune system. A number of technical, regulatory and commercial challenges still exist to bring AMP-based drugs into clinical development and commercialization. The challenges include low metabolic stability due to degradation by proteolysis, chemical stability during storage, regulatory hurdles related to manufacture and the high costs of production [18]. These issues might be overcome by using clever modifications and formulation strategies, such as their incorporation into well-designed drug delivery vehicles [20].

AMPs are generally amphipathic molecules consisting of <45 amino acids, of which a substantial fraction are normally hydrophobic residues, and having a positive net charge [21]. The latter is an important property, driving the adsorption towards the slightly negatively charged phospholipid head groups and lipopolysaccharides (LPS) of the bacterial membrane. This facilitates a selective quick and strong interaction with bacterial membranes, compared to mammalian cell membranes. The mammalian cell membrane is mostly composed of zwitterionic phospholipids and cholesterol, and has a neutral charge, resulting in weaker interactions with positively charged AMPs. This is further illustrated in Figure 1 below.

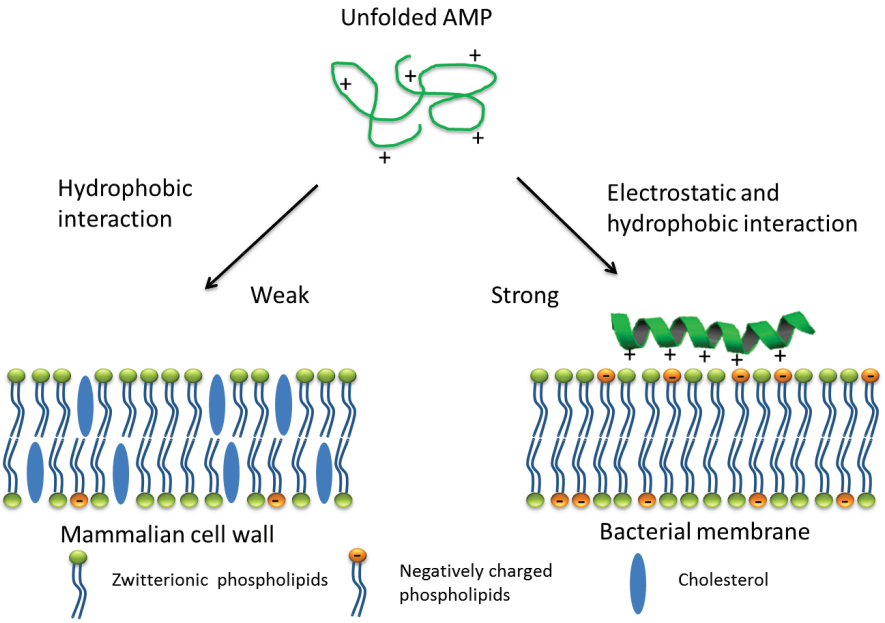

Figure 1. A simplified illustration of the interaction of an AMP with a mammalian cell wall membrane and a bacterial membrane. AMP interacts more strongly with the bacterial membrane due to the presence of negatively charged phospholipids, compared to a mammalian cell wall membrane.

There are several models describing the mode of action of AMPs. The most common modes involves the barrel-stave, carpet and toroidal pore models, which are illustrated in Figure 2 [6]. These models have in common that the presence of AMP results in the formation of pores/defects within the bacterial membrane, leading to rupture and finally death of the bacteria. In the barrel-stave model, the hydrophobic parts of a number of peptides interact with the hydrophobic tail region of the membrane in a ring (="the barrel"). Since it is very energetically unfavorable for a single peptide to penetrate the membrane, this mechanism of action usually occurs above a threshold concentration. At least a few peptides interacting together is believed to cause local membrane thinning, facilitating the insertion of peptides into the membrane [22]. The "stave" refers to individual transmembrane spokes within this round barrel, which can be individual peptides or peptide aggregates. The carpet mechanism of AMPs is similar to the effect of a surfactant detergent removing grease from laundry or dirty dishes. The model suggests that a localized high concentration of peptides results in changes to membrane fluidity, causing membrane dissolution and rupture. Similar to the barrel-stave model, the toroidal pore mechanism usually occurs above a threshold concentration. The peptides induce positive curvature effects upon binding to the membrane, resulting in the formation of membrane-spanning pores lined with polar peptide surfaces and phospholipid head groups [22]. The toroidal-pore mode is commonly considered to be an important mechanism in facilitating AMPs translocation through the membrane to reach intracellular targets. Normally only 5-60 minutes is enough for the AMPs to induce membrane defects [23, 24]. AMPs often change their secondary structure upon membrane interaction.

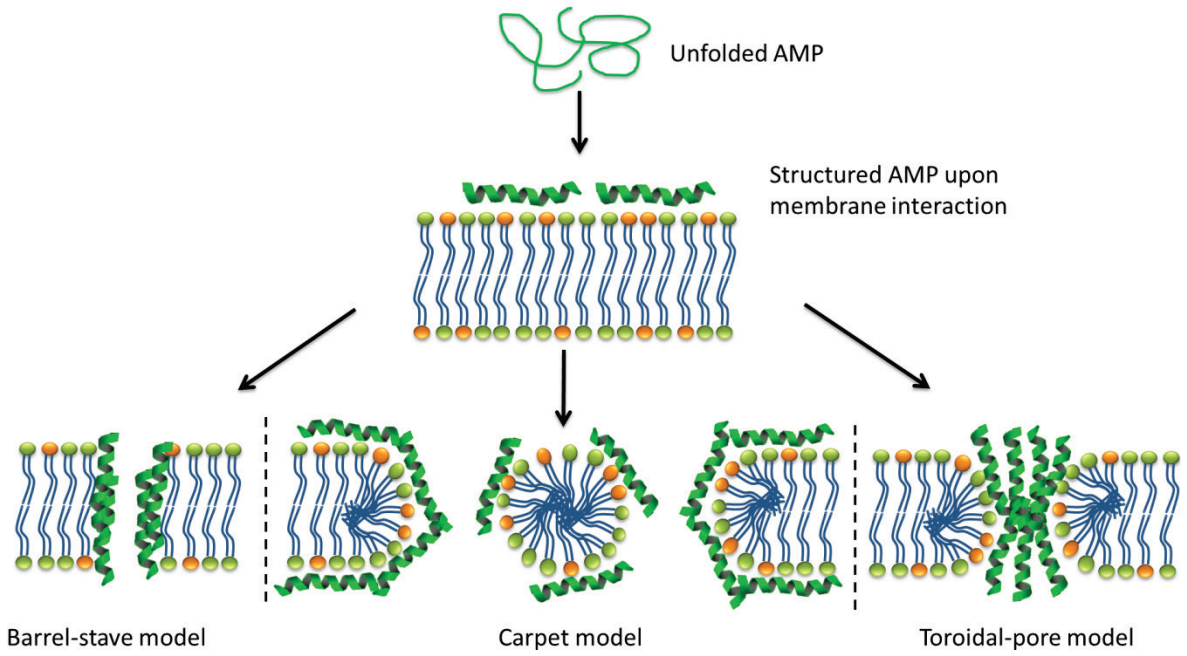

Figure 2. Models commonly used to describe the mechanism of killing bacteria by AMPs. AMPs are usually unstructured in aqueous solution and a conformation change is often observed upon adsorption and insertion into a bacterial membrane. If the AMP targets internal receptors of the cell, translocation through the membrane into the cytoplasm can also occur (not shown in illustration).

1.3. Antimicrobial peptides in this thesis

Three water soluble AMPs; AP114, DPK-060 and LL-37 were investigated in this thesis. They are different in terms of size, charge, hydrophobicity, secondary structure as well as antimicrobial activity. Schematic representations of the secondary structures of the AMPs are presented in Figure 3 and a summary of their physicochemical properties is found in Table 1.

Table 1. Properties of the antimicrobial peptides used in this thesis. MW=molecular weight, AA= amino acid. Note that the secondary structure of LL-37 normally changes from predominantly random coil conformation in solution to α-helix upon membrane adsorption.

Peptide	Sequence	MW (Da)	% hydrophobic AA	Net charge (pH 5.5)	Secondary structure	Antibacterial activity
AP114	GFGCNGPWNEDDLRCHNHCKSI-KGYKGGYCAKGGFVCKCY	4411	40	+4.6	β-sheet, α-helix	Gram-positive
DPK-060	GKHKNKGKKNGKHNGWKWWW	2503	20	+8.5	Random coil	Broad spectrum
LL-37	LLGDFFRKSKEKIGKEFKRIVQR-IKDFLRNLVPRTES	4491	35	+6.3	random coil, α-helix	Broad spectrum

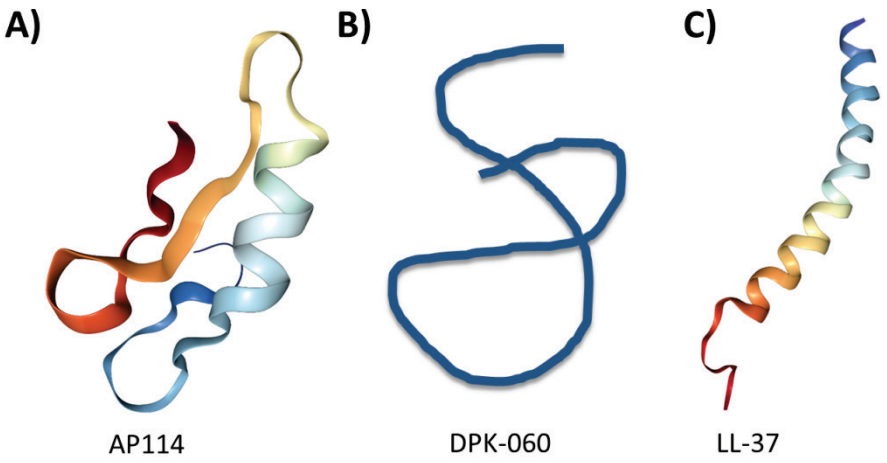

Figure 3. Schematic representations of the α-helical and β-sheet containing plectasin derivative AP114 (A), random coil DPK-060 (B) and α-helical LL-37 peptides. Illustrations A and C were adapted from RCSB Protein Data Bank [25].

The first AP114, also known as NZ2114 in the literature, is a plectasin derivative derived from the fungus *Pseudoplectania nigrella* ("ebony cup" or "svart vårskål" in Swedish). It kills bacteria by translocation through the bacterial membrane, inhibiting the membrane biosynthesis, through targeting of the cellular precursor Lipid II [26, 27]. Hence, the mechanism of action for AP114 differs from the more traditional killing models that involve membrane rupture and lysis of the bacteria. Translocation through the membrane may be according to the toroidal-pore mechanism. AP114 kills Gram-positive bacteria, including *Staphylococcus aureus* and its methicillin resistant variety (MRSA), making it a novel candidate for treatment of pneumonia.

DPK-060 is a broad-spectrum antimicrobial peptide, also known as GKH17-WWW. It is an improved derivative of endogenous human protein kininogen. Due to the three additional tryptophan amino acids at the C-terminal, it withstands enzymatic degradation by infection-

affiliated proteases, without being cytotoxic and possesses enhanced antimicrobial activity [28]. DPK-060 is intended for topical administration to treat a variety of infected skin conditions. The mode of action is believed to be a combination of induction negative curvature strain, thinning and local packing defects in the phospholipid polar head group regions [28]. The therapeutic effect was confirmed by clinical phase II studies as treatment for infections in atopic dermatitis and acute external otitis [14].

LL-37 is the only known human peptide in the cathelicidin family. LL-37 is an important part of the innate immune system of the skin and other soft tissues. It is a broad spectrum bactericide, also having immunomodulatory properties [29, 30]. In addition, LL-37 also promotes healing of chronic wounds [30-32]. Thus, LL-37 is an interesting candidate for topical treatment of bacterial infections. The secondary structure of LL-37 normally changes from mainly random coil in aqueous environment to α-helix upon membrane interaction, especially in the presence of negatively charged lipids and LPS [6, 33, 34]. The peptide is sensitive to proteolytic degradation by enzymes, which has so far limited its therapeutic use [32, 35]. It is suggested that LL-37 uses a toroidal pore/carpet-like mechanism of action [36]. However the exact mechanism of action is debated and is also suggested to depend upon the concentration [33].

1.4. Lyotropic liquid crystals and self-assembly

An amphiphile is a molecule consisting of two distinct regions; a water soluble “hydrophilic” part and an oil soluble “hydrophobic” part. Liquid crystalline (LC) phases form spontaneously upon hydration of certain amphiphilic molecules, e.g. polar lipids. The driving force for this self-assembly process of polar lipids is the *hydrophobic effect* [37, 38]. It strives to minimize unfavorable interactions between the regions of the amphiphile molecule with the solvent. Depending on the concentration of solvent and the nature of the amphiphile, organization into different structurers occurs. There are three main types of LC phases: lamellar, hexagonal and cubic phases. The LC phases are schematically illustrated in Figure 4 below. A LC phase can be of “oil-in-water” (normal) or “water-in-oil”-type (reversed), depending on the orientation of the hydrophobic parts in the self-assembly. A reversed phase is said to have a “negative” curvature. In general, amphiphiles having a double hydrophobic chain or a bulky single one, tend to form reversed structurers.

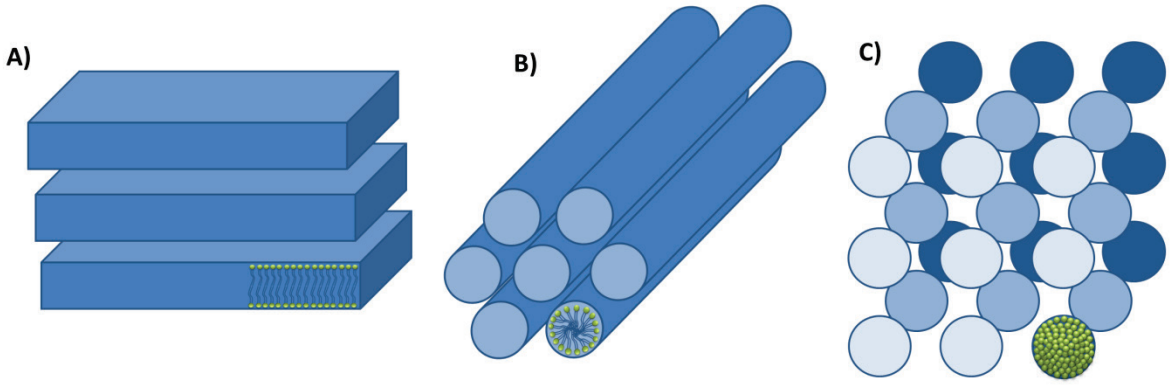

Figure 4. Schematic representation of the three major groups of liquid crystals; lamellar (A), hexagonal (B) and micellar cubic phase (C).

The lamellar phase (L_α) consists of lipid bilayer sheets separated by water layers. The lamellar phase is symmetrical around the middle of the bilayer and has as zero curvature. The hexagonal phase is built up by long cylindrical micelles, organized in a hexagonal pattern. The hexagonal phase can be "normal" H_I as illustrated in Figure 4 B (positive curvature), or "reversed" H_{II} (negative curvature). In the latter situation, the hydrophobic tails are pointing outwards and water is trapped inside the cylinders surrounded by the polar head groups. The cubic phase can be discrete cubic or bicontinuous cubic. A discrete cubic phase is built up by micelles packed in a cubic lattice (see Figure 4 C). The bicontinuous cubic structurers are constituted of continuous water channel systems separated by lipid bilayers, folded in three dimensions [39]. These phases can also be illustrated as rod-like micelles, forming a porous structure in three dimensions. The average curvature is zero in these structurers, mathematically represented by minimal surfaces. Three bicontinuous cubic structurers with minimal surfaces are known to-date: Im3m (P, primitive), Pn3m (D, diamond) and Ia3d (G, gyroid) [40-42]. These bicontinuous phases are illustrated in Figure 5. The cubic structurers can be normal or reversed, depending on the water content and structure of the amphiphile.

The three reversed bicontinuous cubic phases can be placed on a curvature scale based on their relative water content, following the "natural" or universal sequence of LC phases [43]. The negative curvature changes as follow: Im3m>Ia3d>Pn3m. In summary, the curvatures of the LC structurers discussed in this thesis are like this (ordered from most negative to least negative curvature): H_{II}>Im3m>Ia3d>Pn3m>L_α. However, not all amphiphile/water mixtures follow the universal progression of LC phases, displaying all of them upon increased hydration level. This can be exemplified by the glycerol monooleate-water system discussed in the next section.

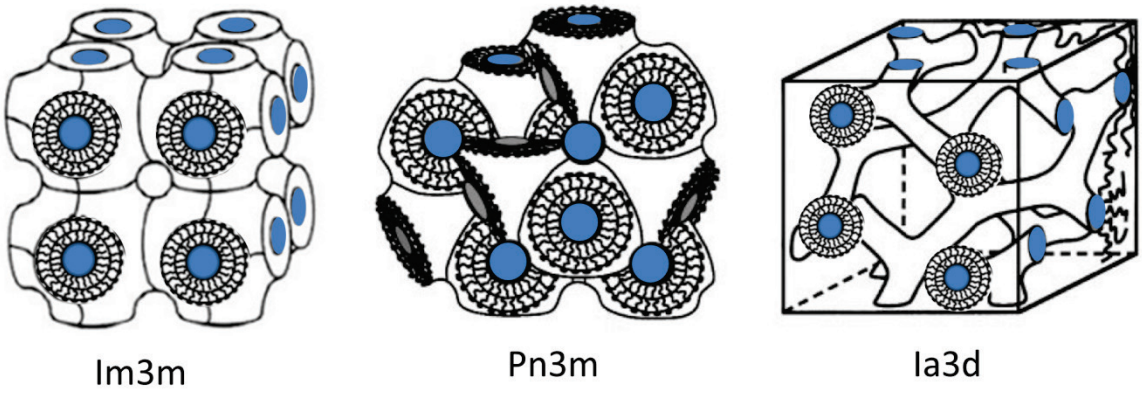

Figure 5. The three types of bicontinuous cubic phases; Im3m, Pn3m and Ia3d. The structurers are constituted of folded lipid bilayers with interwoven water channels.

1.5. Lipid-based liquid crystals in drug delivery

LC phases of polar lipids are of great interest for drug delivery purposes. This is due to their capability to encapsulate a broad range of drugs, ranging from hydrophobic to hydrophilic, as well as amphiphilic ones. In particular bicontinuous cubic phases have gained a lot of attraction since their discovery and structural determination decades ago [44-47]. One of the most extensively studied polar lipids in drug delivery is glycerol monooleate (GMO). GMO is known to have very rich phase behavior with water, making room for many interesting drug delivery opportunities [48]. Moreover, these systems are said to be biocompatible as well as degradable in the body [37, 49, 50]. The GMO molecular structure and phase diagram can be found in Figure 6. At low hydration levels, a lamellar phase is formed. Increasing the water content results in the formation of reversed bicontinuous cubic structurers, or reversed hexagonal at elevated temperatures. Due to the relatively small polar head group and double-bond in the hydrophobic tail, increasing the bulkiness, reversed LC structurers are formed. Addition of guest molecules to the GMO-water system can drastically change the phase behavior. Depending on the nature of the introduced guest molecules, e.g. the polarity and molecular structure, the molecules will be located at different positions in the structure [51]. For example, the addition of oleic acid increases the negative curvature and a reversed hexagonal phase is formed at room temperature [52]. Incorporation of hydrophilic (in the aqueous channels), hydrophobic (in the lipid bilayers) and amphiphilic (at the bilayer-water interface) drugs are possible [53]. It has been shown that the addition of lipophilic compounds to the GMO/water LC cubic system induces transition to a reversed hexagonal phase (increased negative curvature), while molecules having pronounced amphiphilic character can induce transition to a lamellar LC phase (decreased negative curvature) [37, 52, 54]. Release of drugs from LC phases depends both on the structure, as well as on the size and hydrophobicity of the encapsulated molecule. Drug release is generally faster from cubic phases, compared to hexagonal phases, due to the presence of large water channels open to the surrounding media [55]. Water channel diameter is typically 3-10 nm for a cubic phase and 1-3 nm in a hexagonal phase. AMPs comprising differences in amphiphilicity can be

prone to induce similar phase transitions when incorporated into such systems. Phase transitions have previously been reported for a variety of protein loaded LC systems [56-62].

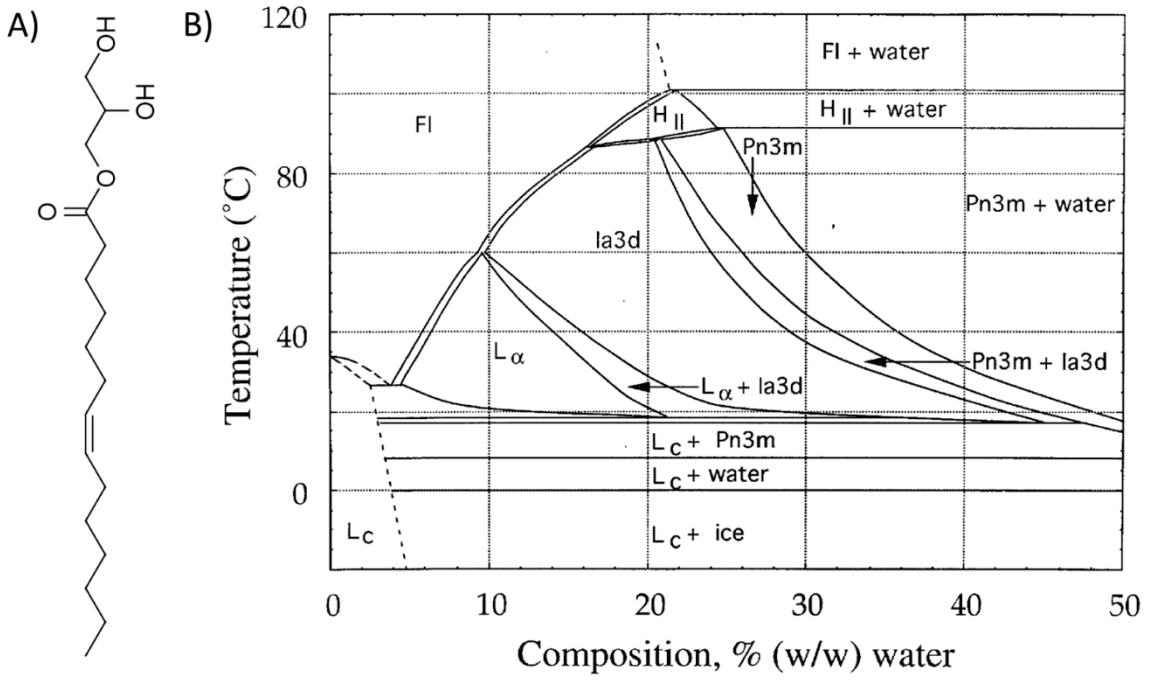

Figure 6. GMO molecular structure (A) and GMO-water phase diagram (B) displaying a rich variety of LC phases dependent on hydration level and temperature. The coexistence of the LC phase with water enables fragmentation of the bulk gel into LCNPs. The phase diagram is reprinted from [48], with permission from Elsevier.

1.6. Liquid crystalline nanoparticles

A practical drawback with LC phases formed of polar lipids is their high viscosity. This is particularly problematic for the rigid and sticky bicontinuous cubic phase, limiting possible the routes of administration [63, 64]. However, these issues can be overcome by the fact that some LC systems can coexist with excess of water (see Figure 6). This enables fragmentation of bulk LC gels into LC nanoparticles (LCNPs), in presence of a suitable stabilizer [65-67]. The most widely used stabilizer for LCNPs is the non-ionic triblock copolymer poly(ethylene oxide−poly(propylene oxide)−poly(ethylene oxide) (PEO_{100}-PPO_{65}-PEO_{100}). This stabilizer is commonly referred to as Poloxamer 407 or P407, but also by its tradenames, such as Lutrol F127 and Pluronic F127. Other stabilizers for LCNPs have also been investigated, for example polyethylene oxide (Myrj), pegylated phytanyl-copolymers, Polysorbate 80, colloidal clay platelets (Laponite), β-caseine and colloidal silica particles [68-74]. Not only GMO can be used to produce LCNPs. Other naturally occurring polar lipids or synthetically produced lipids can be used such as glycerol dioleate, diglycerol monooleate, soy phosphatidylcholine and phytantriol [75-80]. Phytantriol has the advantage of being more chemically stable, compared to glyceride-based lipids, due to the lack of ester bonds susceptible to cleavage by lipases and being hydrolyzed [81]. Dispersions of cubic, hexagonal

and lamellar LC phases as referred to as cubosomes, hexosomes and liposomes, respectively. By dispersing the LC, one can overcome the sticky and viscous nature of the LC gels, which can be advantageous from a drug delivery perspective. Polar peptides and proteins can be incorporated in LCNPs, potentially offering some degree of protection from chemical and proteolytic degradation [38, 63, 82-84], making them an interesting alternative for delivery of AMPs.

1.6.1. Preparation of liquid crystalline nanoparticles

LCNPs can be prepared by fragmentation of bulk LC gels using a combination of high shearing mixers and sonication [65] or high pressure homogenization using a microfluidizer [66]. Sonication of bulk LC gel usually results in particles with small sizes (typically 100-200 nm in diameter) and with narrow particle size distribution. Another preparation method involves dilution of an isotropic mixture of lipid and ethanol with a solution of stabilizer, commonly referred to as "the hydrotrope method" [85]. The hydrotrope method is advantageous since it does not involve any high energy dispersion steps and avoids local heating of the sample, making it suitable for LCNPs loaded with sensitive drugs. Compared with sonicated or microfluidized-formed particles, hydrotrope-formed particles are usually larger in size (>200 nm) and characterized by a broader size distribution. However, all these preparation protocols have the drawback that they also produce a large fraction of vesicles in addition to the desired LCNPs, usually cubosomes or hexosomes. This has been confirmed by cryo-TEM imaging of the particle dispersions. By fine tuning the preparation protocols (sample composition and processing temperature) the fraction of vesicles can be reduced [86]. Another way to reduce the number of vesicles is to heat treat the sonicated or microfluidized dispersions in an autoclave [87]. This treatment has several advantages, namely: i) reducing the number of small vesicles, ii) narrowing down the overall particle size distribution and iii) the sterilizing of the final particle dispersion such that it is suitable for pharmaceutical use. Heat-treatment of LCNPs close to the cloud-point of the stabilizer P407 (>100 °C) is known to reduce the fraction of vesicles due to diminished solubility and stabilizing efficacy of the polymer, resulting in vesicle fusion, hence narrowing the particle size distribution [87-89]. An illustration of the different LCNP preparation techniques and a summary of their advantages/disadvantages are presented in Figure 7 and Table 2, respectively.

Table 2. Summary of the different attributes associated with the different preparation protocols of LCNPs.

Preparation method	Advantages	Disadvantages	Drug loading procedure
Sonication or microfluidization	• Small particles • Narrow particle size distribution	• Local heating during fragmentation • Non sterile sample	Pre-loading (or post-loading)
Sonication or microfluidization followed by heat-treatment or sterilization	• Sterile material • Narrow particle size distribution • Reduction of vesicles	• Not suitable for heat sensitive drugs • Drugs can induce phase separation of particles during heat-treatment	Pre-loading (non-heat sensitive drugs) Post-loading (heat sensitive drugs)
Hydrotrope	• No expensive dispersion equipment needed • Low energy consumption	• Sensitive to processing geometry and mixing rate • Usually larger particle size • Non sterile sample	During dilution of isotropic lipid/ethanol mixture

Drug loading into LCNPs is typically performed by adding the drugs either to the molten lipid phase (lipophilic drugs) or to the water phase (hydrophilic drugs) during the preparation of the LC gel, prior dispersion into nanoparticles. This procedure will hereafter be referred to as "pre-loading". However, peptide and protein drugs are often sensitive to high temperature, which may be induced by high shearing rates during fragmentation or during sterilization of the formulations. Hence, the number of preparation techniques for producing drug-loaded LCNPs with a high degree of uniformity is limited for these types of actives. A second formulation strategy is to allow water soluble drugs to adsorb onto the surface of pre-formed heat-treated LCNPs by means of electrostatic and/or hydrophobic interactions, hereafter referred to as "post-loading". LCNPs usually have a slightly negatively ζ-potential, sufficient to attract positively charged molecules, such as AMPs. A third way to load active substance into LCNPs is to mix them into the isotropic lipid/ethanol mixture, prior to the dilution and precipitation of particles in the hydrotrope method. Pre- and post-loading of AMPs are investigated in **Paper 1-3** and **5**, while LCNPs prepared via the hydrotrope method are part of **Paper 5**.

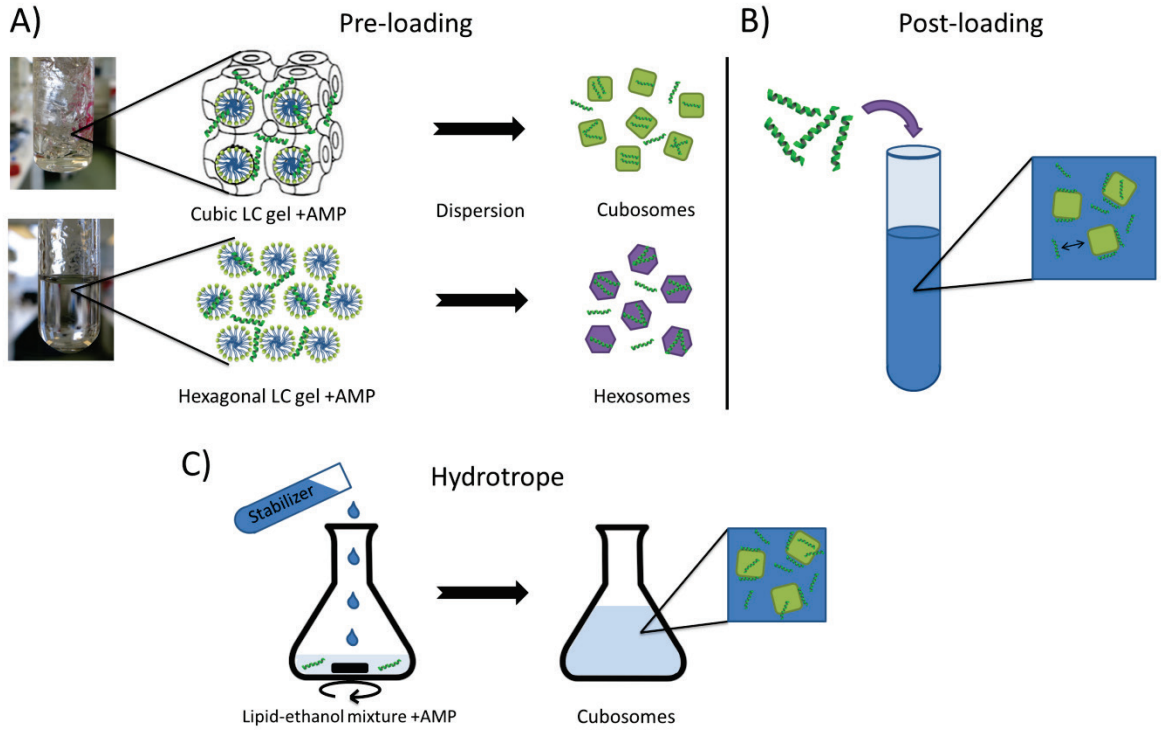

Figure 7. Illustration of the preparation of LCNPs and AMP loading strategies investigated in this thesis. Dispersion of LC gels pre-loaded with AMP (A), Post-loading of AMPs onto pre-formed cubosomes (B) and hydrotrope loading, where an isotropic mixture of lipid, ethanol and peptide is diluted until cubosome precipitation occurs (C).

1.6.2. Liquid crystalline nanoparticles as drug delivery vehicles

LCNPs have previously been investigated as carriers for several peptides and proteins. Examples include insulin (pre-loading) [90], ovalbumin (pre-loading and hydrotrope-loading) [91-93], somatostatin (post-loading) [94], cyclosporine A (pre-loading) [95, 96] and protein vaccines (hydrotrope-loading) [91]. These studies report encouraging results in terms of observed blood glucose levels (insulin, *in vivo*, rat), sustained release properties (ovalbumin, *in vitro* and *in vivo*, rat), increased half-life time (somatostatin, *in vivo*, rat), increased peptide skin penetration (cyclosporine A, *in vivo*, mice) and high entrapment and sustained release properties (protein vaccines, *in vitro*). Lipid based colloidal systems have been shown to effectively deliver and transport drugs to and through the skin as they can help keep skin lipids fluid [97-99]. LCNPs have been shown to enhance the skin penetration and delivery of several active substances, such as peptides, vitamins, herbal extracts, vaccine adjuvants and anti-inflammatory drugs with no observed skin irritation [93, 100-102]. Powder formulations are usually advantageous for other routes of administration, e.g. pulmonary. A LCNP forming powder could impel for pulmonary administration that may be more difficult to achieve with the LCNP dispersions, and result in a longer shelf-life of the formulation. Few studies have investigated powder formulations that form LCNPs upon re-hydration. A protective matrix, e.g. starch, celluloses or sugars, is necessary to add to these formulations to prevent particle aggregation and to protect the sample from collapse, due to osmotic pressure and stress induced by the freezing and drying procedures [103]. Spray-drying, freeze-drying and spray-freeze drying of LCNP dispersions or precursor mixtures are the techniques that have been investigated previously to produce powders of LCNPs [104-109]. LCNPs intended for the topical delivery of LL-37 is discussed in **Paper 5** and LCNP-forming powders for delivery of AP114 in **Paper 3**.

Based on their reported sustained release properties and ability to protect drugs from proteolytic degradation, LCNPs are interesting as drug delivery vehicles for a variety of sensitive peptides, including AMPs, through different routes of administration.

2. AIMS

The overall aim of this thesis is to investigate the use of cubosomes and hexosomes as drug delivery vehicles for the AMPs AP114, DPK-060 and LL-37. Different methodologies for preparing the LCNPs were evaluated, as illustrated in Figure 7. Phase behavior, antimicrobial effect and proteolytic protection of the AMP-loaded particles were studied. The antimicrobial effect before and after exposure to proteolytic enzymes was studied *in vitro* and *ex vivo*, in order to determine if the formulations could preserve, or even enhance, antimicrobial activity. The specific aims of the papers included in this thesis are:

Paper 1: To study how cubic and hexagonal LC gels are affected by AMP incorporation and to investigate the antimicrobial effect of AMP-loaded LCNPs.

Paper 2: To investigate the post-loading methodology of the AMPs onto cubosomes. Association of the AMP with the cubosomes was monitored by different experimental techniques and the antibacterial properties and effect after exposure to proteolytic enzymes were studied.

Paper 3: To evaluate whether LCNP forming powders can be made by freeze-drying, using disaccharides as a protective matrix for the delivery of AP114.

Paper 4: To study how LL-37 loaded cubosomes interact with bacteria and bacterial mimicking lipid bilayers in order to gain insight regarding the mode of action, as illustrated in Figure 8 below.

Paper 5: To study the suitability of LL-37 loaded cubosomes for topical administration to treat bacterial infections.

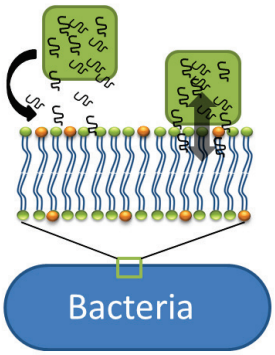

Figure 8. Do peptides need to be released from the cubosome in order to give rise to a bactericidal effect, or does the antimicrobial unit consist of the AMP-loaded cubosome itself?

3. EXPERIMENTAL

3.1. Preparation of liquid crystalline gels

LC gels were prepared by mixing either molten GMO or a GMO/OA-mixture at 45-50 °C with a water solution with or without AMP, resulting in LC gels containing 0, 0.5, 1.0 and 1.5 weight (wt) % peptide (if nothing else stated). The samples were mixed with a spatula, centrifuged at 3000 rotations per minute for 1 hour and allowed to equilibrate at room temperature for at least 1 week prior to further use. The lipid to water ratio was chosen to obtain the cubic Ia3d phase (70:30 GMO:water, wt % [48, 110]) or hexagonal phase (64:16:20 GMO:OA:water, wt % [52, 54]), in order to investigate the impact of the peptide on curvature. In **Paper 3**, where disaccharides (lactose, trehalose and sucrose) were investigated as protective matrices for LCNP forming powders. LC gels containing 2.5 and 5 wt % sugar were prepared. The gels had an overall composition of 68.25:29.25:2.5 GMO:water:sugar (wt %). Moreover, samples containing AP114 were prepared with an overall composition of 67.5:29.0:2.5:1.0 GMO:water:sugar:AP114 (wt %). GMO was obtained from two different manufacturers. RYLO MG 19 Pharma (Danisco A/S, Grindsted, Denmark) with a composition of minimum 95% monoglycerides, maximum 3% diglycerides, maximum 2% triglycerides and a fatty acid content of min. 88% oleoyl (C18:1) was used in **Papers 1** and **2**. Capmul-90 EP/NF (Abitec Corp., Columbus, USA) with a composition of 93.3 and 6.3% mono and di-glycerides, respectively, and a C18:1 (oleyl content) >95% was used in **Papers 3-5**. Super-refined oleic acid NF-LQ-(MH) (Croda, Inc., Snaith, U.K.) was used.

3.2. Preparation of liquid crystalline nanoparticles

Three different LCNP preparation methodologies were investigated and compared in the thesis, described below.

3.2.1. Pre-loading

Dispersions of the LC phases were made by fragmenting 0.5 g LC gel in 9.5 g acetic acid buffer (5 mM, pH 5.5) containing 0.5 or 1.0 % P407, using an Ultra-Turrax high shear mixer (IKA T25, Staufen, Germany) operated at 15000 rpm for 1-2 min. The coarse dispersion was ultra-sonicated using a Vibra-Cell VC 750 (Sonics and Materials Inc., Newton, USA) equipped with a 6 mm probe and operated at 40% of its maximum power in pulse mode (3 s on followed by 7 s off) for a total time of 5 min (cubic GMO dispersions) or 10 min (hexagonal GMO/OA dispersions). The samples were cooled with cold tap water during the sonication. The final particle concentration in these samples was approximately 50 mg/mL (5 w %) and the peptide concentration was 0.25, 0.5 or 0.75 mg/mL, corresponding to 0.5, 1.0 or 1.5 w % peptide in dispersed gels. Samples prepared by the pre-loading methodology were investigated in **Paper 1** and **3-5**.

3.2.2. Post-loading

Particles used for post-loading of AMP were prepared by dispersing a pre-formed cubic LC gel (GMO:water 70:30) in the same way as was done for the pre-loaded samples but without added peptide, followed by a heat-treatment cycle. The heat-treatment was done using a Laboklav 25 autoclave (SHP Steriltechnik AG, Schloss Detzel/Satuelle, Germany) at 121°C

for 20 min. Thereafter, samples containing 5, 10 or 50 mg/mL cubosomes with an AMP content of 0.10 mg/mL (for 5 and 10 mg/mL cubosomes, **Paper 2**) and 0.5, 1.5 and 3.0 mg/mL (for 50 mg/mL cubosomes, **Paper 5**) were prepared in 5 or 20 mM sodium acetate buffer (pH 5.5).

3.2.3. Hydrotrope

0.35 g molten GMO (45 °C) was mixed with 0.35 mL ethanol (99.5 %) to form an isotropic solution. Next, 300 µL of LL-37 dissolved in acetic acid buffer (20 mM, pH 5.5) was added dropwise to the GMO under magnetic stirring at 500 rpm, followed by the slow addition of 8.7 g buffer containing 0.5 % P407. Samples were prepared at LL-37 concentrations of 0.5, 1.5 or 3.0 mg/mL. The final concentration of particles (assuming 30 w % water in the final cubosomes) was 50 mg/mL. Cubosomes loaded with LL-37 were prepared using the hydrotrope methodology in **Paper 5**.

Preparation of LCNP forming powders

LC gels containing disaccharides were dispersed as for pre-loaded samples. More sugar was thereafter added to the dispersion, to reach a final dry weight of 80 % sugar in the formulation (lipid:sugar ratio 1:4). The dispersions were heat-treated in sealed septum flasks for 60 min in an oil bath kept at 100 °C. AP114 containing dispersions were not heat-treated to avoid thermal degradation of the peptide. Next, the disaccharide containing LCNPs were freeze-dried using an Epsilon 2-4 LSCplus (Martin Christ Gmbh, Germany) freeze dryer. The samples were first frozen at -40 °C for 2 h on the tempered plate inside the dryer at atmospheric pressure, followed by drying at 0.1 mbar (equivalent to -42°C ice sublimation temperature) and +4 °C for at least 18 h. Final drying of the samples was performed at 0.001 mbar at +20 °C for 4 h. LCNP forming powders were investigated in **Paper 3**.

3.3. Analytical methods

3.3.1. Dynamic light scattering

Dynamic light scattering (DLS) is a common tool to determine the hydrodynamic radius and size distribution of sub-µm particles in solution. A monochromatic laser beam is shined on the sample and the fluctuation in backscattered light is monitored as function of time. The fluctuations are due to the Brownian motion of the particles in the sample. When the intensity is correlated at several time points, the scattered intensity will remain similar at the beginning, but will differ at longer times due to differences in movement of particles of various sizes. This allows for determination of the diffusion constant, D, which is used to calculate the hydrodynamic radius (R_h) according to the Stoke-Einstein's relation, assuming spherical particles:

$$D = \frac{k_B T}{6\pi\eta R_h} \quad (1)$$

where k_B is the Bolzmann constant, T is the temperature and η the viscosity of the surrounding medium. In this work, DLS was used to measure the particle size and particle size distribution of the LCNPs. The particles were diluted to 1-2.5 mg/mL in water or buffer and analyzed in a Zetasizer Zen3600 instrument (Malvern Instruments Ltd., Worcestershire, U.K.) using

disposable plastic cuvettes. Refractive index was set to 1.47 and 1.33 for the LCNPs and water, respectively.

3.3.2. ζ-potential

The ζ-potential of the particles was determined indirectly by measuring electrophoretic mobility. When an electric field is applied across a dispersion, charged particles migrate toward the electrode of opposite charge. The speed of migration is proportional to the magnitude of the zeta potential. Samples were diluted to a particle concentration of 1-2.5 mg/ml and analyzed in disposable measuring cells at 25 °C. Measurements were made in a Zetasizer Zen3600 (Malvern Instruments Ltd., Worcestershire, U.K.). Each sample was measured in triplicate.

3.3.3. Small angle x-ray scattering

Small angle x-ray scattering (SAXS) is a powerful technique to determine average shape and size of colloidal structures in the 1-100 nm range. Almost any type of sample can be analyzed, such as liquids, solids, gases, gels etc. The thickness of the sample needs to be thin enough to ensure that part of the incident beam is transmitted through, and scattered by the material. The incident x-ray beam needs to be well-collimated (narrow and focused) and monochromatic (very precise wavelength, λ) in order to get high quality data. The intensity of the scattered beam is recorded exclusively at low scattering angles ($2\theta<10°$) onto a 2D detector. Materials having long range nanostructures, like LC phases, will give rise to specific patterns on the detector. The detector image is radially integrated into an intensity I versus scattering vector q plot. Plotting the intensity as function of scattering vector makes the recorded intensity profile independent of λ and eases comparison of data recorded with different x-ray sources. The scattering vector q is defined as:

$$q = \frac{4\pi}{\lambda}\sin(\theta) \qquad (2)$$

Different lattice planes separated by a distance d_{hkl} in the LC structures give rise to constructive interference on the detector, seen as peaks in the diffractogram. This is what we call "Bragg diffraction" and is described according to Bragg's law:

$$n\lambda = 2d_{hkl}\sin\theta, \qquad n = 1, 2, 3 \ldots \qquad (3)$$

The distance between the observed Bragg peaks in a diffractogram is like a fingerprint for the various LC structures. This means that the ratio between the q-values at the adjacent peaks follows a known pattern for different structurers. Combining equations 2 and 3 gives the relation between the spacing between the lattice planes and scattering vector:

$$q = \frac{2\pi \cdot n}{d_{hkl}} \qquad n = 1, 2, 3 \ldots \qquad (4)$$

For a lamellar phase, the lattice spacing is the same throughout the structure and is equal to the lattice constant, a. Hence, equation 4 is used to calculate the lattice parameter of a lamellar phase. For a hexagonal phase ordered in two dimensions (Miller indices h and k), the distances between all possible lattice planes are given by:

$$d_{h,k} = \frac{a\sqrt{3}}{2\sqrt{h^2 + k^2 + hk}} \qquad h, k = 0, 1, 2, 3 \ldots \qquad (5)$$

where a is the distance from the center of one rod to the center of a neighboring rod in the lattice. Again, combining with Bragg's equation (3) peaks are expected at q-values according to:

$$q = \frac{4\pi}{a\sqrt{3}} \sqrt{h^2 + k^2 + hk} \qquad h, k = 0, 1, 2, 3 \ldots \qquad (6)$$

For a cubic phase, all lattice planes are given by:

$$d_{h,k,l} = \frac{a}{\sqrt{h^2 + k^2 + hk}} \qquad h, k, l = 0, 1, 2, 3 \ldots \qquad (7)$$

where a is the lattice constant, i.e. the length of any side of the cubic unit cell. Bragg peaks are expected to appear at q-values:

$$q = \frac{2\pi}{a} \sqrt{h^2 + k^2 + hk} \qquad h, k, l = 0, 1, 2, 3 \ldots \qquad (8)$$

The absence of specific reflections from specific lattice planes makes it possible to discriminate between the different cubic phases. However, this requires that reflections from three lattice planes at minimum are present in the diffractograms. A summary of Bragg peak ratios for LC structurers of interest in this thesis are presented in Table 3. If the lattice parameter a, the length of the amphiphilic molecule l (1.8 nm for GMO) and the volume fraction of amphiphile $\theta_{\text{amphiphile}}$ is known, it is possible to calculate the dimension of the aqueous domains in the LC phases. Mathematical expressions are presented in Table 3.

Table 3. Peak spacing ratios used for detection of different LC phases and mathematical approximations of the dimension of the aqueous domains in the phases, adapted from reference [110].

LC structure	Crystallographic space group	Adjacent peak ratios	Water channel diameter *d* (nm)
Lamellar	-	1:2:3:4:5:…	$a(1\text{-}\theta_{\text{amphphile}})$
Hexagonal, (H_I, H_{II})	-	1:$\sqrt{3}$:2:$\sqrt{7}$:3:…	a-2l
Cubic	Im3m	$\sqrt{2}$: $\sqrt{4}$: $\sqrt{6}$: $\sqrt{8}$: $\sqrt{10}$: ...	2(0.305a-l)
Cubic	Pn3m	$\sqrt{2}$: $\sqrt{3}$: $\sqrt{4}$: $\sqrt{6}$: $\sqrt{8}$: ...	2(0.391a-l)
Cubic	Ia3d	$\sqrt{6}$: $\sqrt{8}$: $\sqrt{14}$: $\sqrt{16}$: $\sqrt{20}$: ...	2(0.248a-l)

In this thesis SAXS was used to identify LC phases in gels and of LCNPs. The lattice parameters were calculated from equations 4, 6 and 8 for lamellar, hexagonal and cubic phases, respectively. SAXS measurements discussed in **Papers 1** and **2** were recorded at the synchrotron beamline I911-SAXS (MAXIV Laboratory, former MAX-Lab, Lund Sweden). Most of the samples analyzed in **Paper 3** were run at the ID02 beamline at the European Synchrotron Radiation Facility (ESRF, Grenoble, France). Complementary measurements were performed using a Mat:Nordic laboratory SAXS instrument (SAXSLAB, Denmark). In **Paper 5**, measurements were carried out on a SAXSpoint 2.0 laboratory instrument (Anton

Paar, Graz, Austria). Liquid crystalline gels were mounted in a multiple sample holder made of steel and fitted between Kapton sheets (sample thickness approximately 1 mm), whereas liquid samples were loaded into quartz capillaries (ID 1.0 or 1.5 mm) mounted in a steel holder. Experimental details are found in the respective papers appended in this thesis.

3.3.4. Cryogenic transmission electron microscopy and tomography

In cryogenic electron microscopy (cryo-TEM), a very thin (<500 nm) aqueous film is vitrified and kept at liquid nitrogen temperature during imaging. Hence, imaging of biological matter such as proteins and colloids in a native hydrated state is achieved. In cryo-TEM an electron beam is accelerated over a high voltage and as the electron beam passes through the thin sample, a 2D projection is monitored on a detector/CCD-camera. The small difference in electron density between water and the studied material, usually the case for biological matter, sometimes makes it hard to acquire images of good contrast. The contrast is usually enhanced by using an under focus of 1-4 µm. The sample preparation is of great importance and is very sensitive to the surrounding temperature and humidity. Therefore, preparations of cryo specimens are done in a well-controlled climate chamber.

In this work, cryo-TEM was used to investigate the appearance of particles present in the LCNP dispersions, to verify DLS and SAXS data. In **Papers 1-3**, a droplet of the LCNP dispersion was placed onto a carbon-coated holey polymer film supported by a copper grid, gently blotted with a filter paper to form a thin liquid film and immediately plunged into liquid ethane at -180 °C. The sample grid was then kept at liquid nitrogen temperature and imaged using a Zeiss LIBRA-120 transmission electron microscope (Carl Zeiss, Oberkochen, Germany).

2D projections are sometimes not precise enough to determine the nanostructure of complex 3D structured samples. Instead, cryogenic electron tomography (Cryo-ET) may be used. In cryo-ET, the sample is tilted (usually from -60 to +60°) and images are acquired at 1-2 ° intervals. The series of images taken is then used to make a "back-projection" and reconstruction of a 3D tomogram, using suitable software. Tilt-series from more than one axis can be used to increase the resolution and precision of the reconstructed void. Cryo-ET was used in this thesis to study how LL-37 loaded cubosomes interacted with mini *Escherichia coli* bacteria (strain P678-54). Cubosomes were incubated with the minicells for 1 h, loaded on a grid and plunge frozen into liquid ethane, using a climate chamber (Vitrobot MARK IV, FEI, Eindhoven, Netherlands). Images were acquired at 4 µm under focus using a FEI Titan Krios electron microscope operating at 300 kV equipped with a Gatan K2 BioQuantum energy filter. Tomogram reconstruction was done with ETOMO software. For sample preparation details, see **Paper 4**.

3.3.5. Quantification of encapsulated antimicrobial peptide

Ultra-filtration was used to separate the LCNPs from the surrounding liquid, to enable quantification of the amount of peptide associated to or encapsulated by the particles. Samples were centrifuged for 30 min through Amicon Ultra filter devices (Ultracel-100K, Merck Millipore Ltd. Corc, Ireland) with a 100 kDa molecular weight cut-off (MWCO). The concentration of peptide in the filtrate was determined using ultra performance liquid

chromatography (UPLC) in **Paper 1**, high performance liquid chromatography (HPLC) in **Paper 2** or by a fluorescamine assay in a plate reader for **Paper 3**. The encapsulation efficacy could then be calculated, as a % of the total added peptide. Details about the liquid chromatography instrumentation and plate-reader measurements are found in **Papers 1**, **2** and **3** respectively.

3.3.6. Release of antimicrobial peptide

Release of AMP from the LCNPs was monitored by dialysis. 1 mL samples were placed in dialysis membranes with a 100 kDa MWCO (Float-A-Lyzer® G2, Spectrum Laboratories Inc., Rancho Dominques, USA) and placed in a buffer solution. A 200 µL sample was withdrawn from the receptor side after 0, 1, 2, 4, 6 and 24 h. The experiments were carried out at 22±1°C. The AMP release was quantified by a fluorescamine assay in a plate reader.

3.3.7. Quartz crystal microbalance with dissipation monitoring

Quartz crystal microbalance with dissipation monitoring (QCM-D) is a sensitive acoustic technique to study surface phenomena such as adsorption, desorption and reactions. Due to the piezoelectric properties of the quartz sensor, the crystal will oscillate if an alternating voltage is applied over the sensor. The resonance frequency, and frequency of overtones, of the sensor are monitored over time and change as material is adsorbed (or desorbed) onto the sensor surface. Water trapped in the adsorbed layers or between adsorbed particles will also oscillate and give rise to frequency shifts. Hence, the signal is a function of both adsorbates and coupled water. If a rigid film with very little coupled water is adsorbed on the sensor, the Sauerbrey relation can be used to calculate the mass (Δm) of the adhered layer giving rise to a frequency shift Δf [111]:

$$\Delta m = -\frac{C\Delta f}{n} \tag{9}$$

where C is 17.7 ng Hz^{-1} m^{-2} and n is the overtone number. It is also possible to calculate the thickness d of the adhered layer if the density ρ of the layer is known:

$$d = \Delta m/\rho \tag{10}$$

For a soft film that contains a substantial fraction of coupled water, the Sauerbrey relation becomes invalid. A soft viscoelastic film will dampen the oscillations of the sensor. The damping energy is called dissipation, D, and describes the viscoelastic properties of the film. The dissipation is determined from the time it takes for the oscillation to stop upon disconnection of the power. Hence, a soft film increases the dissipation. D is defined as:

$$D = \frac{E_{lost}}{2\pi E_{stored}} \tag{11}$$

where E_{lost} is the energy lost during one oscillation cycle and E_{stored} is the total energy stored in the oscillator.

QCM-D was used in **Paper 5** to study how LL-37 loaded cubosomes interact with a bacterial mimicking lipid bilayer. An E1 instrument (Q-Sense, Sweden) and silicon dioxide sensors were used for the experiments. Lipid bilayers were made by vesicle deposition. Tip-sonicated

liposomes were prepared from 1,2-dimyristoyl-*sn*-glycero-3-phosphocholine (hDMPC, C14:0) and 1,2-dimyristoyl-*sn*-glycero-3-phospho-(1'-rac-glycerol) sodium salt (hDMPG, C14:0) at a 75:25 mol % ratio. After recording a stable baseline in water (<1 Hz drift/10 min), a solution of 1 µg/mL poly-L-lysine was flowed over the sensor for 15 min to facilitate quick adsorption of negatively charged vesicles into a bilayer. Next, the cell was rinsed with water followed by flowing in liposomes at 0.1 mg/mL for 30 min. After recording a stable baseline in 5mM sodium acetate pH 5.5, the samples were flowed onto the bilayer (cubosomes 1.6 mg/mL loaded with LL-37 at µg/mL, cubosomes 1.6 mg/mL or LL-37 at 16 µg/mL). The samples were pumped in for a period of 1 h, followed by rinsing with buffer. The flowrate was 50 µL/min and the temperature was 37 °C. Experiments were performed at least in triplicate to ensure reproducibility.

3.3.8. Neutron reflectivity

Neutron reflectivity (NR) is a powerful tool to study phenomena at interfaces, providing quantitative structural and compositional information. A highly collimated beam of neutrons is pulsed onto a macroscopically flat surface and the intensity of the reflected beam is monitored as function of neutron wavelength. The reflected beam intensity carries information about the thickness and composition of layers perpendicular to the surface. The composition is related to the nuclear property scattering length density (SLD), which is analogous to the refractive index of light. The SLD depends on the molecular and isotopic compositions of the bulk materials and interfacial layers. By performing additional measurements with different isotopic composition of the solvent, one can model the data simultaneously in order to obtain a unique solution for the composition of the surface structure. Hence, multiple scattering profiles can be measured and fitted to a structural model of the interface. The models presented in this thesis are divided into layers perpendicular to the interface characterized by a thickness, an SLD and roughness and hydration parameters.

Neutron reflection measurements were carried out at the CRISP reflectometer [112, 113] at ISIS Neutron and Muon source (Rutherford Appleton Laboratory, Didcot, UK). Measurements were performed using custom made flow cells fitted with well-polished silicon (111) blocks of low surface roughness [114]. The sample cells were connected to an HPLC pump to enable switching between contrasts. The temperature was kept at 37°C during the experiments. Three incident angles of 0.33, 0.65 and 1.45° were used to cover the q-range of interest (0.01-0.3 $Å^{-1}$).

The bare silicon surfaces were characterized in two contrasts, H_2O and D_2O, to determine the surface roughness and thickness of the silicon dioxide layer. Next, freshly sonicated liposomes in water mixed with calcium chloride solution to a concentration of 0.2 mg/mL in 2 mM $CaCl_2$ and injected into the cell. The vesicles were of 1,2-dimyristoyl-d54-*sn*-glycero-3-phosphocholine (dDMPC, C14:0) and 1,2-dimyristoyl-d54-*sn*-glycero-3-[phospho-*rac*-(1-glycerol)] sodium salt (dDMPG, C14:0) dDPMC:dDMPG 75:25 mol %. Excess vesicles were removed after 20 min by rinsing with water and then buffer (5mM sodium acetate pH 5.5). The lipid bilayer was characterized in H_2O-buffer ("h-buffer", SLD $-0.56 \cdot 10^{-6}$ $Å^{-2}$), buffer with the same SLD as the silicon block (contrast matched silicon, "CmSi-buffer", buffer mixture resulting in SLD $2.07 \cdot 10^{-6}$ $Å^{-2}$) and D_2O-buffer ("d-buffer", SLD $6.34 \cdot 10^{-6}$ $Å^{-2}$).

Cubosomes loaded with LL-37, reference cubosomes and pure LL-37 were then introduced on bilayers in three different cells and allowed to equilibrate for 1 h. The cells were subsequently rinsed with h-buffer and the samples were characterized at the same three contrasts again. The reflectivity profiles were modelled using RasCAL [115] and Trikk software [116]. The models are discussed in more details in section **4.4**. An experimental resolution of 5 % (ΔQ/Q) was used to fit the data and was determined from experimental data. Experimental and modeled parameters are found in the *Supplementary information* to **Paper 4**.

3.3.9. Super resolution confocal fluorescent microscopy

Airyscan is a novel improvement of the resolution and signal-to-noise of a confocal microscope. Compared to a standard confocal microscope, the light is not blocked by a small pinhole in front of the detector. Instead, the whole Airy pattern is imaged onto a detector array consisting of 32 individual detector elements. Each detector acts like a very small pinhole. The signals from all detector elements can be calculated to their correct position, producing an image with 1.7 times better resolution than a standard confocal microscope.

Images of bacteria and cubosomes were acquired using a Zeiss LSM 880 Airyscan microscope (Carl Zeiss Microscopy GmbH, Jena, Germany) equipped with a 32-element GaAsP detector. The lipophilic fluorescent dye octadecyl rhodamine B (Molecular probes, Invitrogen Inc., Eugene, USA) was added to cubosomes (0.02 wt % of the GMO). 300 µL green fluorescent protein (GFP) expressing *Escherichia coli* (GFP-EC) suspension ($6 \cdot 10^6$ CFU/mL) was incubated for 1 h with i) cubosomes loaded with LL-37, ii) cubosomes, iii) LL-37 or buffer as reference. A few drops of each sample were placed in 35 mm glass bottomed Petri dishes (ibidi GmbH, Martinsried, Germany). Excess liquid was aspirated away and a 2% molten agar solution was poured over the samples to immobilize the bacteria. Samples were imaged using a 63x/NA1.4 oil objective (Zeiss) using the "Airyscan Fast" settings in super resolution mode. The settings resulted in pixel resolution of 0.04 µm in XY and z-stacks were acquired at 0.1 µm intervals using a piezo drive.

3.4. In vitro studies

3.4.1. Microorganisms

The bacteria used to study the antimicrobial efficacy of the LCNPs in this thesis were *Staphylococcus aureus* (SA), reference strain ATCC 25923 and 29213, methicillin-resistant *Staphylococcus aureus* (MRSA) clinical strain No. 0702E0196, *Pseudomonas aeruginosa* (PA), reference strain ATCC 27853, ATCC PA01 and clinical strain No. 0704C0134, *Escherichia coli* (EC), reference strain ATCC 25922 and ATCC 25922GFP (GFP-EC), and ESBL *E. coli*, clinical strain 9007550201, and *Acinetobacter baumannii (*AB*)*, AYE reference strain ATCC BAA-1710.

3.4.2. Minimum inhibitory concentration

Minimum inhibitory concentration (MIC) tests were used as a first screen of antimicrobial activity of the AMP-loaded LCNPs. The MIC value is defined as the lowest concentration of the test item that inhibits growth of planktonic bacteria, as detected by the unaided eye. In **Papers 1**, **2** and **3** serial two-fold dilutions of the tested AMP-loaded LCNP samples were

prepared in brain heart infusion broth (BHI) (BioMérieux, France) for AP114 containing samples or in 1% BHI in water (BHI_{100}) for DPK-060 and LL-37 containing samples. The density of the microorganism suspension was adjusted to approximately $3.3 \cdot 10^6$ CFU/mL (for SA) or to approximately $1.5 \cdot 10^7$ CFU/mL (for PA, EC, AB). An aliquot of 100 µL of the bacterial suspension was added to the wells of a sterile 96-well plate together with 100 µL of the tested sample. Positive controls containing only the medium and the bacterial suspension (growth control) and negative controls, containing the medium and the tested sample without the bacterial suspension (sterility control), were also prepared. The plates were incubated at 37°C for 24 hours. The MIC was defined as the lowest concentration of the sample that completely inhibited the growth of the bacteria.

3.4.3. Time-kill assay

A time-kill assay was used to evaluate the bactericidal properties of the AMP-loaded LCNPs as function of time. In this assay, the test item is mixed with a bacterial suspension and small aliquots are withdrawn during an incubation period. The withdrawn samples are subjected to serial dilutions and plated on agar plates. After incubation of the plates overnight, the bacterial concentration in the test item at different time points was determined as CFU/mL. Time-kill assays were performed in **Papers 1**, **2** and **3** as described below.

20 µL of the inoculum (prepared in BHI for AP114 containing samples or BHI_{100} for DPK-060 and LL-37 containing samples) was added to a test tube containing 1.98 mL of the tested sample diluted in BHI or BHI_{100}. The samples containing the tested LCNPs and controls were incubated at 37°C. At each sampling time of 0, 3, 6 and 24 h an amount of 100 µL was withdrawn from each tube. Serial 100-fold dilutions were prepared when necessary. A 100 µL aliquot of the diluted and/or undiluted sample was plated on agar plates. After incubation of the agar plates for 24 hours at 37 °C, the colonies were counted and the bacteria concentration was calculated.

3.4.4. Ex vivo pig skin wound infection model

The ability of LL-37 loaded cubosomes to reduce a topical bacterial infection was examined by an *ex vivo* pig skin model. The pig skin was obtained from a mixed breed of Yorkshire, Hampshire and Swedish pigham. The model has previously been proved to be suitable for testing of AMP containing samples [117-120]. Moreover, pig skin is generally considered as a good model for human skin [121].

Punch biopsies were made in the shaved and cleaned skin, approximately 0.5–1 mm deep and 3 mm in diameter. Each biopsy was infected by the addition of 100 µL of an SA bacteria suspension (10^7 CFU/mL) and incubated for two hours at 37 °C. 100 µL of the cubosome samples, pure LL-37 or BHI_{100} (negative control) was added to each wound and incubated for 4 hours at 37 °C. The bacteria were harvested by adding 500 µL of Kligman buffer followed by rubbing the wound area gently with a plastic loop. The suspension was transferred to a 5 mL tube with 1 mL 2X diluted Kligman buffer. The procedure was repeated once and the two fractions of bacteria suspension from the infected area were pooled. The bacteria suspension was diluted in 10-fold steps and seeded on horse blood agar plates. The plates were incubated

at 37 °C overnight followed by counting the colonies. Each sample was tested on five infected wounds.

3.4.5. Proteolytic protection and bactericidal effect after proteolysis

Proteolytic protection was investigated of the AMP-loaded LCNPs after incubation with the proteolytic enzymes *Pseudomonas aeruginosa* elastase (PE) or human neutrophil elastase (HNE) for 6 hours. Any peptide degradation was visualized by gel electrophoresis (Tris-Tricine sodium dodecyl sulfate polyacrylamide (SDS-PAGE) gels) using coomassie brilliant blue staining. A radial diffusion assay was performed on the formulations before and after incubation with elastases, using EC and SA bacteria, to evaluate bactericidal properties. The samples were placed in punched wells in an agarose gel containing bacteria. The antimicrobial activity of samples was visualized as a clear zone around each well after overnight incubation at 37 °C. Experimental details are found in **Papers 2** and **5**.

3.4.6. In vitro skin irritation

The skin irritating potential of LL-37 loaded cubosomes was investigated according to OECD TG 439 [122] using the In Vitro EpiDerm^{TM} Skin Irritation Test (EPI-200-SIT, MatTek In Vitro Life Science Laboratories, Bratislava, Slovakia) in **Paper 5**. The model contains human-derived epidermal keratinocytes, cultured to form a multilayered highly differentiated model of the human epidermis. It consists of organized basal, spinous and granular layers, and a multilayered stratum corneum containing intercellular lamellar lipid layers arranged in patterns analogous to those found *in vivo*. The test is supposed to be a stand-alone replacement for *in vivo* animal testing.

Test items, positive (5 % sodium dodecylsulfate (SDS)) and negative control (Dulbecco's phosphate-buffered saline (DPBS) without Ca^{2+} and Mg^{2+} were added to the skin models for 60 minutes, at which point in time they were rinsed with DPBS and allowed to recover in assay medium for 42 hours in the incubator. Then, methylthiazolyldiphenyl-tetrazolium bromide (MTT) solution was added to the skin models, followed by an additional 3 h incubation at 37±1 °C in 5±1% CO_2. MTT solution was removed, 2-propanol added and the plates were shaken rapidly for two hours. The individual skin models were homogenized and transferred to a 96-well plate for absorbance measurement at 570 nm followed by calculation of the viability of the keratinocyte cells, relative to the negative control. Skin irritation is predicted if the remaining relative cell viability is below 50 %.

4. RESULTS AND DISCUSSION

The following part discusses the main findings of the papers included in the thesis. The results presented and discussed in sections **4.1** and **4.2** predominantly originate from **Papers 1** and **2**. Data discussed in section **4.3** are from **Papers 2** and **5**, while the results presented and discussed in sections **4.4-4.6** are from **Papers 3**, **4 and 5**.

4.1. Influence of antimicrobial peptides on the phase behavior of liquid crystalline gels

The effect of incorporating the AMPs AP114, DPK-060 and LL-37 into cubic (GMO:water 70:30 wt %) and hexagonal (GMO:OA:water 16:4:80 wt %) LC gels was studied using synchrotron SAXS. Results showed that the AMPs affected the cubic LC gel in different ways. As can be seen in the diffractograms in Figure 9, the LC structure was kept for LL-37 (E), changed to another cubic symmetry in the case of DPK-060 (C) or gradually turned into a hexagonal phase when AP114 (A) was added. The LC structure of the hexagonal gels was unchanged upon incorporation of any of the AMPs at the studied concentrations. Thus, the hexagonal phase was found to be more robust upon peptide addition. The calculated lattice parameters for the LC phases can be found in **Paper 1**. The reference cubic gel (without any peptide) belonged to the Ia3d space group, with a lattice parameter of 141.3 Å, in good agreement with phase diagrams found in the literature for a GMO:water 70:30 gel [48, 110]. When the AP114 peptide (highest percentage of hydrophobic residues and lowest net charge among the tested AMPs) was added to the system, the structure gradually turned into the reversed hexagonal phase. Hence, AP114 is suggested to interact strongly with the hydrophobic parts of the GMO membranes, thus increasing negative curvature. Interestingly, the cubic Pn3m phase was detected at lower AP114 additions (0.25 and 0.5 wt %). This transition corresponds to a decrease in negative curvature. Transitions from Ia3d to Pn3m, and also further to H_{II}, have previously been observed for other lipophilic molecules or amphiphilic peptides incorporated into GMO-based LC phases [123].

Another factor to consider is the size of the water channels in the LC phases in relation to the size of the AMPs. The sizes of the peptides are approximately 2.7 nm for AP114 (1/2 unit cell consisting of 2 plectasin molecules [124]), 2 nm for DPK-060 (determined by DLS [120]) and 5 nm for the LL-37 in α-helical conformation [125]. The water channel diameter of the reference Ia3d cubic phase (for calculations, see Table 3) is approximately 3.4 nm. Hence, both AP114 and DPK-060 can theoretically fit into the aqueous channels of the cubic phase. In the case of AP114, this is still possible at low concentrations, where only the cubic Pn3m phase was detected (d=3.0 nm at 0.25 % AP114 loading). In this situation a strong interaction with the polar head groups of the GMO molecules in the water domain might explain the decrease in negative curvature, going from cubic Ia3s to Pn3m. At higher concentrations of AP114, more peptide seems to be located further into the hydrophobic parts of the GMO-bilayers, increasing negative curvature. Possibly this occurs because it is energetically beneficial for the system. The water channel diameter of the hexagonal phase at 1.5 w %

AP114 loading is 2.2 nm making it hard for the AP114 molecule to fit into the aqueous domains. This indicates that AP114 is actually taking part in the LC structure as an amphiphile, and not solely located in the hydrophilic or hydrophobic domains.

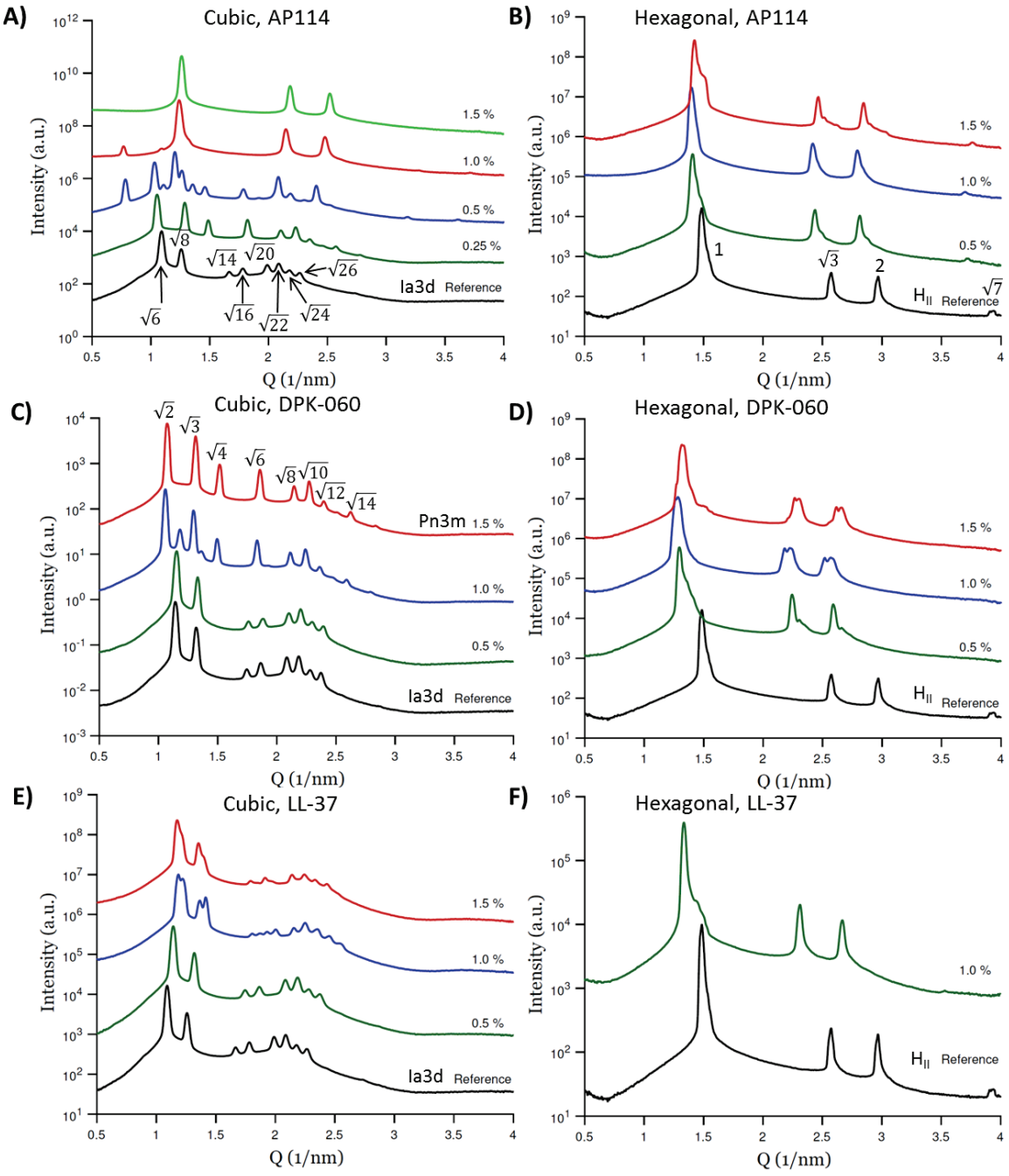

Figure 9. SAXS diffractograms of cubic GMO:water 70:30 wt % (A, C, and E) and hexagonal GMO:OA:water 64:16:20 wt % (B, D and F) LC gels containing AP114, DPK-060 and LL-37 at different concentrations (wt %). Representative peak spacing ratios for the cubic Ia3d (A), hexagonal (B) and cubic Pn3m (C) symmetries are indicated. Measurements were made at beamline I911-SAXS at MAX-Lab.

As seen for AP114 at low concentrations, DPK-060 changed the structure from cubic Ia3d to cubic Pn3m above 0.5 % peptide addition. This is probably a result of DPK-060 being the most hydrophilic and smallest peptide among the examined AMPs. It also carries the highest positive net charge. DPK-060 is believed to interact strongly with the hydrophilic head groups of GMO, resulting in a decreased negative curvature. DPK-060 with its approximately 2 nm size, when in a highly flexible random coil conformation is very likely to fit into the water channels of the cubic Ia3d structure. This may further explain the formation of a cubic phase with less negative curvature.

LL-37 did not affect the cubic Ia3d structure, indicating that the peptide is mostly located in the water domains of the structure or is penetrating the bilayer interfaces without significantly changing the curvature, at the concentrations studied here. LL-37 is usually present in equilibrium between monomers, dimers and trimers at the concentrations used in this thesis [126], making the interpretation a bit harder. Hence, a single 5 nm long LL-37 molecule can theoretically fit into the 3.4 nm water channels of the Ia3d phase, if oriented in parallel. If oriented perpendicularly, LL-37 does not fit into the water channels. However, at much higher LL-37 loadings (≥3 %), a transition from cubic Ia3d to a lamellar phase was observed (data presented in **Paper 5**) in line with data presented in other studies [127]. The transition from a predominantly random coil conformation to α-helical upon interaction with GMO-membranes may also affect the packing of molecules. Moreover, strong electrostatic interactions in combination with steric effects at higher concentrations at the polar head groups of GMO may also play a role in the decrease in negative curvature.

As mentioned earlier, the hexagonal gels kept their LC structure upon peptide addition. However, the lattice parameter for the H_2 phase without AMP (48.9 Å) was found to increase, represented by peak shifts to lower q-values upon peptide incorporation. The observed increase in lattice parameter indicates a swelling of the structure. The most hydrophobic peptide, AP114, showed the smallest increase in lattice parameter. The reason for this could be that the peptide is mostly located in the lipophilic parts of the structure, thus increasing the bulkiness and length of the hydrophobic tails, without changing the diameter of the water channels. This is further supported by the fact that the water channel diameter of the reference hexagonal gel is only 1.3 nm. Hence, it is unlikely that any of the three AMPs are only present in the water channels of the hexagonal phase. The greatest swelling was observed for DPK-060. Due to its high positive net charge and pronounced hydrophilicity, DPK-060 is likely most prone to interact with the polar head groups in the water domains of the hexagonal structure, thus swelling the cylinders diameters, resulting in an increased lattice parameter. Moreover, electrostatic repulsion between the positive charges of the AMPs may play a role in the increase in the lattice parameter.

4.2. Antimicrobial peptide-loaded liquid crystalline nanoparticles

The following section discusses the results obtained from the different types of LCNPs. Only cubosomes were selected to investigate in the post-loading approach. This was due to difficulties in retaining the hexagonal LC symmetry of the particles upon the heat-treatment of the hexagonal system, as revealed by SAXS (unpublished data). Moreover, the hexagonal LCNPs did not show any antimicrobial activity (section **4.2.2**) and were therefore excluded.

4.2.1. Physicochemical characterization

Three different peptide loading approaches were investigated for LCNPs in this thesis: pre-, post- and hydrotrope-loading, as previously illustrated in Figure 7 in section **1.6.1**. For the pre-loaded cubosomes and hexosomes, the AMPs were added into the LC gel before dispersion into nanoparticles by high-shear mixing followed by ultra-sonication. The cubosomes used for post-loading were prepared in the same way, but with no AMP incorporated in the LC gel from the start and with an additional heat-treatment cycle of the sonicated dispersion in an autoclave. This treatment is known to narrow the particle size distribution and to fuse smaller vesicles together into cubosomes or sometimes into larger vesicles. Typical particle size distributions for cubosomes prepared by pre-, post- and hydrotrope methods and for hexosomes prepared by pre-loading are presented in Figure 10 (particles did not contain any AMP). As can be seen from the figure, the pre-loaded cubosomes (green solid line) displayed the smallest mean particle size. Hexosomes (red solid line), prepared using the same methodology, were found to be larger with a slightly broader particle size distribution. The heat-treatment of cubosomes used for post-loading (dashed green line) resulted in particles larger than the pre-loaded cubosomes, but with a narrow size distribution, as expected from the literature [87]. A reduction in the number of small vesicles was observed after the heat-treatment, as was observed in the cryo-TEM images presented in Figure 14 A and I. The cubosomes prepared by the hydrotrope method (blue line) resulted in the largest particles with a broad particle size distribution as expected due to the low energy input during the preparation.

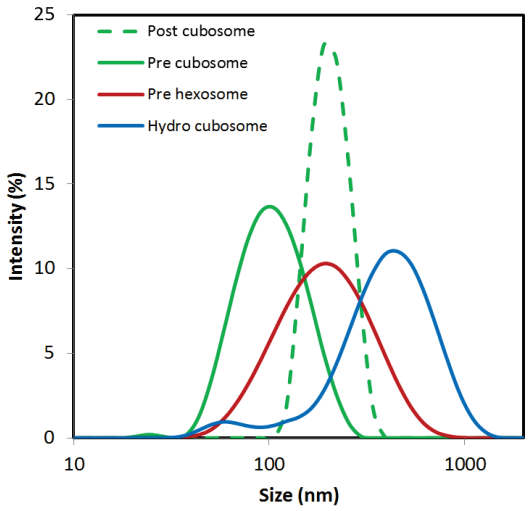

Figure 10. Comparison of particle size distributions obtained for cubosomes and hexosomes without any AMP, prepared by different methodologies.

The AMP-loaded cubosomes were characterized in terms of particle size, ζ-potential and peptide loading efficacy. Results for the pre-loaded cubosomes and hexosomes are illustrated in Figure 11. For the cubosomes, the mean particle size was in the range of 100-130 nm with a narrow particle size distribution (polydispersity index, PDI <0.160. The mean particle size for the hexosomes was in the range 140-170 nm and showed a slightly broader distribution (PDI <0.220). In general, pre-loaded cubosomes encapsulated less peptide (41-86%), compared to the hexosomes using the same methodology (>94%). SAXS measurements revealed that all pre-loaded cubosomes displayed presence of particles with cubic Im3m structure, see Figure 13. The only exception was at high AP114-loading where an H_{II} phase was also detected, in accordance with SAXS of the bulk LC gels. SAXS diffractograms for the pre-loaded cubosomes and hexosomes are presented in Figure 13. The size of the water channels in the Im3m phase is approximately 4.0 nm (a=12.5 nm), slightly larger than in the bulk Ia3d gel (3.4 nm). A swelling of the cubic structure upon dispersion is likely due to the equilibrium in excess water. The water pores in the hexagonal phase observed in AP114-containing cubosomes is 2.4 nm (a=6.0 nm) compared to 1.9 nm (a=5.5 nm) in the pre-loaded hexosomes. The observed differences in encapsulation efficacy between the cubic and hexagonal particles is in good agreement with the literature, showing that encapsulation and release is generally faster from cubic phases due to the presence of larger and open water channels [55]. The water channels in a reversed hexagonal phase are smaller and often said to be more closed to the surrounding medium, resulting in more efficient encapsulation of substances and slower release.

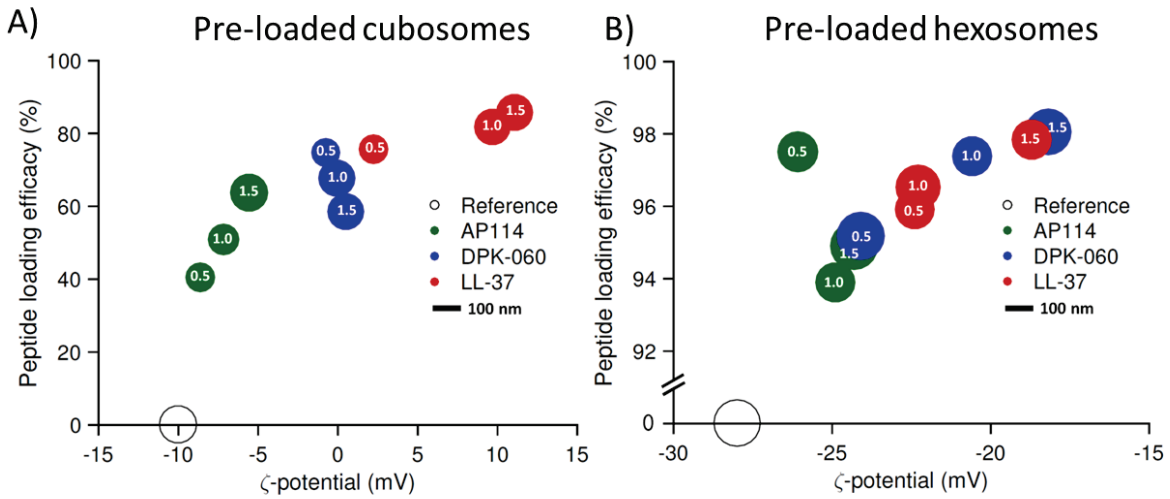

Figure 11. Peptide loading efficacy plotted as function of ζ-potential, for pre-loaded cubosomes (A) and hexosomes (B). The diameter of the bubbles is proportional to the mean particle size. The cubic reference equals 127 nm and the hexagonal 159 nm (unfilled circles). Numbers inside circles represent initial peptide loading (wt %) in dispersed gels. Samples were measured after dilution in MilliQ-water.

The ζ-potential for the pre-loaded references (no AMP) cubosomes and hexosomes were always negative and became less negative or positive upon peptide incorporation, indicating presence of the positively charged AMPs on the cubosome and hexosome surfaces. The hexosomes were found to have more negative ζ-potential, compared to the cubosomes, as a consequence of the presence of negatively charged oleic acid molecules at pH 5.5, just above

the pK_a ~4.8 [54]. The presence of negatively charged oleic acid may also play a role in the encapsulation of the AMPs in the hexosomes, since it facilitates for strong electrostatic interactions between the carrier and load.

Similar trends in peptide encapsulation efficacy and ζ-potential, as for pre-loaded cubosomes, were observed for post-loaded cubosomes. Data is presented in Figure 12. Again, the properties of the peptides (size, charge and hydrophobicity) strongly affected the association to the cubosome particles. Two concentrations of cubosomes were investigated, 5 and 10 mg/mL, with a fixed concentration of the AMPs, 0.10 mg/mL.

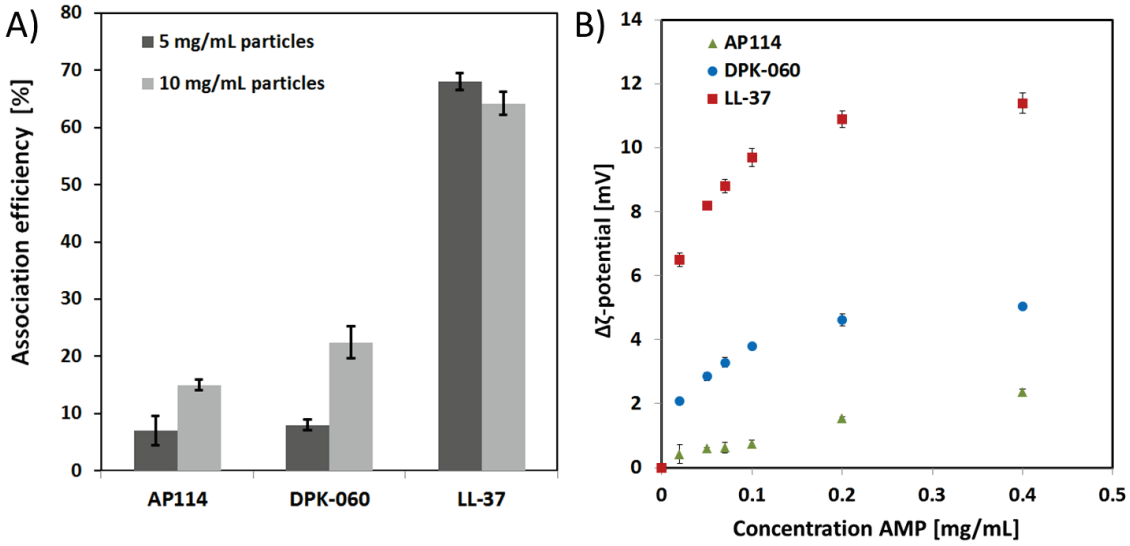

Figure 12. Peptide association efficacy for post-loaded cubosomes (A) and peptide association to cubosomes monitored as change in ζ-potential (B). Data indicates adsorption of peptides on the particle surfaces. Cubosome concentration was 1 mg/mL in the ζ-potential scan. The ζ-potential of the cubosomes without addition of peptide was – 1.5 mV in 5 mM sodium acetate buffer pH 5.5. Data is presented as mean values ± standard deviation (n=3).

The samples containing 5 mg/mL cubosomes showed only 7-8 % association of the peptides AP114 and DPK-060. If the concentration of cubosomes was increased from 5 to 10 mg/mL, the AMP association to the particles more than doubled. Interestingly, LL-37 with properties intermediate between AP114 and DPK-060 in terms of hydrophobicity and net charge, showed a much higher degree of association (>60 %) independent of the particle concentration. This indicates that the adsorbing/aggregating of LL-37 on the particles is independent of the available cubosome surface area. The properties of AP114 comprising the lowest positive net charge (+4.6), a large fraction hydrophobic residues (40%) and a high molecular weight (4.4 kDa), did not favor a strong association onto the cubosomes. The increase in cubosome-associated AP114 and DPK-060 upon doubling the particle concentration indicates a sensitive equilibrium between adsorbed and non-adsorbed peptide. One may believe that electrostatic interactions are the most important factor influencing peptide association to cubosomes. However this hypothesis does not hold in case of DPK-060 (net charge +8.5 at pH 5.5), which has the highest positive net charge among the studied AMPs, but still showed lower adsorption compared to LL-37 (net charge +6.3 at pH 5.5). The presence of positively charged AMPs on the cubosome outer surfaces was further indicated by

the increase in ζ-potential upon peptide addition, in line with data for pre-loaded cubosomes, see Figure 12 B. The ζ-potential was always slightly negative (in absolute values) at the lowest peptide concentrations and became increasingly positive at higher concentrations. LL-37 showed largest change in ζ-potential, in good agreement with the peptide association efficacy data, indicative of a high degree of association to the cubosomes. A strong association of LL-37 onto cubosomes was also indicated by the transition from a mainly random coil conformation to more α-helical upon interaction with the cubosomes, as revealed by circular dichroism measurements (for details see **Paper 2**). This observation is in good agreement with data reported previously, which also indicated an increase in α-helicity upon adsorption of LL-37 onto lipid membranes [29, 128]. It seems to be more energetically favorable for LL-37 to adopt α-helical conformation when adsorbed to the cubosomes, as opposed to random coil in the aqueous phase, driving the adsorption process. Peptide hydrophobicity, net charge, molecular weight as well as how they adsorbs onto the cubosomes are the most important factors in the association process. SAXS-data of the post-loaded cubosomes is found in Figure 13 G. No difference was observed upon peptide adsorption onto the cubosomes and the cubic Im3m structure remained. This indicates that the peptides do not penetrate into the particles, as locally high concentrations of e.g. AP114 have been shown to induce phase transitions. Particles loaded with LL-37 prepared by the hydrotrope method also showed the presence of a cubic Im3m phase, as revealed by SAXS (discussed in more detail in **Paper 5**).

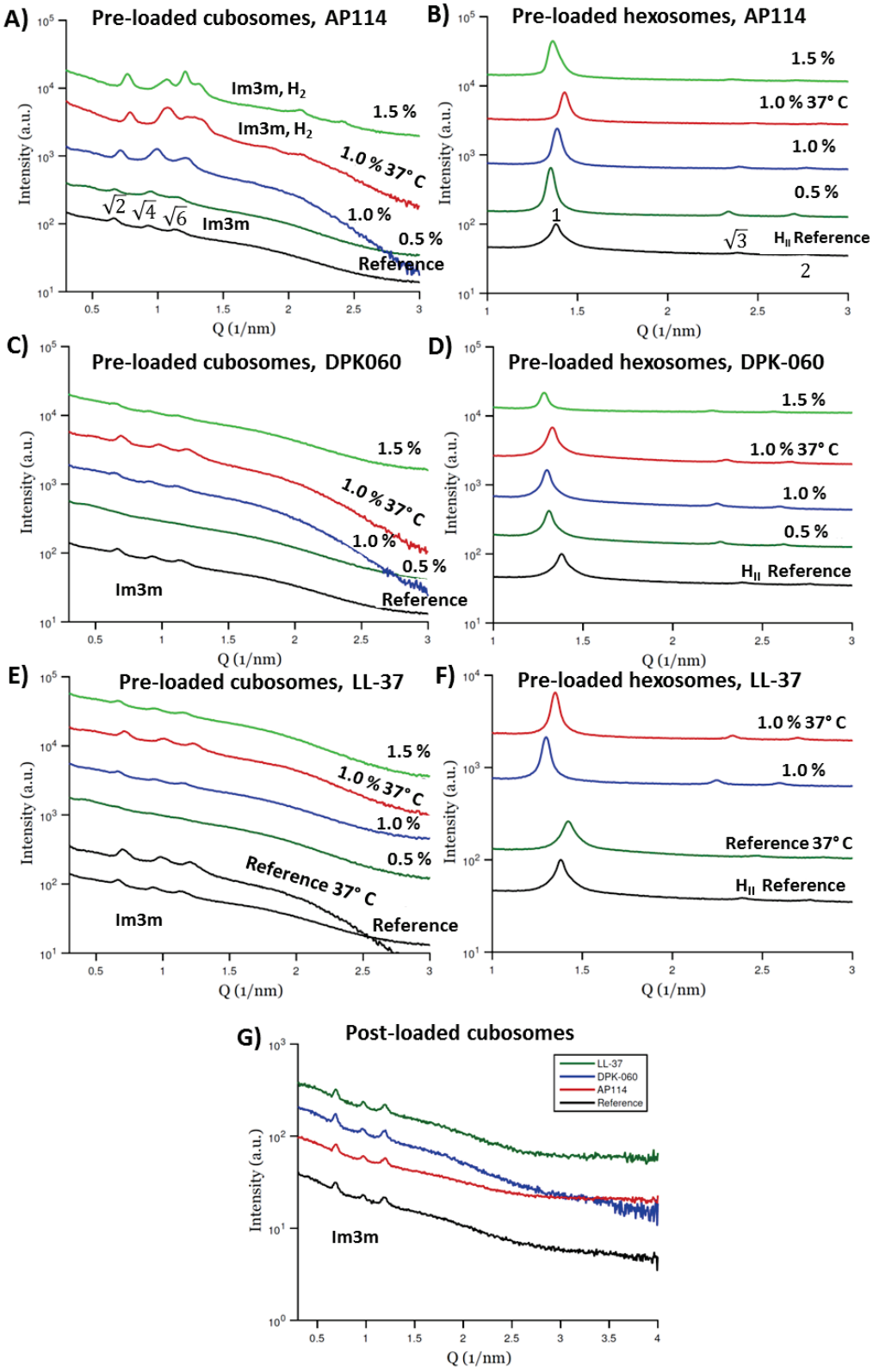

Figure 13. SAXS diffractograms of pre-loaded cubosomes and hexosomes (A-F) and post-loaded cubosomes (G). The peptide loading in % reflects the initial peptide content in the undispersed LC gel for the pre-loaded particles (A-F). The particle concentration was 50 mg/mL for pre-loaded samples and 10 mg/mL for post-loaded. Representative peak spacing ratios for the cubic Im3m (A) and hexagonal (B) symmetries are marked in the figure.

Cryo-TEM images of both pre-loaded cubic and hexagonal dispersions as well as post-loaded cubosomes, presented in Figure 14, indicate the presence of dense particles with internal structure, in agreement with the observed diffraction peaks revealed by SAXS. The cubosome particles did sometimes carry vesicular structures at their edges. The hexosome particles were found to be more round-shaped, with a blurred internal structure. This is probably because the hexosomes are not "single crystals". Instead, the particles are likely constituted of many domains of hexagonal structure, oriented in different directions. From Figure 14 A, the repeating distance in the cubosome particles was measured to be approximately 90-95 Å in the images, in good agreement with the calculated lattice spacing from the (110) reflection in the SAXS-data, calculated at 95.5 Å. Images of the post-loaded cubosomes (Figure 14 I-L) indicates a reduction in the fraction of small vesicles. Moreover the particles were found to be of more homogenous size, as suggested by the DLS measurements and by the literature [87]. This was expected since these particles were heat-treated, resulting in a more narrow size distribution. No apparent difference was observed between the cubosome with or without AMPs, in line with the SAXS-data, showing only the presence of the cubic Im3m phase.

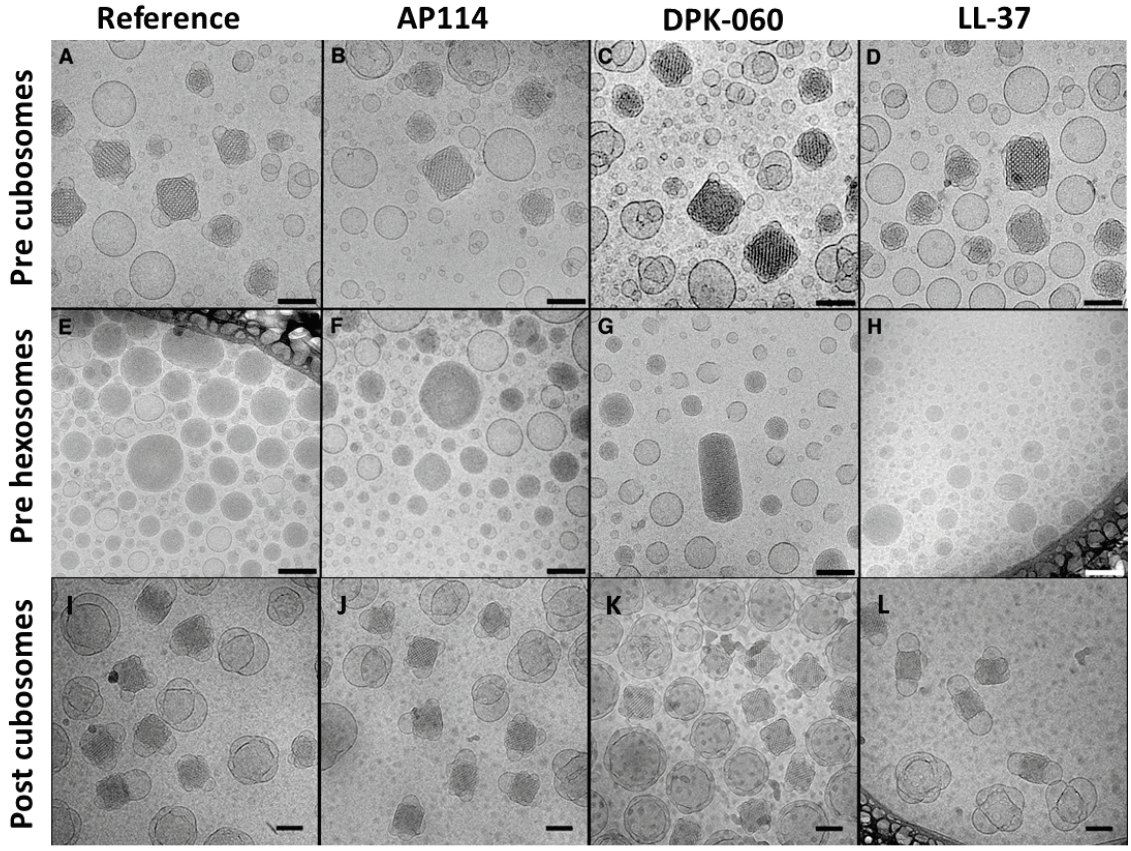

Figure 14. Cryo-TEM images of pre- and post-loaded LCNPs. Pre-loaded GMO-based cubosomes (A-D) and GMO/OA-based hexosomes (E-H) were loaded with 1 wt % AMP prior to dispersion, resulting in a final concentration of 500 µg/mL. Post-loaded cubosomes (I-L) contained 100 µg/mL AMP and the particle concentration was 10 mg/mL. Scale bars equal 100 nm.

The release of AMP from the cubosomes was monitored by dialysis in 5 mM sodium acetate buffer (post-loaded) or in 20 mM sodium acetate buffer (hydrotrope) at pH 5.5. Results are presented in Figure 15 and show that the release of AP114, DPK-060 and LL-37 from the

cubosome particles was drastically reduced at higher ionic strength. Moreover, when the ionic strength of the buffer was increased four-fold, in case of hydrotrope cubosomes (Figure 15 D), no release was observed. This indicates that the interaction between the AMPs and cubosomes are both electrostatic and hydrophobic in nature. These data are further discussed in the next section regarding the antimicrobial effect of the particles (section **4.2.2**). Release from pre-loaded cubosomes and hexosomes indicated that only the "free" non-encapsulated peptide was transferred across the dialysis membrane. This conclusion was drawn since the quantity of the released peptide (unpublished data) agreed perfectly with the amount of peptide not encapsulated by the particles, as quantified by UPLC (Figure 11 B). Hence, one may hypothesize that the peptides like to be part of the LC structures, and are not prone to diffuse or leak out from the LC particles over time.

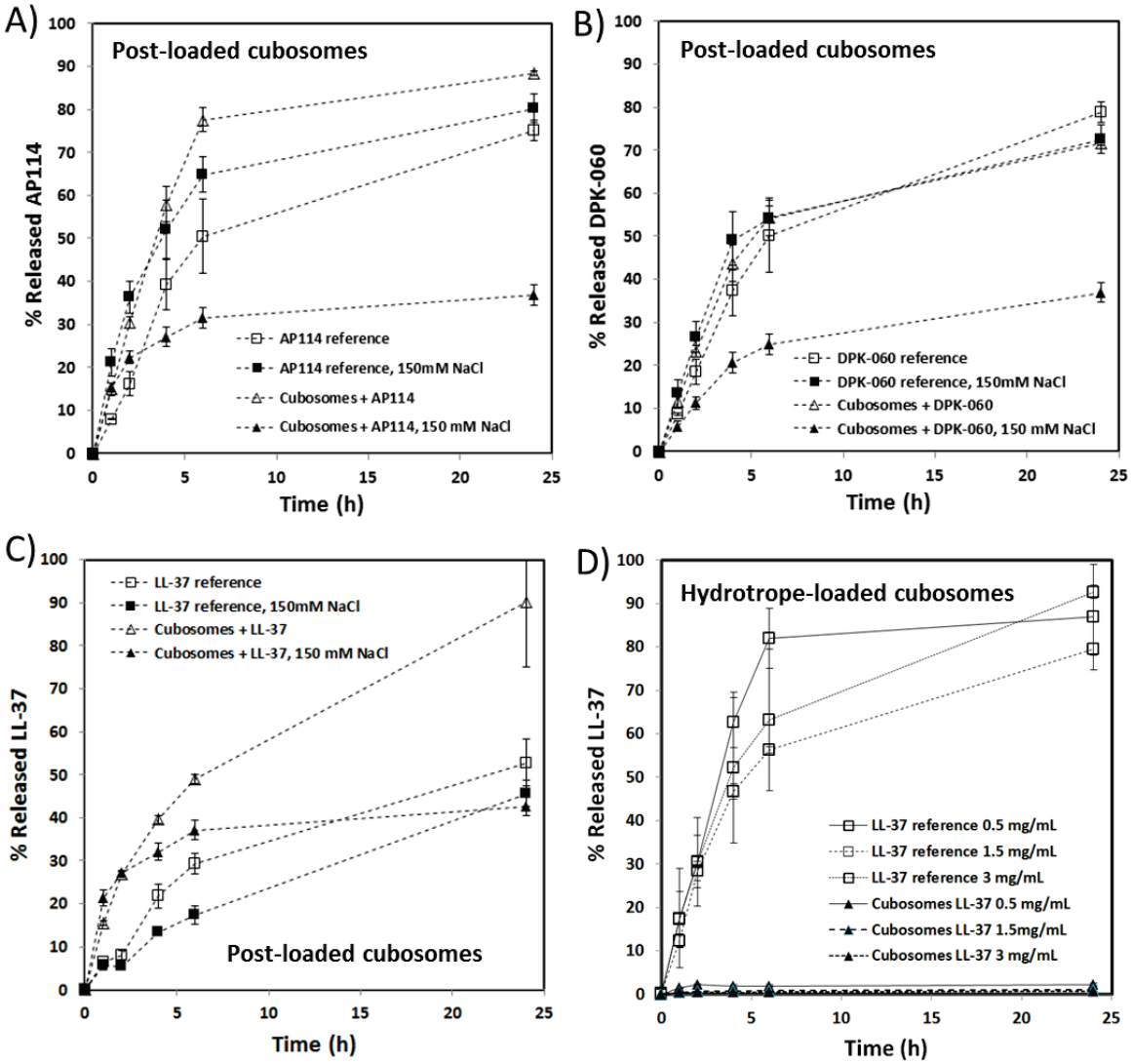

Figure 15. Release of AMP from cubosomes post-loaded with AP114 (A), DPK-060 (B) and LL-37 (C) and LL-37 loaded hydrotrope cubosomes (D). The release of AMPs from cubosomes was found to be slower at higher ionic strength. The release was measured in 5 mM sodium acetate buffer at pH 5.5 with or without 150 mM NaCl in A-C and in 20 mM sodium acetate buffer at pH 5.5 in D. Data is presented as mean ± standard deviation (n=2).

4.2.2. Antimicrobial effect

The first screening of the antimicrobial activity of peptide-loaded cubosomes and hexosomes was done by minimum inhibitory concentration (MIC) tests using 7 different bacterial strains. MIC data of pre- and post-loaded cubosomes are presented in Table 4. Pre-loaded hexosomes did not display any antimicrobial activity (MIC >16 μg/mL) for all tested strains, and were therefore excluded from the table. The reason for the reduced antimicrobial activity of hexosomes might be a combination of electrostatic and encapsulation effects. As can be seen in Figure 11 B, hexosomes displayed a more negative ζ-potential, compared to the cubosomes. If delivery of peptide and killing of bacteria is solely a result of particle-bacteria interaction, the more negatively charged hexosomes may interact less with the negatively charged bacterial membranes. The high encapsulation of AMPs in the hexosomes also seems to be non-beneficial for the killing efficiency. It might be the case that the AMPs are too strongly bound and stuck inside the hexosomes for good killing of bacteria. No apparent difference concerning the two different particle concentrations (i.e. 5 mg/mL and 10 mg/mL) was observed for the post-loaded cubosomes, and therefore only data for 10 mg/mL particles is shown here.

Table 4. MIC values for pure peptide (Ref) and for pre- and post-loaded cubosomes. Pre-loaded particles contained 500 μg/mL AMP and post-loaded 100 μg/mL before dilution. Samples containing AP114 were only tested against SA and MRSA, since the peptide is known to only kill gram-positive strains.

	MIC values (μg/mL)								
	AP114			**DPK-060**			**LL-37**		
	Ref	**Pre**	**Post**	**Ref**	**Pre**	**Post**	**Ref**	**Pre**	**Post**
S. aureus	8	8	8-16	4	2-4	1-2	8-16	>16	>16
MRSA	4	4	4	4	2-4	2	8-16	>16	>16
P. aeruginosa	-	-	-	8	16	8-16	8-16	>16	8-16
***P. aeruginosa* clinical strain**	-	-	-	16	8-16	8	8-16	8	8-16
E. coli	-	-	-	8	2-4	4	16	16	8-16
ESBL *E. coli* clinical strain	-	-	-	4-8	2-4	2-4	16	>16	≥16
A. Baumannii	-	-	-	4-8	16	16	16	>16	≥16

In general, AP114 and DPK-060 loaded cubosomes had similar antimicrobial effect compared to unformulated peptide. LL-37 containing samples showed a slight reduction in its usually broad spectrum activity, and were only active against gram-negative strains. The reason for this could be that the peptide needs to be delivered in different ways for different bacteria in order to adsorb sufficiently and penetrate the membrane. Interestingly, the activity of the pre- and post-loaded cubosomes was very similar in the MIC tests. This is somewhat striking, since the degree of encapsulated or cubosome-associated AMP usually differed (lower encapsulation of the post-loaded cubosomes). For example, pre-loaded cubosomes with DPK-060 with an encapsulation efficacy of over 60 % performed as well as post-loaded cubosomes, with an association of DPK-060 of only 22 %. Hence, one might have expected a lower activity for the pre-loaded cubosomes if only free peptide contributed to bactericidal activity, which was not the case. These findings indicate that the observed antimicrobial effect of the particles is not solely due to the free non-encapsulated peptide. Moreover, the LL-37 loaded cubosomes displayed a very high encapsulation efficacy (80 % for pre-loaded and 60 % for post-loaded), still showing good effect against gram-negative bacteria, such as EC. Therefore, these findings suggest that particle-bacteria interactions contribute to the bacterial killing.

This is further investigated in section **4.4.** None of the reference particles displayed any antimicrobial effect in the MIC tests.

The formulations with promising antimicrobial activity in the MIC tests were further investigated by time-kill assays. Data for pre- and post-loaded cubosomes on EC are presented in Figure 16. Interestingly, post-loaded cubosomes with DPK-060 appeared to be slightly more effective against EC (Figure 16 B) at 4 µg/mL, compared to pure DPK060 at the same concentration. Pre-loaded DPK-060 and LL-37 cubosomes displayed a preserved antimicrobial effect on EC (Figure 16 A and C). Similar bactericidal properties of LL-37 loaded in GMO-based cubosomes was recently confirmed by other research groups [127]. These findings further support the hypothesis that peptide-loaded cubosomes may be the antibacterial unit, and not only the "free" non-encapsulated peptide. Hence, release of AMP from the cubosomes is not a necessity in order to kill bacteria. The 1-2 dilutions lower MIC for DPK-060 pre-loaded cubosomes on EC could not be confirmed by the time-kill assay. Post-loaded LL-37 cubosomes displayed a preserved activity on EC at 16 µg/mL and performed better than pure peptide at 8 µg/mL. This moderate increase in activity may contribute to the unexpected antimicrobial activity of post-loaded reference cubosomes during the first 3 hours on EC (Figure 16 B and D). The reason for this effect remains unclear as it was not observed in the MIC test. However, the pre-loaded reference particles never exhibited any antimicrobial effect in the time-kill assays.

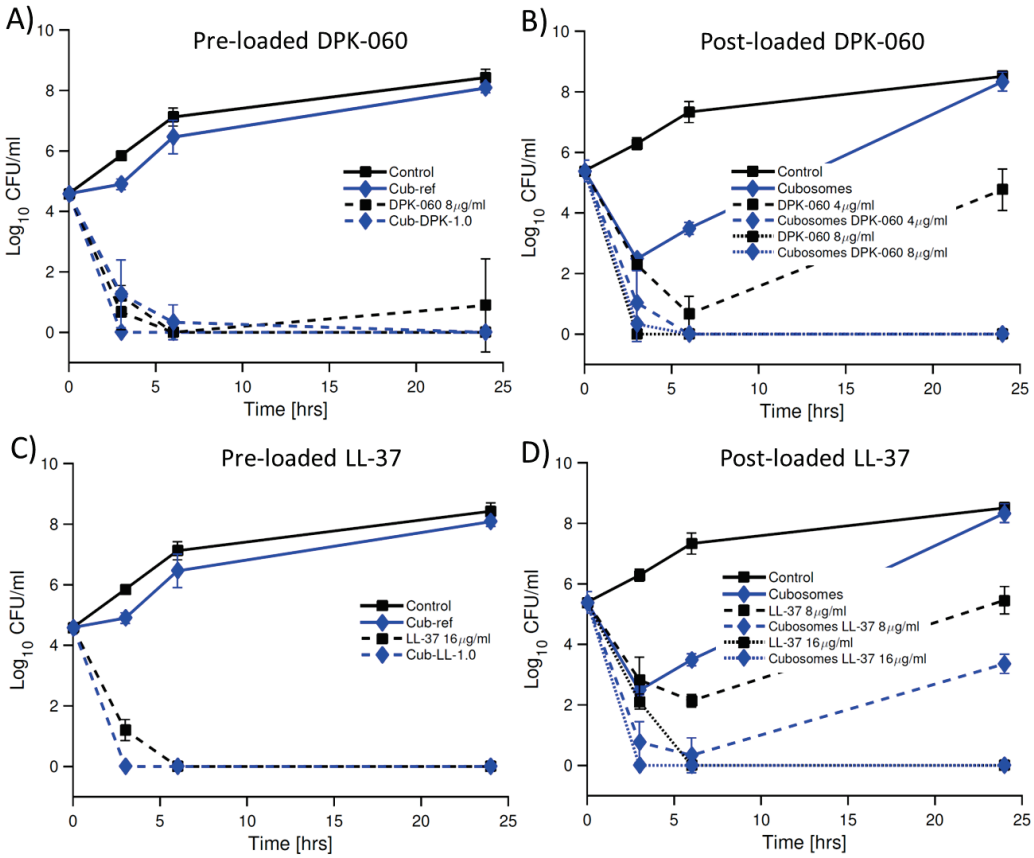

Figure 16. Time-kill curves for pre- and post-loaded cubosomes with peptides DPK-060 (A and B) and LL-37 (C and D) at selected AMP concentrations on *Escherichia coli*. Each data point is represented by mean ± standard deviation (n=3).

The release experiments can provide further insight to the *in vitro* antibacterial effect of the AMP loaded cubosomes. The BHI and BHI_{100} medium used for these *in vitro* studies contains roughly the same ionic strength as the 5 mM sodium acetate buffer, or with 150 mM NaCl, used in the release experiments (Figure 15). For a majority of the AMP loaded cubosomes, the bacterial killing reached its maximum after 6 hours incubation. If the release is as low in the BHI media for AP114 as in the buffer with 150 mM NaCl (only 30% released peptide after 24 hours), one would probably not expect such good antimicrobial effect, unless the peptide-loaded particle itself contributes to bacterial killing. The DPK-060 loaded cubosomes displayed a very similar release profile to reference peptide in the buffer without NaCl. Hence, one can expect very similar bacterial killing *in vitro*, which also was the case. The slightly synergistic effect observed for DPK-060 loaded cubosomes on SA and EC in the MIC-tests cannot fully be explained by the differences in the release profiles. Data suggest the slight increase in activity can instead be attributed to a particle-bacteria interaction.

4.3. Proteolytic protection of LL-37

One of the biggest obstacles with AMPs, such as LL-37, is their sensitivity to proteolysis in the presence of proteases at the site of infection. Therefore, the proteolytic stability of pure LL-37 and LL-37 loaded in cubosomes was investigated. This was done by exposing the samples to two relevant enzymes; *Pseudomonas aeruginosa* elastase (PE) and human neutrophil elastase (HNE). After incubation with the elastases the degradation of peptide was monitored by gel-electrophoresis. Data for pre-, post- and hydrotrope-loaded cubosomes with LL-37 are presented in Figure 17. AP114 and DPK-060 were not degraded by the elastases and are excluded from this discussion (data is presented in **Paper 2**).

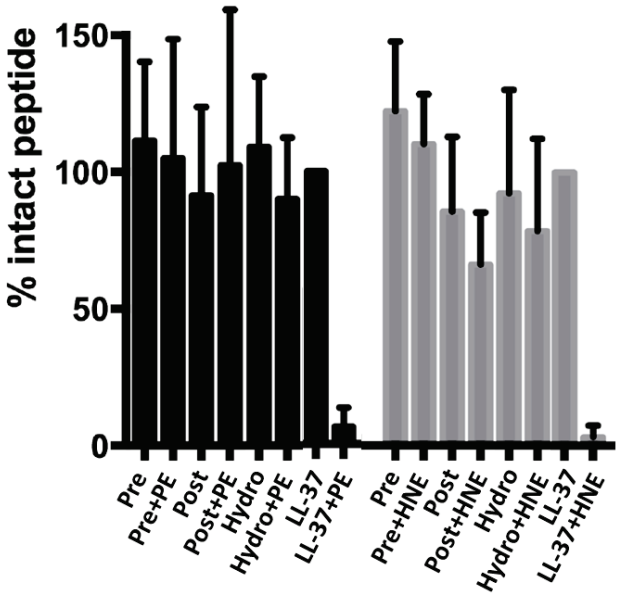

Figure 17. Proteolytic protection of LL-37 loaded in cubosomes. Samples were subjected to PE (black bars) or HNE (gray bars). Pure LL-37 was almost totally degraded by the elastases, whereas the cubosomes protected the peptide from degradation.

Pure LL-37 was found to be degraded by both PE and HNE, in line with data found in literature [129]. Interestingly, pre-, post- and hydrotrope-loaded cubosomes protected LL-37 from degradation by PE and HNE. Previously it was shown that the AMP melittin adsorbed onto lipid-disk particles was protected from the proteolytic attack of trypsin [130]. It was hypothesized that the polyethylene glycol (PEG) stabilizer located on the rim of the particles provided steric hindrance, thereby efficiently blocking peptide-enzyme interaction. The block copolymer PEO-PPO-PEO (P407) used as stabilizer for the cubosome particles, may protect LL-37 from enzymatic degradation in a similar way in case of the post-loaded cubosomes. Moreover, it has been shown that LL-37 is protected from proteolysis while adsorbed onto lipid membranes (liposomes) [126], in line with the data presented in this thesis. For the pre and hydrotrope-loaded cubosomes most of LL-37 is encapsulated within the interior of the particles, which is most likely the main reason for protection against enzymatic attacks.

A radial diffusion assay (RDA) was used to investigate the antibacterial effect of pre-, post-, and hydrotrope-loaded cubosomes before (controls) and after incubation with PE or HNE. Results for post-loaded cubosomes are presented in Figure 18 below.

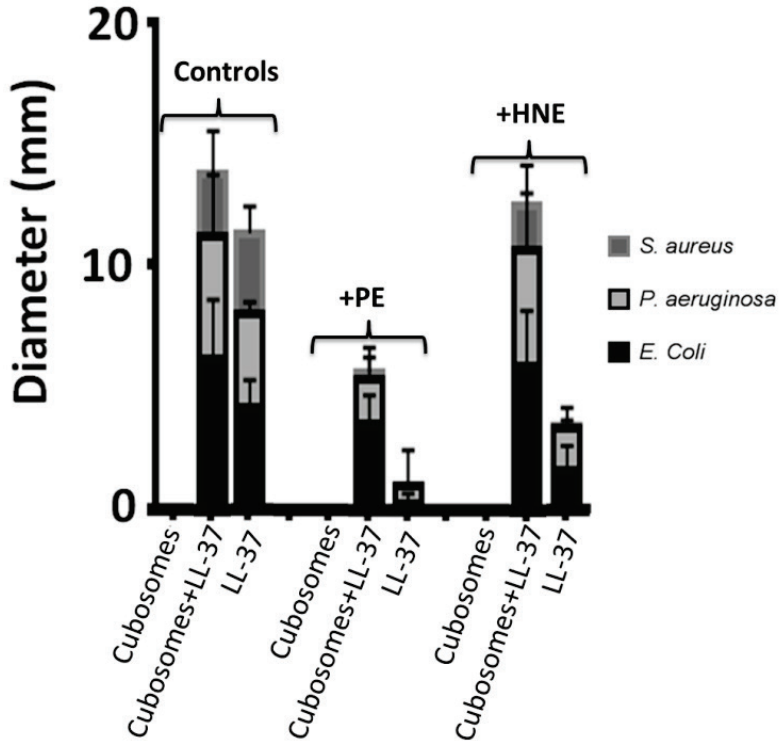

Figure 18. Bactericidal effect of post-loaded cubosomes before and after incubation with PE or HNE on SA, PA and EC, using RDA. Larger diameters correspond to more effective bacterial killing. Data is presented as mean + standard deviation (n=5 for EC, and n=4 for PA and SA).

It was found that the LL-37 loaded cubosomes killed SA, PA and EC before enzyme incubation. The good antimicrobial effect against SA was not observed previously in the MIC and time-kill assays. However, the MIC and time-kill assays were performed on planktonic bacteria, compared to the RDA, where the bacteria are fixated in an agarose gel. The variations in bacterial killing can be attributed to the differences in the *in vitro* methods. Interestingly, a significantly better bactericidal effect of the LL-37 loaded cubosomes was

observed after proteolysis compared to unformulated LL-37. These observations are in line with the proteolysis data, which indicated that cubosomes protect LL-37 from degradation by the enzymes. The same trend was observed for pre- and hydrotrope cubosomes loaded with LL-37 (data presented and discussed in **Paper 5**).

In summary, all three types of cubosomes protect the proteolytic sensitive peptide LL-37 from proteolysis, resulting in a significantly improved antibacterial effect after enzyme exposure, compared to pure LL-37.

4.4. Interaction of liquid crystalline nanoparticles with model and bacterial membranes

The understanding of the interaction of drugs and delivery vehicles with bacterial and cell membranes is of great interest in order to predict the mode of action [131, 132]. Hence, it is important to study how AMP-loaded cubosomes interact with bacteria and bacterial membranes, to identify the drug delivery mechanism. What is the antibacterial unit; is it the peptide alone, or is it the peptide-loaded cubosome?

QCM-D and NR are powerful techniques to study how drugs and nanoparticles interact with mammalian or bacterial mimicking lipid bilayers [133]. The interaction between mammalian mimicking bilayers and cubosomes has been studied previously [134, 135]. Results indicate that there is an interaction between the cubosomes and the lipid bilayers, consisting of dioleoyl phosphatidylcholine (DOPC), resulting in extensive material exchange between the cubosome and bilayer. It was shown that by modifying the composition of the cubosomes, for instance through the addition of the biologically active lipid palmitoyl phosphatidylserine (DPPS), the affinity to membranes was enhanced [136, 137].

In this thesis, the interactions between cubosomes loaded with LL-37 (pre-loading) and EC bacteria as well as with bacterial mimicking lipid bilayers were studied. The rationale for choosing these systems was the previously reported effective killing of EC, despite a large fraction of peptide beeing associated with the cubosome (data presented in section **4.2.1** and **4.2.2**). Therefore, it can be hypothesized that a cubosome-bacteria interaction exists that gives rise to the bacterial killing. Negatively charged bilayers consisting of mixtures of DMPC and DMPG were used and have been shown to be an appropriate model for bacterial membranes [138]. However, DMPC/DMPG bilayers are a very simplified model for gram-negative bacteria such as EC. The cell envelope of gram-negative bacteria consists of an inner and an outer membrane separated by a layer of proteoglycan [139]. Moreover, lipopolysaccharides (LPS) are attached to the outer membrane, all of which are also neglected by this model. Cubosome-bilayer interactions were studied using QCM-D. Data is presented in Figure 19. Bilayers were formed by vesicle deposition, displaying a Δf of approximately -25 Hz and ΔD close to zero. No spreading among overtones was observed, indicative of the formation of a thin and rigid adsorbed bilayer (data shown in *Supplementary information* to **Paper 4**) [140]. The Sauerbrey relation (see equation 9 in section **3.3.7**) gives an adsorbed mass of 4.4 mg/m^2 and a layer thickness of 4.9 nm, assuming a density of lipids of 0.9 g/cm^3. As the QCM-D

signal includes contributions from the water associated to the layer, these values are most likely slightly overestimated. Data shows that initially LL-37 loaded cubosomes quickly adsorbs onto lipid bilayer, as seen by the drastic decrease in frequency and increase in dissipation. The strong adsorption of cubosome particles on the surface occurs as interpreted from the large change in both Δf (-70 Hz) and ΔD ($45 \cdot 10^{-6}$). Moreover, the spreading of overtones and dissipation further indicate the highly viscoelastic nature of the adsorbed layer. Interestingly, cubosomes without LL-37 behaved differently. Only a small increase in both frequency and dissipation was observed, suggesting weak affinity of the cubosomes to the bilayer. This may be due to material loss from the bilayer, from transient adsorption of the cubosomes, resulting in a softer and more hydrated bilayer. LL-37 on its own did not cause any large changes in frequency, indicating no net loss or gain from the bilayer. However, the dissipation increased slightly over time, probably as a result of softening of the layer. The small changes in frequency and dissipation are in line with previous work, where LL-37 was exposed to DMPC/DMPG and phosphatidylcholine (PC) bilayers using QCM-D [33, 141]. The data does not indicate adsorption of LL-37 on top of the bilayer, as one would then expect the frequency to decrease as a consequence of peptide adsorption. Instead, it is more likely that it penetrates and/or aggregates into the bilayer and possibly forming pores, as suggested in the literature [142].

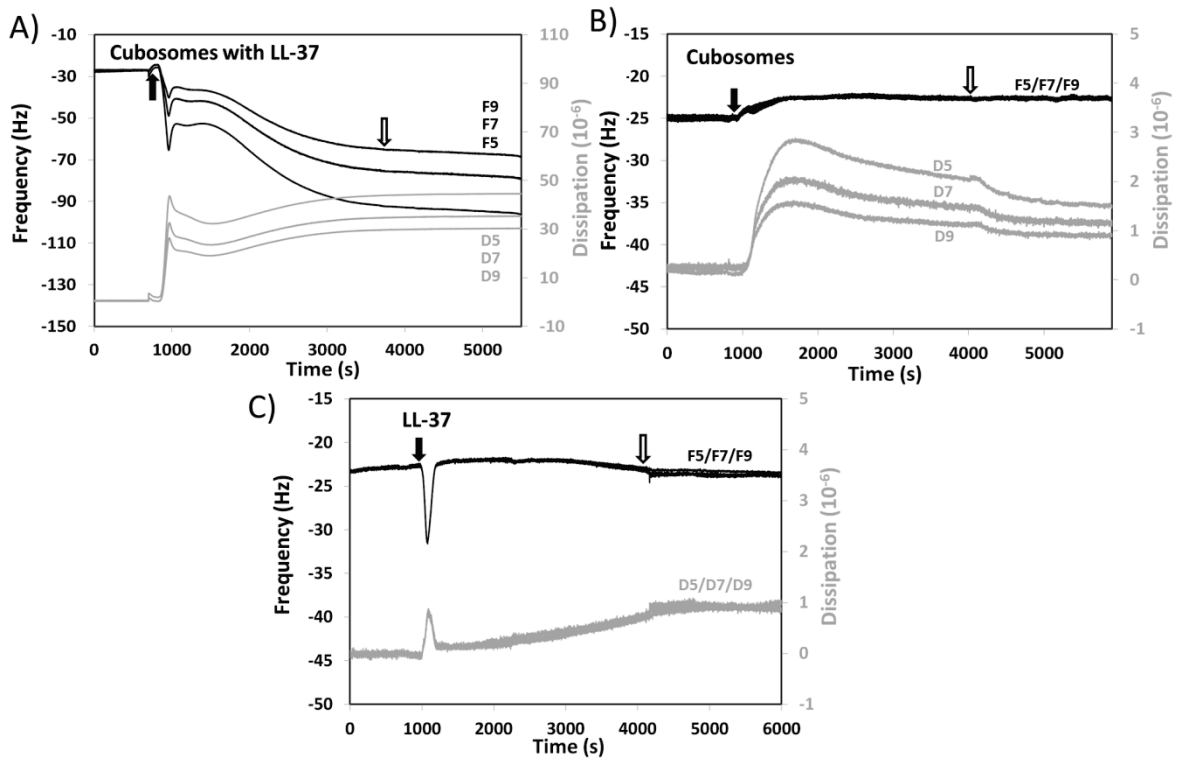

Figure 19. QCM-D data of supported DMPC:DMPG bilayers upon exposure to pre-loaded cubosomes with LL-37 (A), cubosomes without LL-37 (B) and LL-37 (C). The concentration of cubosomes and LL-37 was 1.6 mg/mL and 16 µg/mL, respectively. Data indicates a strong affinity of the LL-37 loaded cubosomes onto the bacterial mimicking bilayer. Addition of sample is indicated by filled arrow and rinse with buffer with unfilled arrow.

The features observed by QCM-D were further investigated by NR measurements. Reflectivity profiles recorded in three different isotropic contrasts (d-buffer, CmSi-buffer and h-buffer) and are presented in Figure 21. The NR experiments were designed to mimic the QCM-D experiments as far as possible, to allow the data to be compared. DMPC and DMPG lipids with deuterated tails were used to achieve a better contrast for neutrons of the tail region of the bilayer, compared to the hydrogenated LL-37 and cubosome adsorbates. A model of the bilayers was constructed, as illustrated in Figure 20. The best fits of the experimental data confirmed the presence of lipid bilayers of high coverage, 4.3 ± 0.1 mg/m^2 with a total thickness of 43.7 ± 1 Å, consisting of 8 Å from the polar head group and 27.7 Å from the tail region (average from data collected from 3 different experiments). Experimental and modeled parameters can be found in the *Supplementary information* to **Paper 4**. The bilayer model was further verified by calculation of the mean molecular area (MMA) to check the area occupied by both the heads and tails agrees. In the three bilayers an average MMA of 57 ± 1 Å^2 was obtained. This value is slightly lower than data found in literature for DMPC (59.9 Å^2) and DMPG (65.1 Å^2), predicting a MMA of 61.2 Å^2 for a 75:25 mixture [143, 144]. The adsorbed mass and thickness is slightly lower compared to the QCM-D data, as expected. The total coverage of the bilayers was >99 %, calculated from the hydration level predicted by the model of the tail region (always less than 1 % water). The total bilayer thickness is slightly lower than reported values for dDMPC:hDMPG 75:25 mol % vesicles, characterized by small angle neutron scattering (SANS), of 46.3 ±1Å [145]. However, the differences may be due to the differences in curvature, hydration and tilting of the bilayer.

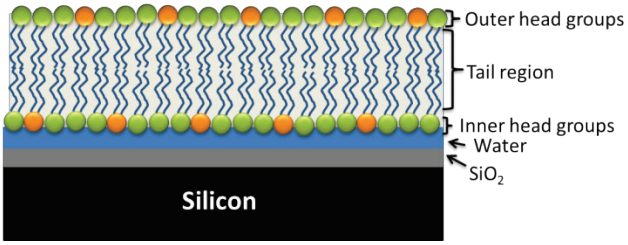

Figure 20. Schematic of the layers used in the models to fit the experimental NR data of the lipid bilayers. In case of when LL-37 was adsorbed, the tail region was split into an inner and outer leaflet. The zwitterionic DMPC is represented by green head groups and the negatively charged DMPG with orange head groups.

The best fit for the bilayer subjected to LL-37 was obtained when the tails were split into an inner and outer leaflet, as shown in Figure 21 C. A similar model was previously successfully used to model how the α-helical AMP aurein 1.2 interacted with bacterial mimicking bilayers [145]. The SLD of the inner and outer tail region was fitted by the software, where a lowering of the SLD suggest the insertion of hydrogenated material into the otherwise fully deuterated tail region. The inner tail leaflet and head groups remained unchanged, indicating no penetration of LL-37 to the inner leaflet of the bilayer. The best fit to experimental data was obtained when the SLD of the outer tail region was $4.23 \cdot 10^{-6}$ Å^{-2} and 24 % water in the layer. From the SLD of the outer tail region, the fraction LL-37 was calculated to be 57 %. Therefore there are only 16 % of the original deuterated lipids left in the outer leaflet of the bilayer. An SLD of 2.20 10^{-6} Å^{-2} for LL-37 and 6.89 10^{-6} Å^{-2} for the deuterated lipid tails was used for the calculation above. These findings are in line with the QCM-D data, indicating insertion of the peptide in the bilayer, and not adsorption on top of it. A model where LL-37

adsorbs on top of the bilayer was also tested. However, it gave poor fit of experimental data, also verifying the conclusion that the peptide must penetrate into the bilayer. The NR data indicates that the helix of the peptide is located in parallel to the surface ("lying"), in contrast to the QCM-D data indicating a similar change through the whole bilayer. If LL-37 was oriented perpendicular ("standing"), the inner leaflet of the bilayer should also have been affected, as the length of LL-37 is approximately 5 nm. Formation of barrel-stave defects within the bilayer is unlikely according to the NR data. However, the beginning of carpet or toroidal pore-like defects by LL-37 is supported. These findings are further supported by literature showing that the LL-37 α-helix is predominantly located parallel to bilayer surfaces, squeezed in between the polar head groups of the lipids [146, 147].

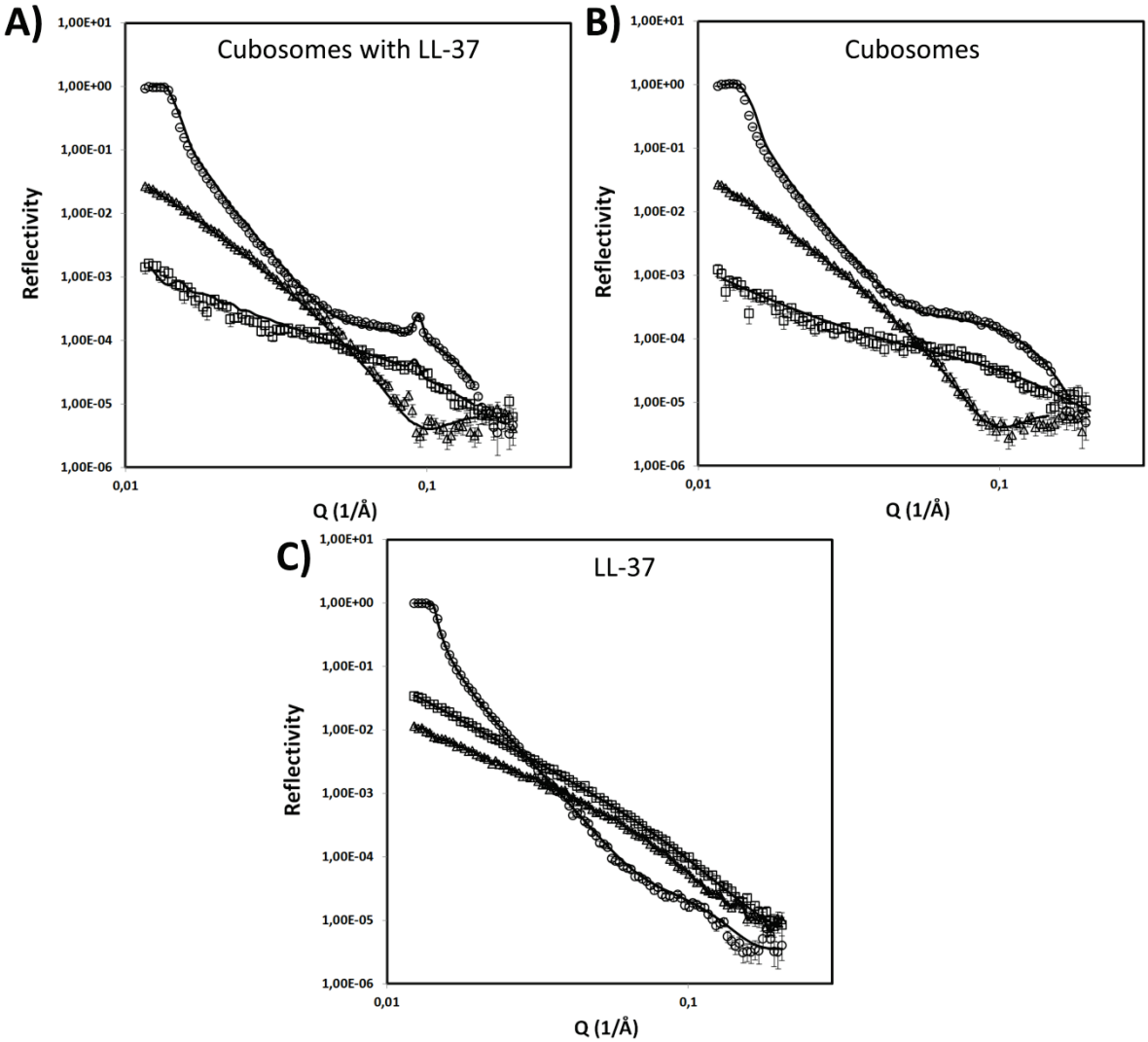

Figure 21. NR data after incubation of pre-loaded cubosomes with LL-37 (A), cubosomes (B) and LL-37 (C) on dDMPC:dDMPG bilayers. Experimental data were collected in three contrasts: d-buffer (circles), CmSi-buffer (squares) and h-buffer (triangles). Solid lines represent best fits.

The first approach used to model the bilayer subjected to cubosomes with LL-37 was to add another layer, consisting of GMO and water, to the top of the bilayer. However, this approach produced a bad fit to experimental data. A more sophisticated model was used, where the cubosome particles were modelled as repeating lamellar structures on top of the lipid bilayer.

This approach proved to be a simple and accurate way to fit the reflectivity profiles from cubosome particles adsorbed onto lipid bilayers [134, 135, 137]. The most striking feature of the reflectivity data for cubosomes loaded with LL-37 (Figure 21 A) is the presence of a Bragg diffraction peak at Q=0.095 $Å^{-1}$ in the d-buffer contrast. The peak indicates presence of a repeating structure in the direction perpendicular to the surface, i.e. the presence of cubosomes. Equation 4 (section **3.3.3**) was used to calculate the repeating distance giving rise to the reflection, 6.6 nm. This is very close to the $d_{(110)}$-reflection observed in SAXS-data. The cubosomes are of Pn3m structure with lattice parameter of ~8.9 nm, resulting in $d_{(110)}$=6.3 nm ($8.9/\sqrt{2}$). Bragg peaks were previously observed by other research groups performing similar experiments, usually located at slightly higher Q-values (~0.14 $Å^{-1}$) [134, 137]. The difference is likely because cubosomes with a different cubic structure (Im3m, a~14 nm) and lattice parameter were used in those experiments. The model giving best fit of the experimental data suggests the number of lamellar repeats to be 35 on top of the bilayer, resulting in a thickness of 214 nm. The calculation is based on the parameters giving the best fit, suggesting that 3.7 nm is occupied by a GMO bilayer separated by 2.4 nm water. The calculated size of the cubosomes is larger than the mean particle size of ~140 nm, as obtained from DLS. This may indicate that large cubosomes are more prone to adsorb, or that smaller cubosomes adsorbs on top of each other. Moreover, the fitted parameters indicate that the bilayer was strongly affected by the LL-37 loaded cubosomes. This is shown as changes in the thickness and SLD of the inner and outer head group and hydrophobic region, indicating presence of a more diffuse bilayer, as observed in the fitted experimental data. This further indicates a strong interaction of the LL-37-loaded cubosomes with the bacterial mimicking bilayer.

The overall shape of the reflectivity curves of the bilayer subjected to cubosomes without LL-37 (Figure 21 B) is very similar to that obtained for cubosomes with LL-37 sample (Figure 21 A). The most obvious difference is the lack of the Bragg peak in the former case. This indicates a slightly different interaction of the cubosomes with the bilayer, which may be due to less adsorption of the cubosomes to the bilayer or because they are localized further away from the bilayer surface. Since only the specular reflection was monitored in the experiments, only structures perpendicular to the surface are measured. Hence, if the repeating structures of the cubosomes are not oriented in parallel to the surface, they will not give rise to Bragg peaks. Therefore, it is not possible to get information from cubosomes randomly oriented and/or too far away from the surface. The reflectivity curves were fitted with a similar model as for the cubosomes with LL-37, with the difference being that the layers of repeating lamellar structure on top (cubosomes) were removed. Since the reflectivity is most sensitive to the layers adjacent to the surface, a curve with a similar overall shape but without the Bragg peak was obtained. As for the cubosomes with LL-37, the model suggests the presence of a compressed bilayer with less order, resulting in more diffuse head and tail-regions, as observed by changes in SLDs and thicknesses in the model.

Strong association of LL-37 loaded cubosomes with bacterial membranes was also observed using super resolution confocal microscopy. Representative images are presented in Figure 22. The fluorescently labeled cubosomes with LL-37 (in red) were frequently located around the EC bacteria, which was not the case for cubosomes without LL-37. Surprisingly, no cell lysis or clear membrane damage could be observed in any of the images. However, the resolution may be too low to visualize the membrane defects normally present in bacteria subjected to AMPs, imaged by scanning electron microscopy (images are presented in **Paper 2**).

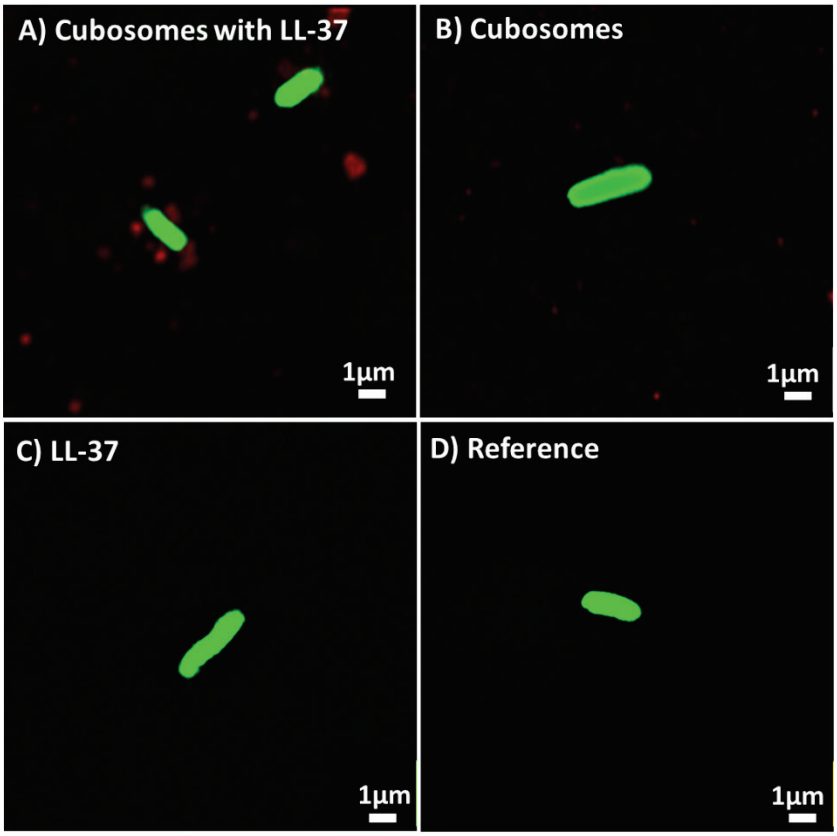

Figure 22. Super resolution confocal microscopy images of GFP producing EC bacteria (green) incubated with cubosomes containing the fluorescent dye octadecyl rhodamine B (red). Images indicate higher affinity of LL-37 loaded cubosomes to the bacteria (A), compared to cubosomes without LL-37 (B).

Cryo-ET was used to visualize the adsorption of cubosomes on bacterial membranes at higher resolution than confocal microscopy. Normally, the size of EC bacteria (~2-3 µm) is too large to fit into the vitrified films (<500 nm) used for cryo-TEM. Bacterial minicells have recently gained increasing interest because of their considerably smaller size, compared to normal bacteria. Minicells are produced by mutant bacteria and due to abnormal cell division, much smaller cells are disbudded [148]. Minicells are normally only 300-400 nm in size, thus more suited for cryo-TEM/ET imaging purposes. In this work, cubosomes were incubated together with mini-EC and plunge-frozen on a grid. A tilt-series of images were reconstructed via back-projection into 3D tomogram slices. Slices from a tomogram of LL-37 loaded cubosomes together with a mini EC cell are presented in Figure 23. The inner (IM) and outer membrane (OM) separated by a peptidoglycan layer of the EC can be seen in the images.

Direct contact and fusion of the cubosome particle with the outer bacterial membrane is observed (indicated by arrow). This indicates that it is possible for cubosomes loaded with LL-37 to merge together with the bacteria. Other membrane defects are also present, just to the right of the cubosome particle, induced by a small cubosome or vesicle. However, cubosomes not containing LL-37 were sometimes also found in direct contact with minicells (data not shown). Due to the very thin ice film in the middle of the grid, particles and minicells are prone to migrate and accumulate close to the edges of the holes. One can only speculate if adsorption of the cubosomes onto the minicells is a consequence of the vitrification procedure or because of physical attraction. However, a substantial fraction of the data presented in this section strongly indicates that adsorption is due to attractive forces between the LL-37 loaded cubosomes and bacteria. The transmembrane potential of bacteria is typically -130 to -150 mV [22]. Hence, there should be an attractive electrostatic force between the cubosomes which have a positive ζ-potential (see Figure 11) when loaded with LL-37.

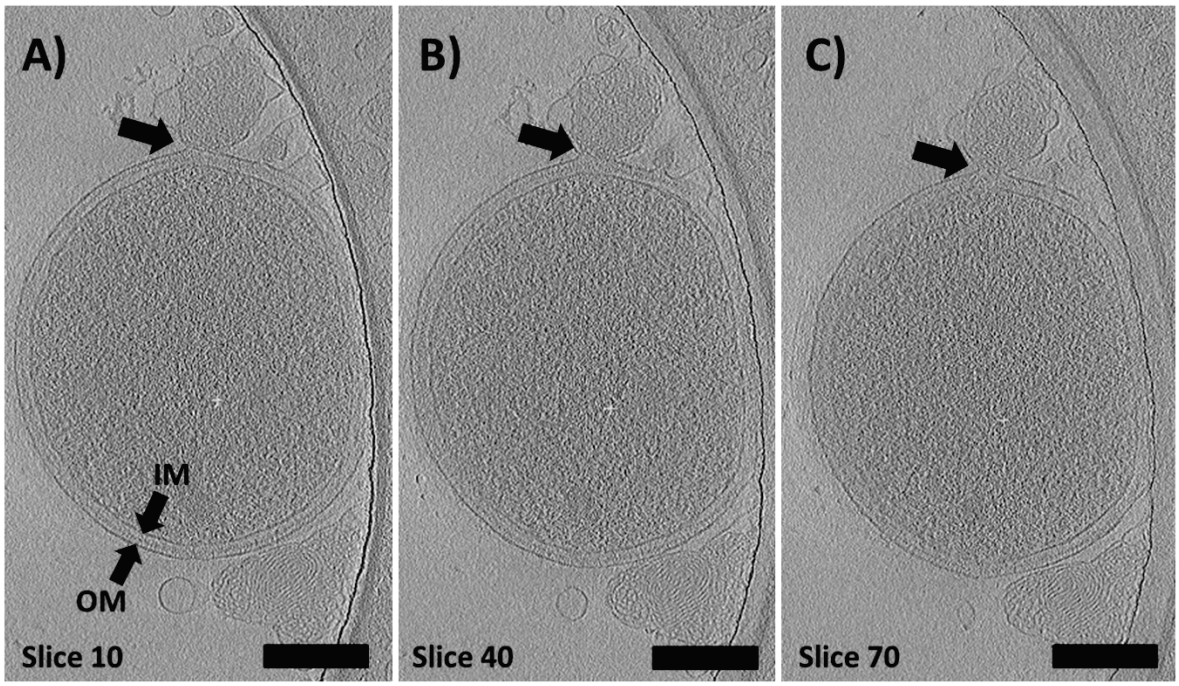

Figure 23. Slices extracted from a tomogram showing fusion of a cubosome particle loaded with LL-37 with the outer membrane (OM) of a mini EC cell, indicated by arrow. IM=inner membrane. Scale-bars equal 200 nm.

The data presented in this section provide evidence that the affinity for a cubosome to adsorb onto bacterial or bacterial mimicking bilayers can be increased by the incorporation of LL-37. By doing so, bacterial killing seems to be a result of direct contact between the cubosome particle and outer membrane of the bacteria. These findings are in good agreement with the previously discussed in vitro studies, presented in section **4.2.2**, also indicating that it is the LL-37 loaded cubosome that is the antimicrobial unit.

4.5. Liquid crystalline nanoparticles forming powders

A powder formulation that forms LCNPs upon hydration can be advantageous to access new routes of administration e.g. pulmonary. Moreover, under certain circumstances the shelf-life of sensitive active substances can be prolonged by the use of dry formulations. This is of particularly great interest for biological drugs, such as peptides and proteins that may be susceptible to hydrolysis and deamidation. In this thesis, the use of three disaccharides; lactose, trehalose and sucrose were investigated as protective matrices for GMO-based powders produced by freeze-drying. Sugars, especially disaccharides, have been shown to serve as effective lyo-protectants for biological membranes [149-151]. The role of disaccharides is to form a vitrified matrix around the lipids and to replace the water in the dry state around the hydrophilic head groups [152]. Disaccharides are usually better than monosaccharides in stabilizing lipid membranes, due to their higher glass transition temperature, resulting in better solid state properties of the dry powders such as improved flowability. A sugar with too low glass transition temperature can result in a powder with stickier properties, especially if subjected to moisture, acting like a plasticizer. The formation of a glassy state of the sugar is important for the effective stabilization of lipid membranes [153]. Hence, they may also be suitable as stabilizers for non-lamellar liquid crystalline (LC) structures such as cubic and hexagonal phases. The sizes of disaccharides are small compared to the water channels in the cubic and hexagonal LC phases, thus facilitating penetration into and stabilization of the structurers.

Bulk LC gels (GMO:water 70:30 wt %) were prepared at two concentrations (2.5 and 5 wt %) of the disaccharides in order to study how the sugars influence the phase behavior. Results show that addition of the disaccharides induced a phase transition from the cubic Ia3d to a mixture of cubic Pn3m and reversed hexagonal phase, as can be seen in the SAXS diffractograms in Figure 24 A. Peaks originating from the hexagonal phase became more prominent as the sugar content increased. Therefore, it was decided to continue investigations with the lower sugar content (2.5 wt %) to maintain as large a fraction of cubic phase as possible. This was due to the previous investigations showing that AMP-loaded hexosomes have reduced antimicrobial activity compared to cubosomes. These observed changes in LC structures are in line with phase diagrams present in literature for the GMO/water/sucrose and GMO/water/trehalose mixtures, also showing formation of a hexagonal phase upon sugar incorporation [154]. It can be speculated that if the sugars replace the water molecules around the GMOs polar head groups they may facilitate a more efficient packing of the head groups. This may explain the increased negative curvature upon disaccharide incorporation. When 1 % AP114 was added to the gels only cubic Pn3m structure was detected as presented in Figure 24 B. This was an unexpected finding since AP114 was previously shown to induce formation of reversed hexagonal phase at the same concentration in the pure GMO/water system (see Figure 9 A section **4.1**). Therefore, one would expect to find a reversed hexagonal phase also in AP114 and disaccharide containing samples, which was not the case. These results indicate that the disaccharide and AP114 molecules interact with the membranes in a synergistic way, which differs from if they were incorporated on their own.

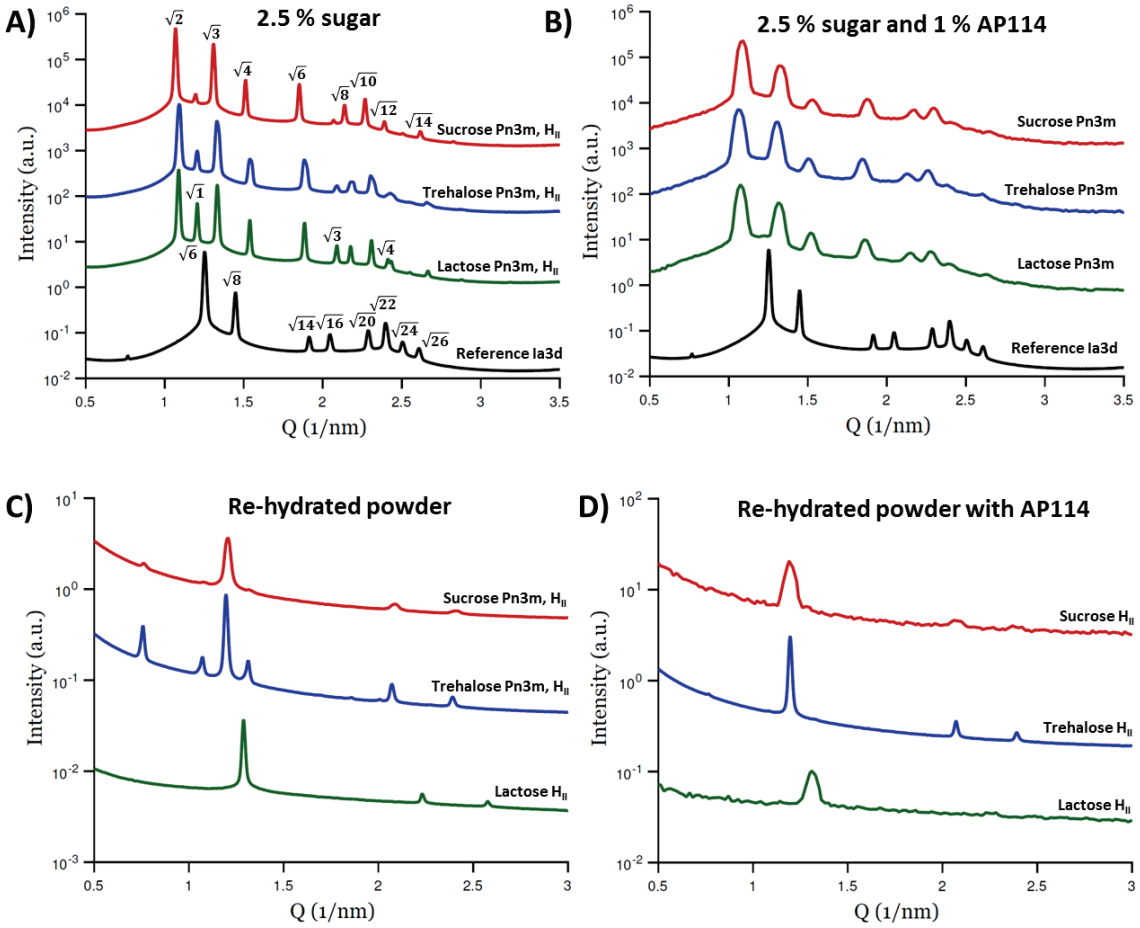

Figure 24. SAXS diffractograms of liquid crystalline gels (A and B) and particle dispersions after freeze-drying followed by rehydration (C and D). Characteristic peak spacing ratios are marked out for cubic Pn3m structure (A: red curve, sucrose), hexagonal (A: green curve, lactose) and cubic Ia3d reference with no sugar (A: black curve, reference). All samples were run at ESRF, except for samples in panel B and the sucrose and lactose samples resented in panel D, which were run at the SAXSLab-instrument.

The bulk LC gels were thereafter dispersed in water with 1 % P407 stabilizer. More disaccharide was added to the dispersion, to reach a final lipid:sugar ratio of 1:4 followed by heat-treatment and freeze-drying. The AP114 containing samples were not heat-treated due to the thermal instability of peptide. The physical appearance of the freeze-dried formulations was brittle and porous cakes that could easily be crushed into a fine powder. The freeze-dried samples were then rehydrated to their original concentration. The samples were further characterized by SAXS, cryo-TEM, DLS, release of AP114, as well as antimicrobial properties. SAXS diffractograms of the rehydrated powders, with and without AP114, are presented in Figure 24 C and D, respectively. The samples mainly indicated the presence of reversed hexagonal phase. The rehydrated powders without AP114 also displayed cubic Pn3m reflections, most prominent for sample containing trehalose. Formulations containing disaccharide and AP114 only showed the presence of reversed hexagonal phase. This observation may be explained by the fact that more sugar is incorporated when the powders are hydrated, when LC structures are re-formed, due to the fact that sugar is in great excess (lipid:sugar 1:4). The presence of the hexagonal phase may therefore be the most prominent

structure in the rehydrated samples due to the incorporation of more than the 2.5 wt % sugar added to the original gel. Another observation is that lactose-containing formulations gave smaller dimensions of the hexagonal structure by 5-6 Å, as can be seen by the shift of peaks to higher *q*-values. The differences in hydrophobicity, solubility of the disaccharides and the number of hydrogen bonding sites between the sugars and the hydrophilic head groups at the GMO molecules may influence the hexagonal phase that is formed. Particle size measurements (DLS) of the rehydrated powders indicated particles with a fairly broad size distribution, compared to particles prior to the freeze-drying cycle. Particle size data is presented in **Paper 3**. Trehalose was found to be the only sugar that could maintain a mono-modal particle size distribution after re-hydration of the powders, thus being the preferred choice of lyo-protectant for GMO-based LCNP forming powders. However, to-date lactose has regulatory approval for pulmonary use. Cryo-TEM investigation of the rehydrated powder with trehalose (no AP114) showed the presence of dense particles, displaying internal liquid crystalline structure, as can be seen in Figure 25 A. Fast Fourier analysis indicated the presence of cubic Pn3m structured particles, observed at different crystallographic orientations [155]. This observation was in line with the SAXS measurements of the same sample also showing presence of cubic Pn3m phase. Peptide encapsulation in the rehydrated powders containing AP114 was quantified using the ultra-centrifuge filtration method. Results showed an encapsulation efficacy of 85 % for lactose containing sample, 88 % for trehalose and 82 % for sucrose. The high degree of encapsulation of AP114 is in line with the data presented previously in section **4.2.1**, showing that higher encapsulation is usually achieved in hexagonal structured particles, compared to cubic particles**.** Hence, the presence of reversed hexagonal phase in the rehydrated formulations probably explains the high encapsulation efficacy. Release of AP114 from the rehydrated powders was studied using dialysis. Data is presented in Figure 25 B.

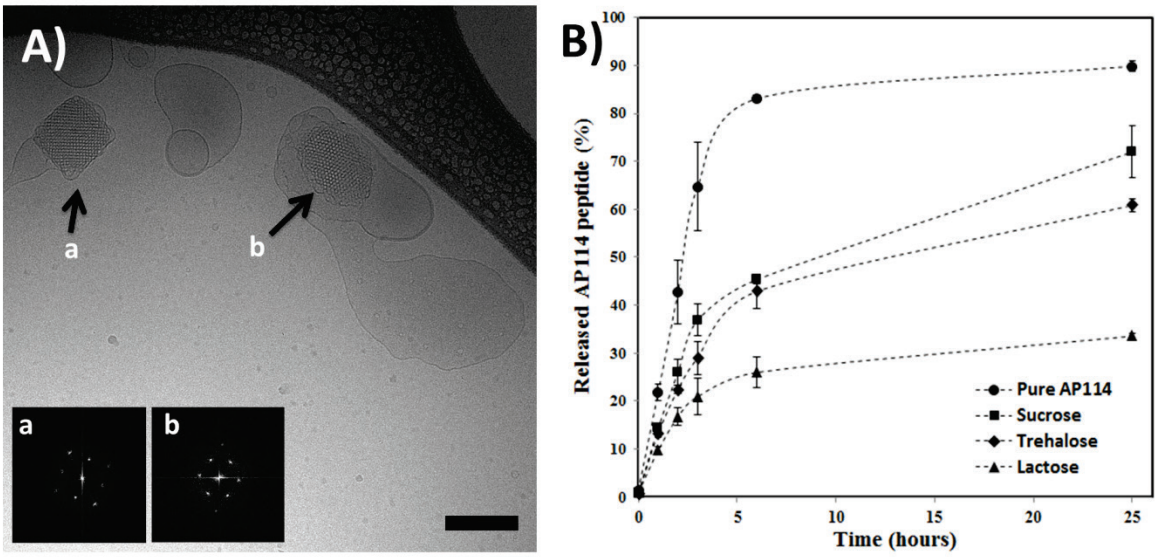

Figure 25. Representative cryo-TEM image of rehydrated freeze-dried powder containing trehalose (without AP114) (A) and release profiles of AP114 from rehydrated powders (B). Inserts in panel A show fast Fourier transforms of particles indicated by arrows. Scale-bar equals 200 nm. All formulations displayed a prolonged release over 25 h, compared to the reference with only peptide. Release data is presented as mean ± standard deviation (n=2).

The release was found to vary depending on which disaccharide was used as the lyo-protectant for the formulations. The lactose containing sample showed a significantly lower and slower release of AP114 during the 25 h dialysis period compared to samples containing trehalose and sucrose. This may be explained by differences in the dimensions of the water channels of the hexagonal structure in the particles. Lactose containing particles have much smaller water pores, 1.9 nm, compared to 2.5 nm in case of trehalose and sucrose. If the size of one AP114 molecule is approximated to be 2.7 nm, it is more challenging for the peptide to diffuse out from the narrower aqueous channels in the lactose containing sample. The size of the water channels in the trehalose and sucrose containing particles is slightly smaller than the AP114 molecule, but might be large enough to allow diffusion out of the structure.

The antibacterial properties of the rehydrated AP114-loaded powders were investigated using MIC and time-kill assays. MIC tests displayed preserved, or slightly increased, antibacterial properties of trehalose and sucrose containing samples, compared to pure peptide. Because AP114 is only active against gram-positive bacteria experiments were only carried out using SA and MRSA bacteria. The lactose containing sample displayed a reduced antibacterial effect in the MIC test. Particles without AP114 did not display any antibacterial activity. Time-kill assays agreed with the MIC-data, showing that trehalose and sucrose containing formulations were most prone to kill bacteria, as can be seen in Figure 26. These findings are in good agreement with the release studies, showing that the formulations with greatest release of AP114 (containing trehalose and sucrose) appeared to be most efficient in killing the bacteria. In the case of AP114, the data presented here and in section **4.2.2** indicates that release of AP114 is important to achieve efficient bacterial killing. This is in contrast to e.g. LL-37 loaded cubosomes, where the antimicrobial effect seems to originate from the peptide-loaded particle itself and is not solely due to the release of peptide. The mode of action is very different for AP114 and LL-37, which might explain the differences. AP114 acts by binding to the bacterial cell wall precursor Lipid II and inhibits membrane biosynthesis, whereas LL-37 is said to have unspecific membrane disruptive and modulating properties. Hence, it might be more important for AP114 to be released in order to translocate into the membrane and find the right receptors. If AP114 is not released from the hexosome particles sufficiently, the mode of action might be inhibited.

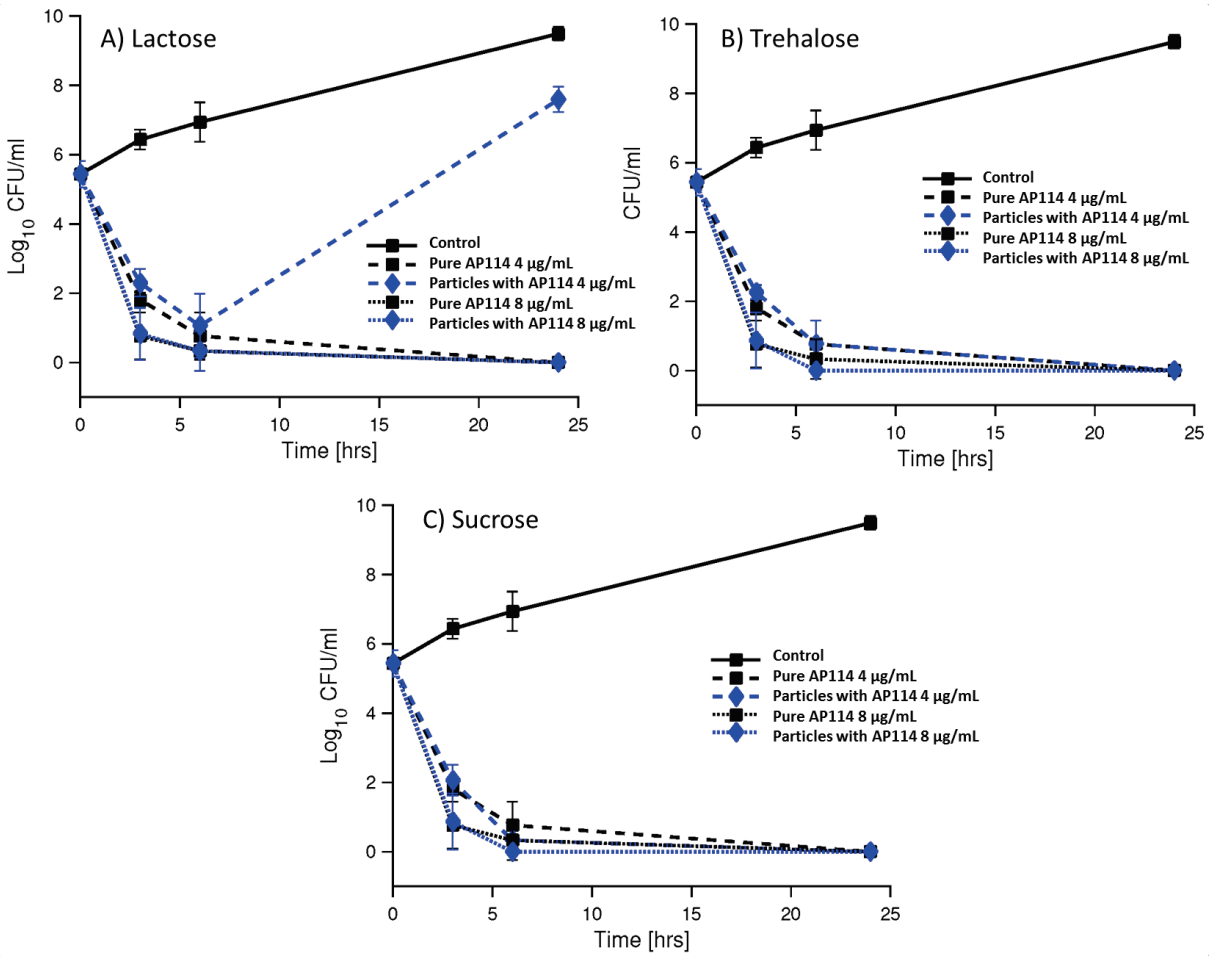

Figure 26. Time-kill curves for rehydrated powders containing AP114 and lactose (A), trehalose (B) and sucrose (C) on MRSA bacteria. All peptide-loaded particles killed the bacteria similar to pure peptide, with the exception of lactose containing particles at 4 µg/mL AP114 that displayed a reduced activity after 6 h incubation. Note that the 8 µg/mL curves with and without particles overlap in A. Data is presented as mean ± standard deviation (n=3). "Control" represents sample without any peptide or particles.

4.6. Liquid crystalline nanoparticles for topical delivery

Treatment of surgical site infections (SSIs), skin and soft tissue infections (SSTIs) and burn wound infections all rely on efficient antibiotic therapies. Hence, topical delivery of AMPs is of great interest for treatment of various skin infections caused by bacteria. The most common bacteria causing skin related infections are SA and its methicillin resistant analogue MRSA, PA and multi-drug resistant variants, *Staphylococcus epidermis* (SE) and EC [156-161]. In this part of the thesis, cubosomes prepared by the three methodologies (pre-, post- and hydrotrope) loaded with LL-37 will be discussed. Formulations of cubosomes may be best suitable for topical administration due to the hemolytic and cytotoxic properties reported previously [37, 76], which can be an obstacle e.g. for intravenous administration.

The release of LL-37 from cubosomes prepared by the hydrotrope method was presented and discussed previously; see Figure 15 D in section **4.2.1**. No release of LL-37 was observed, and that was also the case for pre- and post-loaded cubosomes (data presented in **Paper 5**).

Moreover, these cubosomes were found to fully protect LL-37 from proteolysis, as presented in Figure 17 in section **4.3**, as a consequence of being fully associated to the cubosomes. The LC structure of the particles discussed in this part of the thesis was investigated by SAXS and can be found in **Paper 5**.

The skin irritating potential of the cubosomes, with and without LL-37, was investigated using an *in vitro* human epidermis model. Results are presented in Figure 27 below. A viability >50 % of the keratinocytes predicts no skin irritation of a sample, according to the standardized test OECD TG 439. The viability of the keratinocyte cells was not negatively affected after exposure to any of the cubosome particles, indicating no skin irritation. No significant difference was observed for cubosomes with or without LL-37. Additionally, neither the preparation methodology nor the size of the corresponding cubosomes had any effect on the cells. Due to the very similar chemical compositions of the samples, any big differences would have been surprising. These findings indicate that GMO-based cubosomes can be used for topical administration of drugs, since they do not induce skin irritation. Potential applications within the field of cosmetics may also be possible.

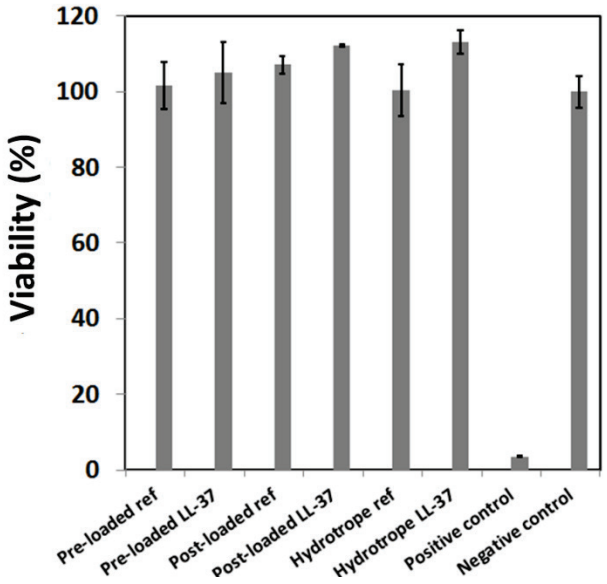

Figure 27. Skin irritation potential of cubosomes presented as viability of keratinocyte cells after exposure to cubosomes with and without LL-37. No skin irritating potential of the samples was found since the viability were always >50 % compared to the negative control.

Results from the *ex vivo* pig skin wound infection model are presented in Figure 28. All cubosomes displayed a reduced bactericidal effect on SA, compared to pure LL-37 at the same concentrations. Pre-loaded cubosomes appeared to be most efficient at 0.5 mg/mL peptide loading. The hydrotrope particles were found to kill bacteria least effectively. On the other hand, pure LL-37 peptide showed the strongest bacterial killing. More than 95% of the bacteria were killed over the 4 h application period, with a dose-response dependency. The observation that the cubosomes reduced the activity of LL-37 was not expected by the previous *in vitro* studies. The delivery mechanism and antibacterial properties of LL-37 loaded cubosomes may differ among planktonic bacteria that are used in the MIC and time-kill assays, compared to the bacteria in this *ex vivo* model. Planktonic bacteria are more easy

accessible for pure LL-37 and while loaded into cubosomes due to the faster diffusion and Brownian motion of the particles. The results here indicate that release of peptide is more important for killing bacteria that are attached to a surface. The *ex vivo* model shows best antibacterial properties for the pre-loaded cubosomes. The small particle size and narrow size distribution (~130 nm, PDI 0.15) of the pre-loaded cubosomes creates a large surface area that appears to be beneficial in the delivery of LL-37, facilitating many interaction points between the particles and bacteria. Moreover, the smaller particles may diffuse faster into the infected wound, thus increasing the possibility to reach many bacteria. This may explain why the much larger hydrotrope particles do not perform as well. Surprisingly, the cubosomes without any LL-37 affected the SA bacteria negatively, especially in case of pre- and post-loaded cubosomes. This is something that was not observed in MIC-tests previously using similar particles. However, the samples were diluted to a much lower particle concentration in the MIC tests (<1 mg/mL) whereas in the *ex vivo* model the cubosome dispersions are applied without further dilution (~50 mg/mL), which may explain the difference in activity. Hence, high cubosome concentrations might be suffocating for the bacteria, thereby suppressing their growth. In summary, the use of cubosomes for topical delivery of LL-37 was found to be a trade-off between proteolytic protection and antimicrobial activity.

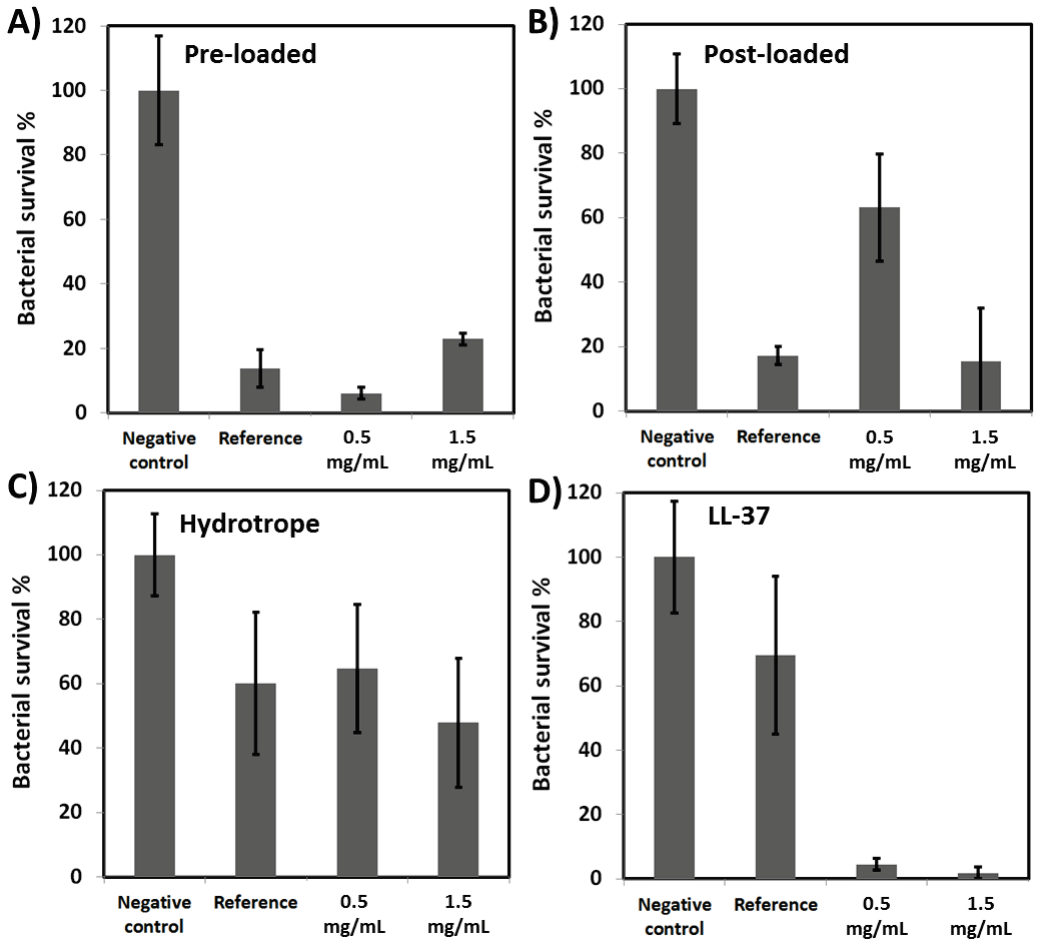

Figure 28. Survival of SA after sample exposure in the *ex-vivo* pig skin wound infection model. Data is presented as % of the viability of negative control (approximately 10^7 CFU/mL). "Reference" refers to cubosome without LL-37 in panel A-C, whilst in D it refers to 20 mM sodium acetate buffer pH 5.5. Negative control is BHI_{100}. Data is presented as mean ± standard error of mean (n=5).

5. CONCLUSIONS

As the number of multi-drug resistant bacteria increases around the globe, the demand for novel antibiotics and efficient treatment strategies is rising. AMPs have recently received great attention in the scientific community. Due to challenges in terms of susceptibility to proteolytic enzymes and high cost of manufacturing, only two AMPs have reached the market. Adequate drug delivery systems, or clever modifications of the peptides, are still needed in order to take more candidates all the way through clinical trials.

In this thesis, it was demonstrated that AMPs could successfully be loaded in cubic and hexagonal LC gels and in LCNPs using different peptide loading strategies. The overall findings are summarized in Table 5. It was demonstrated that the AMPs strongly influenced the curvature and LC structure of the cubic GMO/water system, while the hexagonal GMO/OA/water system was more robust. Size, net charge, hydrophobicity and concentration of the AMPs were important factors, influencing both the phase behavior and degree of association to the LCNPs. The LC structure of the particles strongly influenced the encapsulation efficacy of the AMPs, and in turn the release and antimicrobial activity, due to different dimensions of the water channels. Cubosomes were found to effectively protect the proteolytic sensitive peptide LL-37 from degradation by infection associated proteases, resulting in a significantly improved bacterial killing after proteolysis compared to pure peptide. However, there seems to be a trade-off between good protection from proteolysis (high encapsulation) and antimicrobial effect. Cubosomes were also demonstrated to be safe for topical administration. By adding disaccharides to the formulations, dry powders could be produced by freeze-drying, that formed LCNPs upon re-hydration. This could lead to increased shelf-life of the formulations and open up for new routes of administration.

Table 5. Summary of the main findings of this thesis.

System	Cubosome	Cubosome	Cubosome	Hexosome
AMP loading strategy	**pre**	**post**	**hydrotrope**	**pre**
AMP loading efficacy	moderate	poor/moderate	excellent*	excellent
Particle uniformity	good	excellent	poor	moderate
Antimicrobial activity	good	good	moderate***	poor
Proteolytic protection	excellent	excellent	excellent	**
Antibacterial effect after proteolysis	good	good	good	**

* As no release was observed, **Not investigated in this thesis, ***Data only from *ex vivo* model

In the design of nanoparticles for delivery of AMPs it is important to consider that different types of AMPs may have different mode of action. This was exemplified by the peptide AP114, which targets specific intracellular receptors (specific mode of action) and therefore needs to be released from the particles to give a sufficient antimicrobial effect. On the other hand, for the detergent-like peptide LL-37 (unspecific mode of action) contact between the peptide loaded particle and the outer bacterial membrane is enough to induce membrane defects, resulting in bacterial killing. The antimicrobial unit in the latter case seems to be the LL-37 loaded cubosomes, not solely due the free peptide. Hence, release of AMP from the LCNP carrier is not a necessity in order to kill bacteria.

6. FUTURE PERSPECTIVES

Most antibiotics, including penicillin, are today taken systemically. This was also the case in the fictional introductory story of this thesis. It means that the whole body is exposed to the drug and not only the bacteria causing the infection. Hence, the good bacteria will also suffer from the treatment. Local treatment overcomes part of these issues. Surgical site infections, burn wound infections and skin and soft tissue infections may all be treated predominantly with locally applied antibiotics in the future to reduce exposure and improve compliance. AMPs may serve as a good drug candidate for treatment of these indications. A formulation with triggered and controlled release properties, that delivers a sufficient dose of AMP over long times would be beneficial to reduce the number of applications. Trigged release is something that could add some extra functionality to LCNP systems. Other research groups have made use of OA to make pH-dependent phase transitions possible, from reversed hexagonal to bicontinuous cubic [54]. This enables the use of the good encapsulation properties of the hexagonal phase at higher pH ($pH>pK_a$) while at lower pH ($pH<pK_a$) cubosomes will form. Moreover, hexosomes may serve as a better choice for encapsulation of chemically unstable peptides, due to the lower water content compared to cubic phases. As discussed in this thesis, both release and antimicrobial properties were found to be superior for particles of cubic LC structure. This was recently used in the design of pH controlled transformations of OA and LL-37 containing lipid particles [162]. Structural alternations due to exposure of lipases is another interesting route that may be used to induce triggered release [79]. Naturally occurring phospholipids, such as soy phosphatidylcholine, are also of great interest. It has been shown that it can be used to modulate the structure of lipid-based LC systems [163]. Due to the ester bond present in the GMO molecule, it is susceptible to hydrolysis, which can limit the shelf-life of the LCNPs. The synthetic lipid phytantriol may therefore serve as an alternative to GMO for further studies, since it has better chemical stability. However, phytantriol is not regulatory approved as an inactive excipient in pharmaceutical formulations to-date [164]. Despite the superior proteolytic protection of sensitive AMPs offered by the cubosomes, the use of peptides that are designed to withstand proteolytic enzymes is probably more beneficial from a regulatory perspective. Chemical stability, e.g. deamidation and hydrolysis of peptides, are issues that need to be carefully considered and addressed before translation into clinical studies.

There are many challenges related to antibiotic resistance development. Decades of careful use of penicillin and other antibiotics, have actually led to fewer antibiotic resistant bacteria from clinical isolates in Scandinavian countries compared to the rest of Europe [165]. However, as people travel around the globe, so do bacteria. No matter if they are of good or bad nature. Antibiotic resistance needs to be tackled on a global basis and we have to take precautions during use of novel substances in order to not repeat history. People worldwide need to be taught that penicillin is not active against viral infections, such as a normal cold. Penicillin can still be bought over the counter in many countries, which is problematic. Moreover, in countries where the health system is increasingly reliant on commercial enterprises, novel difficulties might emerge. Similar to checking reviews before going to a

new restaurant or buying a new car, patients will look up reviews for different clinics. Doctors may prescribe unnecessary amounts of antibiotics as a result of pressure from patients in order to lower the risk of bad reviews of the clinic. Also, it can be hard to motivate big pharma companies to spend a lot of resources on developing cheap drugs like penicillin that cures the patients in one week or two.

The best is of course to not get a bacterial infection at all. However, sometimes you can't help it. Maybe preventive actions are needed as much as new antibiotics? Washing your hands properly, and listening to and trusting your medical doctor may also serve as an efficient treatment. Moreover, it is important to remember that bacteria are essential for many functions of our body. Research points out that the complex fauna of bacteria located in our intestines is important for our immune system. Keeping the good bacteria in good shape minimizes the risk of letting the bad guys take over. Who knows, "probiotics" might become as important as antibiotics in the future.

7. REFERENCES

1. Yap, M.-N.F., *The Double Life of Antibiotics.* Missouri medicine, 2013. **110**(4): p. 320-324.
2. Pierson, E., D.T. Hung, and A.E. Clatworthy, *Targeting virulence: a new paradigm for antimicrobial therapy.* Nature Chemical Biology, 2007. **3**(9): p. 541-548.
3. Coates, A.R.M., G. Halls, and Y. Hu, *Novel classes of antibiotics or more of the same?* British Journal of Pharmacology, 2011. **163**(1): p. 184-194.
4. Czaplewski, L., et al., *Alternatives to antibiotics-a pipeline portfolio review.* Lancet Infect Dis, 2016. **16**(2): p. 239-51.
5. WHO, *Antimicrobial resistance: global report on surveillance*. 2014.
6. Pasupuleti, M., A. Schmidtchen, and M. Malmsten, *Antimicrobial peptides: key components of the innate immune system.* Critical reviews in biotechnology, 2012. **32**(2): p. 143-171.
7. Zeya, H.I. and J.K. Spitznagel, *Cationic proteins of polymorphonuclear leukocyte lysosomes. II. Composition, properties, and mechanism of antibacterial action.* J Bacteriol, 1966. **91**(2): p. 755-62.
8. Zeya, H.I. and J.K. Spitznagel, *Antibacterial and enzymic basic proteins from leukocyte lysosomes: separation and identification.* Science, 1963. **142**(3595): p. 1085-7.
9. Boman, H.G., I. Nilsson, and B. Rasmuson, *Inducible antibacterial defence system in Drosophila.* Nature, 1972. **237**(5352): p. 232-235.
10. Hultmark, D., et al., *Insect immunity. Purification and properties of three inducible bactericidal proteins from hemolymph of immunized pupae of Hyalophora cecropia.* Eur J Biochem, 1980. **106**(1): p. 7-16.
11. Steiner, H., et al., *Sequence and specificity of two antibacterial proteins involved in insect immunity.* Nature, 1981. **292**(5820): p. 246-8.
12. Zasloff, M., *Magainins, a class of antimicrobial peptides from Xenopus skin: isolation, characterization of two active forms, and partial cDNA sequence of a precursor.* Proc Natl Acad Sci U S A, 1987. **84**(15): p. 5449-53.
13. Wang, G., et al., *Antimicrobial Peptides in 2014.* Pharmaceuticals, 2015. **8**(1): p. 123-150.
14. Eckert, R., *Road to clinical efficacy: challenges and novel strategies for antimicrobial peptide development.* Future Microbiology, 2011. **6**(6): p. 635-651.
15. Hancock, R.E.W. and H.-G. Sahl, *Antimicrobial and host-defense peptides as new anti-infective therapeutic strategies.* Nature biotechnology, 2006. **24**(12): p. 1551-1557.
16. Fox, J.L., *Antimicrobial peptides stage a comeback.* Nat Biotechnol, 2013. **31**(5): p. 379-82.
17. Fjell, C.D., et al., *Designing antimicrobial peptides: form follows function.* Nat Rev Drug Discov, 2011. **11**(1): p. 37-51.
18. Mahlapuu, M., et al., *Antimicrobial Peptides: An Emerging Category of Therapeutic Agents.* Frontiers in Cellular and Infection Microbiology, 2016. **6**.
19. Andersson, D.I., D. Hughes, and J.Z. Kubicek-Sutherland, *Mechanisms and consequences of bacterial resistance to antimicrobial peptides.* Drug Resistance Updates, 2016. **26**: p. 43-57.
20. Nordström, R. and M. Malmsten, *Delivery systems for antimicrobial peptides.* Advances in Colloid and Interface Science, 2017. **242**: p. 17-34.
21. Hancock, R.E.W. and R. Lehrer, *Cationic peptides: a new source of antibiotics.* Trends in Biotechnology, 1998. **16**(2): p. 82-88.
22. Yeaman, M.R. and N.Y. Yount, *Mechanisms of antimicrobial peptide action and resistance.* Pharmacol Rev, 2003. **55**(1): p. 27-55.
23. Nakajima, Y., et al., *Antibacterial activity and mechanism of action of tick defensin against Gram-positive bacteria.* BBA - General Subjects, 2003. **1624**: p. 125-130.
24. Wu, M. and R.E.W. Hancock, *Interaction of the cyclic antimicrobial cationic peptide bactenecin with the outer and cytoplasmic membrane*. 1999, WAVERLY PRESS INC: United States. p. 29.
25. Rose, A.S., et al., *NGL viewer: web-based molecular graphics for large complexes.* Bioinformatics, 2018: p. bty419-bty419.
26. Schneider, T., et al., *Plectasin, a Fungal Defensin, Targets the Bacterial Cell Wall Precursor Lipid II.* Science, 2010. **328**(5982): p. 1168-1172.
27. Fischer, R.L., et al., *Plectasin is a peptide antibiotic with therapeutic potential from a saprophytic fungus.* Nature, 2005. **437**(7061): p. 975-980.
28. Schmidtchen, A., et al., *Boosting Antimicrobial Peptides by Hydrophobic Oligopeptide End Tags.* Journal of Biological Chemistry, 2009. **284**(26): p. 17584-17594.
29. Dürr, U.H.N., U.S. Sudheendra, and A. Ramamoorthy, *LL-37, the only human member of the cathelicidin family of antimicrobial peptides.* BBA - Biomembranes, 2006. **1758**(9): p. 1408-1425.

30. Ramos, R., et al., *Wound healing activity of the human antimicrobial peptide LL37.* Peptides, 2011. **32**(7): p. 1469-1476.
31. Gronberg, A., et al., *Treatment with LL-37 is safe and effective in enhancing healing of hard-to-heal venous leg ulcers: a randomized, placebo-controlled clinical trial.* Wound Repair Regen, 2014. **22**(5): p. 613-21.
32. Strömstedt, A.A., et al., *Evaluation of Strategies for Improving Proteolytic Resistance of Antimicrobial Peptides by Using Variants of EFK17, an Internal Segment of LL-37.* Antimicrobial Agents and Chemotherapy, 2009. **53**(2): p. 593-602.
33. Shahmiri, M., et al., *Membrane Core-Specific Antimicrobial Action of Cathelicidin LL-37 Peptide Switches Between Pore and Nanofibre Formation.* Scientific Reports, 2016. **6**: p. 38184-38184.
34. Sood, R., et al., *Binding of LL-37 to model biomembranes: Insight into target vs host cell recognition.* Biochimica et Biophysica Acta (BBA) - Biomembranes, 2008. **1778**(4): p. 983-996.
35. Sieprawska-Lupa, M., et al., *Degradation of human antimicrobial peptide LL-37 by Staphylococcus aureus-derived proteinases.* Antimicrob Agents Chemother, 2004. **48**(12): p. 4673-9.
36. Vandamme, D., et al., *A comprehensive summary of LL-37, the factotum human cathelicidin peptide.* Cellular Immunology, 2012. **280**(1): p. 22-35.
37. Milak, S. and A. Zimmer, *Glycerol monooleate liquid crystalline phases used in drug delivery systems.* International Journal of Pharmaceutics, 2015. **478**(2): p. 569-587.
38. Chen, Y., P. Ma, and S. Gui, *Cubic and Hexagonal Liquid Crystals as Drug Delivery Systems.* BioMed Research International, 2014.
39. Demurtas, D., et al., *Direct visualization of dispersed lipid bicontinuous cubic phases by cryo-electron tomography.* Nature communications 2015. **6**: p. 8915.
40. Lynch, M.L. and P.T. Spicer, *Bicontinuous liquid crystals*. 2005: CRC press.
41. Hyde, S.T., *Bicontinuous structures in lyotropic liquid crystals and crystalline hyperbolic surfaces.* Current Opinion in Solid State and Materials Science, 1996. **1**(5): p. 653-662.
42. Hyde, S.T., *Identification of Lyotropic Liquid crystalline Mesophases*, in *Handbook of Applied Surface and Colloid Chemistry*, K. Holmberg, Editor. 2001, John Wiley & Sons, Ltd. p. 299-332.
43. Fong, C., T. Le, and C.J. Drummond, *Lyotropic liquid crystal engineering-ordered nanostructured small molecule amphiphile self-assembly materials by design.* Chemical Society Reviews, 2012. **41**(3): p. 1297.
44. Larsson, K., *Cubic lipid-water phases: structures and biomembrane aspects.* The Journal of Physical Chemistry, 1989. **93**(21): p. 7304-7314.
45. Larsson, K., *Periodic minimal surface structures of cubic phases formed by lipids and surfactants.* Journal of Colloid and Interface Science, 1986. **113**(1): p. 299-300.
46. Luzzati, V. and F. Husson, *The structure of the liquid-crystalline phases of lipid-water systems.* The Journal of Cell Biology, 1962. **12**(2): p. 207-219.
47. Rivas, E., et al., *Structure of the Cubic Phases of Lipid-Water Systems.* Nature, 1968. **220**(5166): p. 485-488.
48. Qiu, H. and M. Caffrey, *The phase diagram of the monoolein/water system: metastability and equilibrium aspects.* Biomaterials, 2000. **21**(3): p. 223-234.
49. Ganem-Quintanar, A., D. Quintanar-Guerrero, and P. Buri, *Monoolein: A Review of the Pharmaceutical Applications.* Drug Development and Industrial Pharmacy, 2000. **26**(8): p. 809-820.
50. Kulkarni, C.V., et al., *Monoolein: a magic lipid?* Physical Chemistry Chemical Physics, 2011. **13**(8): p. 3004-3021.
51. Caboi, F., et al., *Addition of hydrophilic and lipophilic compounds of biological relevance to the monoolein/water system. I. Phase behavior.* Chemistry and Physics of Lipids, 2001. **109**(1): p. 47-62.
52. Borné, J., T. Nylander, and A. Khan, *Phase Behavior and Aggregate Formation for the Aqueous Monoolein System Mixed with Sodium Oleate and Oleic Acid.* Langmuir, 2001. **17**(25): p. 7742-7751.
53. Mulet, X., B.J. Boyd, and C.J. Drummond, *Advances in drug delivery and medical imaging using colloidal lyotropic liquid crystalline dispersions.* Journal of Colloid and Interface Science, 2013. **393**(0): p. 1-20.
54. Salentinig, S., L. Sagalowicz, and O. Glatter, *Self-Assembled Structures and pKa Value of Oleic Acid in Systems of Biological Relevance.* Langmuir, 2010. **26**(14): p. 11670-11679.
55. Bisset, N.B., B.J. Boyd, and Y.-D. Dong, *Tailoring liquid crystalline lipid nanomaterials for controlled release of macromolecules.* International Journal of Pharmaceutics, 2015. **495**(1): p. 241-248.
56. Angelova, A., et al., *Interaction of the Peptide Antibiotic Alamethicin with Bilayer- and Non-bilayer-Forming Lipids: Influence of Increasing Alamethicin Concentration on the Lipids Supramolecular Structures.* Archives of Biochemistry and Biophysics, 2000. **378**(1): p. 93-106.
57. Angelova, A., et al., *Proteocubosomes: Nanoporous Vehicles with Tertiary Organized Fluid Interfaces.* Langmuir, 2005. **21**(9): p. 4138-4143.

58. Angelova, A., et al., *Structural organization of proteocubosome carriers involving medium- and large-size proteins.* Journal of Drug Delivery Science and Technology, 2005. **15**(1): p. 108-112.
59. Angelova, A., et al., *Dynamic control of nanofluidic channels in protein drug delivery vehicles.* Journal of Drug Delivery Science and Technology, 2008. **18**(1): p. 41-45.
60. Angelov, B., et al., *Protein-Containing PEGylated Cubosomic Particles: Freeze-Fracture Electron Microscopy and Synchrotron Radiation Circular Dichroism Study.* The Journal of Physical Chemistry B, 2012. **116**(26): p. 7676-7686.
61. Angelova, A., et al., *Protein entrapment in PEGylated lipid nanoparticles.* International Journal of Pharmaceutics, 2013. **454**(2): p. 625-632.
62. Angelov, B., et al., *Multicompartment Lipid Cubic Nanoparticles with High Protein Upload: Millisecond Dynamics of Formation.* ACS Nano, 2014. **8**(5): p. 5216-5226.
63. Shah, J.C., Y. Sadhale, and D.M. Chilukuri, *Cubic phase gels as drug delivery systems.* Advanced Drug Delivery Reviews, 2001. **47**(2–3): p. 229-250.
64. Yaghmur, A. and O. Glatter, *Characterization and potential applications of nanostructured aqueous dispersions.* Advances in Colloid and Interface Science, 2009. **147–148**(0): p. 333-342.
65. Gustafsson, J., et al., *Cubic Lipid−Water Phase Dispersed into Submicron Particles.* Langmuir, 1996. **12**(20): p. 4611-4613.
66. Gustafsson, J., et al., *Submicron Particles of Reversed Lipid Phases in Water Stabilized by a Nonionic Amphiphilic Polymer.* Langmuir, 1997. **13**(26): p. 6964-6971.
67. Larsson, K., *Aqueous dispersions of cubic lipid–water phases.* Current Opinion in Colloid & Interface Science, 2000. **5**(1–2): p. 64-69.
68. Chong, J.Y.T., et al., *Novel Steric Stabilizers for Lyotropic Liquid Crystalline Nanoparticles: PEGylated-Phytanyl Copolymers.* Langmuir, 2015. **31**(9): p. 2615-2629.
69. Chong, J.Y.T., et al., *High-Throughput Discovery of Novel Steric Stabilizers for Cubic Lyotropic Liquid Crystal Nanoparticle Dispersions.* Langmuir, 2012. **28**(25): p. 9223-9232.
70. Larsson, K. and F. Tiberg, *Periodic minimal surface structures in bicontinuous lipid–water phases and nanoparticles.* Current Opinion in Colloid & Interface Science, 2005. **9**(6): p. 365-369.
71. Muller, F., A. Salonen, and O. Glatter, *Phase behavior of Phytantriol/water bicontinuous cubic Pn3m cubosomes stabilized by Laponite disc-like particles.* Journal of Colloid and Interface Science, 2010. **342**(2): p. 392-398.
72. Muller, F., A. Salonen, and O. Glatter, *Monoglyceride-based cubosomes stabilized by Laponite: Separating the effects of stabilizer, pH and temperature.* Colloids and Surfaces A: Physicochemical and Engineering Aspects, 2010. **358**(1–3): p. 50-56.
73. Zhai, J., et al., *Revisiting β-Casein as a Stabilizer for Lipid Liquid Crystalline Nanostructured Particles.* Langmuir, 2011. **27**(24): p. 14757-14766.
74. Bhatt, A.B., T.J. Barnes, and C.A. Prestidge, *Silica nanoparticle stabilization of liquid crystalline lipid dispersions: impact on enzymatic digestion and drug solubilization.* Curr Drug Deliv, 2015. **12**(1): p. 47-55.
75. Johnsson, M., et al., *Aqueous Phase Behavior and Dispersed Nanoparticles of Diglycerol Monooleate/Glycerol Dioleate Mixtures.* Langmuir, 2005. **21**(11): p. 5159-5165.
76. Barauskas, J., et al., *Interactions of lipid-based liquid crystalline nanoparticles with model and cell membranes.* International Journal of Pharmaceutics, 2010. **391**(1–2): p. 284-291.
77. Barauskas, J. and T. Landh, *Phase Behavior of the Phytantriol/Water System.* Langmuir, 2003. **19**(23): p. 9562-9565.
78. Fraser, S.J., et al., *Controlling nanostructure and lattice parameter of the inverse bicontinuous cubic phases in functionalised phytantriol dispersions.* Journal of Colloid and Interface Science, 2013. **408**(0): p. 117-124.
79. Wadsäter, M., et al., *Formation of Highly Structured Cubic Micellar Lipid Nanoparticles of Soy Phosphatidylcholine and Glycerol Dioleate and Their Degradation by Triacylglycerol Lipase.* ACS Applied Materials & Interfaces, 2014. **6**(10): p. 7063-7069.
80. Wadsater, M., et al., *Structural effects of the dispersing agent polysorbate 80 on liquid crystalline nanoparticles of soy phosphatidylcholine and glycerol dioleate.* Soft Matter, 2015. **11**(6): p. 1140-1150.
81. Nguyen, T.-H., et al., *Phytantriol and glyceryl monooleate cubic liquid crystalline phases as sustained-release oral drug delivery systems for poorly water soluble drugs I. Phase behaviour in physiologically-relevant media.* Journal of Pharmacy and Pharmacology, 2010. **62**(7): p. 844-855.
82. Rizwan, S.B., et al., *Bicontinuous cubic liquid crystals as sustained delivery systems for peptides and proteins.* Expert Opinion on Drug Delivery, 2010. **7**(10): p. 1133-1144.
83. Angelova, A., et al., *Self-Assembled Multicompartment Liquid Crystalline Lipid Carriers for Protein, Peptide, and Nucleic Acid Drug Delivery.* Accounts of Chemical Research, 2010. **44**(2): p. 147-156.

84. Guo, C., et al., *Lyotropic liquid crystal systems in drug delivery.* Drug Discovery Today, 2010. **15**(23–24): p. 1032-1040.
85. Spicer, P.T., et al., *Novel Process for Producing Cubic Liquid Crystalline Nanoparticles (Cubosomes).* Langmuir, 2001. **17**(19): p. 5748-5756.
86. Akhlaghi, S.P., et al., *Impact of preparation method and variables on the internal structure, morphology, and presence of liposomes in phytantriol-Pluronic® F127 cubosomes.* Colloids and Surfaces B: Biointerfaces, 2016. **145**: p. 845-853.
87. Barauskas, J., et al., *Cubic Phase Nanoparticles (Cubosome†): Principles for Controlling Size, Structure, and Stability.* Langmuir, 2005. **21**(6): p. 2569-2577.
88. Demurtas, D., et al., *Direct visualization of dispersed lipid bicontinuous cubic phases by cryo-electron tomography.* Nature Communications, 2015. **6**: p. 8915.
89. Kuntsche, J. and H. Bunjes, *Influence of preparation conditions and heat treatment on the properties of supercooled smectic cholesteryl myristate nanoparticles.* European Journal of Pharmaceutics and Biopharmaceutics, 2007. **67**(3): p. 612-620.
90. Chung, H., et al., *Self-assembled "nanocubicle" as a carrier for peroral insulin delivery.* Diabetologia, 2002. **45**(3): p. 448-451.
91. Rizwan, S.B., et al., *Preparation of phytantriol cubosomes by solvent precursor dilution for the delivery of protein vaccines.* European Journal of Pharmaceutics and Biopharmaceutics, 2011. **79**(1): p. 15-22.
92. Gordon, S., et al., *Chitosan hydrogels containing liposomes and cubosomes as particulate sustained release vaccine delivery systems.* Journal of Liposome Research, 2012. **22**(3): p. 193-204.
93. Rattanapak, T., et al., *Comparative study of liposomes, transfersomes, ethosomes and cubosomes for transcutaneous immunisation: characterisation and in vitro skin penetration.* Journal of Pharmacy and Pharmacology, 2012. **64**(11): p. 1560-1569.
94. Cervin, C., et al., *A combined in vitro and in vivo study on the interactions between somatostatin and lipid-based liquid crystalline drug carriers and bilayers.* European Journal of Pharmaceutical Sciences, 2009. **36**(4-5): p. 377-385.
95. Lopes, L., et al., *Reverse Hexagonal Phase Nanodispersion of Monoolein and Oleic Acid for Topical Delivery of Peptides: in Vitro and in Vivo Skin Penetration of Cyclosporin A.* Pharmaceutical Research, 2006. **23**(6): p. 1332-1342.
96. Lai, J., et al., *Pharmacokinetics and enhanced oral bioavailability in beagle dogs of cyclosporine A encapsulated in glyceryl monooleate/poloxamer 407 cubic nanoparticles.* International journal of nanomedicine, 2010. **5**: p. 13-23.
97. Jain, S., et al., *Recent Advances in Lipid-Based Vesicles and Particulate Carriers for Topical and Transdermal Application.* Journal of Pharmaceutical Sciences, 2017. **106**(2): p. 423-445.
98. Sala, M., et al., *Lipid nanocarriers as skin drug delivery systems: Properties, mechanisms of skin interactions and medical applications.* International Journal of Pharmaceutics, 2018. **535**(1): p. 1-17.
99. Zhai, Y. and G. Zhai, *Advances in lipid-based colloid systems as drug carrier for topic delivery.* Journal of Controlled Release, 2014. **193**: p. 90-99.
100. Lopes, J.L.C., et al., *Liquid crystalline phases of monoolein and water for topical delivery of cyclosporin A: Characterization and study of in vitro and in vivo delivery.* European Journal of Pharmaceutics and Biopharmaceutics, 2006. **63**(2): p. 146-155.
101. Lopes, L.B., F.F.F. Speretta, and M.V.L.B. Bentley, *Enhancement of skin penetration of vitamin K using monoolein-based liquid crystalline systems.* European Journal of Pharmaceutical Sciences, 2007. **32**(3): p. 209-215.
102. Seo, S.R., et al., *In vivo hair growth-promoting efficacies of herbal extracts and their cubosomal suspensions.* Journal of Industrial and Engineering Chemistry, 2013. **19**(4): p. 1331-1339.
103. Abdelwahed, W., et al., *Freeze-drying of nanoparticles: Formulation, process and storage considerations.* Advanced Drug Delivery Reviews, 2006. **58**(15): p. 1688-1713.
104. Avachat, A.M. and S.S. Parpani, *Formulation and development of bicontinuous nanostructured liquid crystalline particles of efavirenz.* Colloids and Surfaces B: Biointerfaces, 2015. **126**: p. 87-97.
105. Moebus, K., J. Siepmann, and R. Bodmeier, *Cubic phase-forming dry powders for controlled drug delivery on mucosal surfaces.* Journal of Controlled Release, 2012. **157**(2): p. 206-215.
106. Nasr, M. and M. Dawoud, *Sorbitol based powder precursor of cubosomes as an oral delivery system for improved bioavailability of poorly water soluble drugs.* Journal of Drug Delivery Science and Technology, 2016. **35**: p. 106-113.
107. Nielsen, L.H., et al., *Microcontainers as an oral delivery system for spray dried cubosomes containing ovalbumin.* European Journal of Pharmaceutics and Biopharmaceutics, 2017. **118**: p. 13-20.
108. Shah, M.H., S.V. Biradar, and A.R. Paradkar, *Spray dried glyceryl monooleate–magnesium trisilicate dry powder as cubic phase precursor.* International Journal of Pharmaceutics, 2006. **323**(1–2): p. 18-26.

109. Spicer, P.T., et al., *Dry Powder Precursors of Cubic Liquid Crystalline Nanoparticles (cubosomes).* Journal of Nanoparticle Research, 2002. **4**(4): p. 297-311.
110. Briggs, J., H. Chung, and M. Caffrey, *The temperature-composition phase diagram and mesophase structure characterization of the monoolein/water system.* Journal de Physique II, 1996. **6**(5): p. 723-751.
111. Höök, F., et al., *Energy Dissipation Kinetics for Protein and Antibody−Antigen Adsorption under Shear Oscillation on a Quartz Crystal Microbalance.* Langmuir, 1998. **14**(4): p. 729-734.
112. Nunez, V., et al., *Improvements to the polarised-neutron reflectometer CRISP.* Physica B: Condensed Matter, 1997. **241-243**: p. 148-150.
113. Penfold, J., R.C. Ward, and W.G. Williams, *A time-of-flight neutron reflectometer for surface and interfacial studies.* Journal of Physics E: Scientific Instruments, 1987. **20**(11): p. 1411.
114. Browning, K.L., et al., *Human Lipoproteins at Model Cell Membranes: Effect of Lipoprotein Class on Lipid Exchange.* Scientific Reports, 2017. **7**(1): p. 7478.
115. Hughes, A., *RasCAL, https://sourceforge.net/p/rscl/wiki/Home/.* ISIS Neutron and Muon source, 2014.
116. Rennie, A.R., *trikk, http://www.reflectometry.net/refprog.htm*. 2018.
117. Björn, C., et al., *Anti-infectious and anti-inflammatory effects of peptide fragments sequentially derived from the antimicrobial peptide centrocin 1 isolated from the green sea urchin, Strongylocentrotus droebachiensis.* AMB Express, 2012. **2**: p. 67-67.
118. Bjorn, C., et al., *Anti-infective efficacy of the lactoferrin-derived antimicrobial peptide HLR1r.* Peptides, 2016. **81**: p. 21-8.
119. Myhrman, E., et al., *The novel antimicrobial peptide PXL150 in the local treatment of skin and soft tissue infections.* Appl Microbiol Biotechnol, 2013. **97**(7): p. 3085-96.
120. Schmidtchen, A., et al., *Boosting antimicrobial peptides by hydrophobic oligopeptide end tags.* J Biol Chem, 2009. **284**(26): p. 17584-94.
121. McDonnell, G., et al., *Clinical correlation of a skin antisepsis model.* Journal of Microbiological Methods, 1999. **35**(1): p. 31-35.
122. OECD, *Test No. 439: In Vitro Skin Irritation - Reconstructed Human Epidermis Test Method*. 2013: OECD Publishing.
123. Yaghmur, A., et al., *Tuning curvature and stability of monoolein bilayers by designer lipid-like peptide surfactants.* PloS one, 2007. **2**(5): p. e479.
124. Mandal, K., et al., *Racemic crystallography of synthetic protein enantiomers used to determine the X-ray structure of plectasin by direct methods.* Protein Sci, 2009. **18**(6): p. 1146-54.
125. Sancho-Vaello, E., et al., *Structural remodeling and oligomerization of human cathelicidin on membranes suggest fibril-like structures as active species.* Scientific Reports, 2017. **7**(1): p. 15371.
126. Oren, Z., et al., *Structure and organization of the human antimicrobial peptide LL-37 in phospholipid membranes: relevance to the molecular basis for its non-cell-selective activity.* Biochemical Journal, 1999. **341**(Pt 3): p. 501-513.
127. Gontsarik, M., et al., *Antimicrobial Peptide-Driven Colloidal Transformations in Liquid-Crystalline Nanocarriers.* The Journal of Physical Chemistry Letters, 2016. **7**(17): p. 3482-3486.
128. Johansson, J., et al., *Conformation-dependent antibacterial activity of the naturally occurring human peptide LL-37.* J Biol Chem, 1998. **273**(6): p. 3718-24.
129. Braun, K., et al., *Membrane interactions of mesoporous silica nanoparticles as carriers of antimicrobial peptides.* Journal of Colloid and Interface Science, 2016. **475**: p. 161-170.
130. Zetterberg, M.M., et al., *PEG-stabilized lipid disks as carriers for amphiphilic antimicrobial peptides.* Journal of Controlled Release, 2011. **156**(3): p. 323-328.
131. Fragneto, G. and M. Rheinstädter, *Structural and dynamical studies from bio-mimetic systems: an overview.* Comptes Rendus Physique, 2007. **8**(7): p. 865-883.
132. Barker, R.D., L.E. McKinley, and S. Titmuss, *Neutron Reflectivity as a Tool for Physics-Based Studies of Model Bacterial Membranes*, in *Biophysics of Infection*, M.C. Leake, Editor. 2016, Springer International Publishing: Cham. p. 261-282.
133. Nylander, T., et al., *Neutron reflectometry to investigate the delivery of lipids and DNA to interfaces (Review).* Biointerphases, 2008. **3**(2): p. FB64-FB82.
134. Vandoolaeghe, P., et al., *Neutron Reflectivity Studies of the Interaction of Cubic-Phase Nanoparticles with Phospholipid Bilayers of Different Coverage.* Langmuir, 2009. **25**(7): p. 4009-4020.
135. Vandoolaeghe, P., et al., *Adsorption of cubic liquid crystalline nanoparticles on model membranes.* Soft Matter, 2008. **4**(11): p. 2267-2277.
136. Shen, H.-H., et al., *The influence of dipalmitoyl phosphatidylserine on phase behaviour of and cellular response to lyotropic liquid crystalline dispersions.* Biomaterials, 2010. **31**(36): p. 9473-9481.
137. Shen, H.-H., et al., *The interaction of cubosomes with supported phospholipid bilayers using neutron reflectometry and QCM-D.* Soft Matter, 2011. **7**(18): p. 8041-8049.

138. Fernandez, D.I., et al., *Structural effects of the antimicrobial peptide maculatin 1.1 on supported lipid bilayers.* European Biophysics Journal, 2013. **42**(1): p. 47-59.
139. Mathews, C.K., K.G. Ahern, and K.E. Van Holde, *Biochemistry*. 3 ed. 2000, San Francisco: Addison Wesley Longman Inc.
140. Richter, R., A. Mukhopadhyay, and A. Brisson, *Pathways of Lipid Vesicle Deposition on Solid Surfaces: A Combined QCM-D and AFM Study.* Biophysical Journal, 2003. **85**(5): p. 3035-3047.
141. Lozeau, L.D., M.W. Rolle, and T.A. Camesano, *A QCM-D study of the concentration- and time-dependent interactions of human LL37 with model mammalian lipid bilayers.* Colloids and Surfaces B: Biointerfaces, 2018. **167**: p. 229-238.
142. Xhindoli, D., et al., *The human cathelicidin LL-37--A pore-forming antibacterial peptide and host-cell modulator.* Biochim Biophys Acta, 2016. **1858**(3): p. 546-66.
143. Kucerka, N., M.P. Nieh, and J. Katsaras, *Fluid phase lipid areas and bilayer thicknesses of commonly used phosphatidylcholines as a function of temperature.* Biochim Biophys Acta, 2011. **1808**(11): p. 2761-71.
144. Pan, J., et al., *Molecular structures of fluid phase phosphatidylglycerol bilayers as determined by small angle neutron and X-ray scattering.* Biochim Biophys Acta, 2012. **1818**(9): p. 2135-48.
145. Rai, D.K. and S. Qian, *Interaction of the Antimicrobial Peptide Aurein 1.2 and Charged Lipid Bilayer.* Scientific Reports, 2017. **7**(1): p. 3719-3719.
146. Henzler Wildman, K.A., D.-K. Lee, and A. Ramamoorthy, *Mechanism of Lipid Bilayer Disruption by the Human Antimicrobial Peptide, LL-37.* Biochemistry, 2003. **42**(21): p. 6545-6558.
147. Sevcsik, E., et al., *Interaction of LL-37 with Model Membrane Systems of Different Complexity: Influence of the Lipid Matrix.* Biophysical Journal, 2008. **94**(12): p. 4688-4699.
148. Farley, M.M., et al., *Minicells, Back in Fashion.* Journal of Bacteriology, 2016. **198**(8): p. 1186-1195.
149. Garvey, C.J., et al., *Phospholipid Membrane Protection by Sugar Molecules during Dehydration—Insights into Molecular Mechanisms Using Scattering Techniques.* International Journal of Molecular Sciences, 2013. **14**(4): p. 8148-8163.
150. Kent, B., et al., *Localization of trehalose in partially hydrated DOPC bilayers: insights into cryoprotective mechanisms.* Journal of The Royal Society Interface, 2014. **11**(95).
151. Lenné, T., et al., *Location of sugars in multilamellar membranes at low hydration.* Physica B: Condensed Matter, 2006. **385**: p. 862-864.
152. Izutsu, K.-I., C. Yomota, and T. Kawanishi, *Stabilization of Liposomes in Frozen Solutions Through Control of Osmotic Flow and Internal Solution Freezing by Trehalose.* Journal of Pharmaceutical Sciences, 2011. **100**(7): p. 2935-2944.
153. Nagase, H., H. Ueda, and M. Nakagaki, *Relationship between Hydrophobic Index of Saccharide and Gel-Liquid Crystal Transition Temperature of the L-[alpha]-Dipalmitoyl Phosphatidylcholine (DPPC)/Saccharide/Water System.* Chemical & Pharmaceutical Bulletin, 1999. **47**(5): p. 607.
154. Söderberg, I. and H. Ljusberg-Wahren, *Phase properties and structure of a monoglyceride/sucrose/water system.* Chemistry and Physics of Lipids, 1990. **55**(2): p. 97-101.
155. Sagalowicz, L., et al., *Study of liquid crystal space groups using controlled tilting with cryogenic transmission electron microscopy.* Langmuir : the ACS journal of surfaces and colloids, 2007. **23**(24): p. 12003-12009.
156. Church, D., et al., *Burn Wound Infections.* Clinical Microbiology Reviews, 2006. **19**(2): p. 403-434.
157. Dryden, M.S., *Complicated skin and soft tissue infection.* Journal of Antimicrobial Chemotherapy, 2010. **65**(suppl_3): p. iii35-iii44.
158. Giacometti, A., et al., *Epidemiology and microbiology of surgical wound infections.* J Clin Microbiol, 2000. **38**(2): p. 918-22.
159. Leaper, D.J., et al., *Surgical site infection - a European perspective of incidence and economic burden.* Int Wound J, 2004. **1**(4): p. 247-73.
160. Lowy, F.D., *Antimicrobial resistance: the example of Staphylococcus aureus.* J Clin Invest, 2003. **111**(9): p. 1265-73.
161. Moet, G.J., et al., *Contemporary causes of skin and soft tissue infections in North America, Latin America, and Europe: report from the SENTRY Antimicrobial Surveillance Program (1998-2004).* Diagn Microbiol Infect Dis, 2007. **57**(1): p. 7-13.
162. Gontsarik, M., et al., *pH-Triggered nanostructural transformations in antimicrobial peptide/oleic acid self-assemblies.* Biomaterials Science, 2018. **6**(4): p. 803-812.
163. Yaghmur, A., et al., *Control of the Internal Structure of MLO-Based Isasomes by the Addition of Diglycerol Monooleate and Soybean Phosphatidylcholine.* Langmuir, 2006. **22**(24): p. 9919-9927.
164. U.S. Food and Drug Administration (FDA). *Inactive Ingredient Search for Approved Drug Products*. [cited 2018 2018-10-11]; Available from: https://www.accessdata.fda.gov/scripts/cder/iig/index.cfm.

165. European Centre for Disease Prevention and Control, *Surveillance of antimicrobial resistance in Europe*. 2016.